Università degli studi di Ferrara

DIPARTIMENTO DI INGEGNERIA

DOTTORATO DI RICERCA IN SCIENZE DELL'INGEGNERIA

Ciclo XXVII

Coordinatore: Prof. Stefano Trillo

Wireless Localization Systems: Statistical Modeling and Algorithm Design

Settore Scientifico Disciplinare ING-INF/03

Dottoranda:
Dott.ssa Stefania Bartoletti

Tutore:
Prof. Ing. Andrea Conti

Cotutore:
Prof. Moe Z. Win

Anni 2012-2014

Sommario

I sistemi wireless per la localizzazione sono essenziali per numerose applicazioni emergenti che si basano sul concetto di *context-awareness*, specialmente nei settori civile, della logistica e della sicurezza. Ottenere una stima accurata della posizione di oggetti target in ambienti indoor, a cui molte di tali applicazioni si rivolgono, è tuttora ostico ed è oggetto di una attività di ricerca fervente a livello mondiale. Le prestazioni di tali sistemi derivano dalla qualità di misure di distanza (ranging) ottenute processando segnali wireless scambiati tra nodi che compongono il sistema di localizzazione. Tali stime di distanza servono da osservazioni per l'inferenza della posizione dei target e la loro qualità dipende dalle proprietà intrinseche della rete e dalle tecniche di processamento del segnale. Pertanto, il progetto di tali sistemi non può prescindere da un accurato modello statistico per l'informazione sulla distanza e da efficienti algoritmi di ranging, localizzazione e tracciamento. Gli obiettivi principali di questa tesi sono: (i) la derivazione di modelli statistici e (ii) il design di algoritmi per diversi tipi di sistemi wireless per la localizzazione, con particolare riguardo verso i sistemi passivi e semi-passivi (sistemi radar attivi, sistemi radar passivi, sistemi di identificazione a radio frequenza). A tal fine, sono stati derivati modelli statistici per l'informazione di distanza, proposti algoritmi di tipo soft-decision e hard-decision a bassa complessità ed analizzati diversi sistemi di localizzazione a banda larga e ultra-larga. L'attività di ricerca è stata condotta anche nell'ambito di diversi progetti, in collaborazione con altre Università ed aziende nazionali ed internazionali, e nell'ambito di un periodo di ricerca di durata annuale presso il Massachusetts Institute of Technology, Cambridge, MA, USA. L'analisi di prestazione dei sistemi descritti, dei modelli derivati e degli algoritmi proposti è stata validata considerando diversi case study in scenari realistici e utilizzando anche risultati ottenuti nell'ambito dei suddetti progetti.

Abstract

Wireless localization systems are essential for emerging applications that rely on context-awareness, especially in civil, logistic, and security sectors. Accurate localization in indoor environments is still a challenge and triggers a fervent research activity worldwide. The performance of such systems relies on the quality of range measurements gathered by processing wireless signals within the sensors composing the localization system. Such range estimates serve as observations for the target position inference. The quality of range estimates depends on the network intrinsic properties and signal processing techniques. Therefore, the system design and analysis call for the statistical modeling of range information and the algorithm design for ranging, localization and tracking. The main objectives of this thesis are: (i) the derivation of statistical models and (ii) the design of algorithms for different wireless localization systems, with particular regard to passive and semi-passive systems (i.e., active radar systems, passive radar systems, and radio frequency identification systems). Statistical models for the range information are derived, low-complexity algorithms with soft-decision and hard-decision are proposed, and several wideband localization systems have been analyzed. The research activity has been conducted also within the framework of different projects in collaboration with companies and other universities, and within a one-year-long research period at Massachusetts Institute of Technology, Cambridge, MA, USA. The analysis of system performance, the derived models, and the proposed algorithms are validated considering different case studies in realistic scenarios and also using the results obtained under the aforementioned projects.

Index

List of Acronyms

PFA probability of false alarm

PD probability of detection

ACK acknowledge

AOA angle-of-arrival

AWGN additive white Gaussian noise

BP band-pass

BPZF band-pass zonal filter

CDF cumulative distribution function

CDMA code division multiple access

CFAR constant false-alarm rate

CIR channel impulse response

CRB Cramèr-Rao bound

CRLB Cramèr-Rao lower bound

ED energy detector

EIRP Equivalent Isotropic Radiated Power

EKF extended Kalman filter

ESD energy-based soft-decision

FCC Federal Communications Commission

FDOA frequency difference-of-arrival

GPS Global Positioning System

HDSA high-definition situation-aware

i.i.d. independent, identically distributed

INR interference-to-noise ratio

IR-UWB impulse radio UWB

ISNR interference-plus-signal-to-noise-ratio

JBSF jump back and search forward

JSD Jensen–Shannon divergence

KF Kalman Filter

KLD Kullback-Leibler divergence

LE localization error

LEO localization error outage

LOS line-of-sight

LS least squares

LTE long term evolution

MAP maximum a posteriori probability

MB maximum bin

MBS maximum bin search

MF matched filter

MIMO multiple-input multiple-output

ML maximum likelihood

MLS maximum likelihood search

MSE mean squared error

MMSE minimum mean square error

MUI multi-user interference

MUR Multistatic radar

NA non-aided

NBI narrowband interference

NLOS non-line-of-sight

OFDM orthogonal frequency division multiplexing

OL obstruction loss

OLOS obstructed line-of-sight

OOA order of arrival

PDF probability distribution function

PDP power delay profile

PF particle filter

PMF probability mass function

PRF pulse repetition frequency

PRP pulse repetition period

PSD power spectral density

RADAR radar

RaDIAL radio detection, identification, and localization

RCS radar cross section

RF radiofrequency

RFID radio frequency identification

RMS root mean square

RMSE root-mean-square error

ROC receiver operating characteristic

RRC root raised cosine

RSS received signal strength

RSSI received signal strength indicator

RTLS real time locating systems

RTT round-trip time

RV random variable

SBS serial backward search

SEO speed error outage

SNR signal-to-noise ratio

SOO signals of opportunity

SR sensor radar

ST simple thresholding

TCS threshold crossing search

TEO tracking error outage

TDOA time difference-of-arrival

TNR threshold-to-noise ratio

TOA time-of-arrival

TOF time-of-flight

TSD threshold-based soft-decision

UHF ultra-high frequency

UWB ultra-wideband

WSN wireless sensor network

WSR wireless sensor radar

WSRN wireless sensor radar network

Chapter 1

Introduction

The evolution of communication and information technologies calls for systems that are increasingly distributed in an operating environment. The fifth generation of wireless systems envisages a large number of applications where sensors embedded in physical objects will be networked with people and other devices [1]. For example, the integration of Global Positioning System (GPS) and inertial sensors into cellular phones marked the beginning of a new era of ubiquitous context-awareness. Internet of things, ubiquitous computing, and autonomous logistic are emerging paradigms that follow this trend. Location inference is a prerequisite for context-awareness and enables a number of new important applications.

Localization and tracking are performed by wireless localization systems that infer the location of objects, devices, and persons—depending on the application—from the processing of wireless signals. The capability of wireless localization systems to operate in indoor and harsh propagation environments is still a challenge and triggers a fervent research activity worldwide. In fact, sub-meter localization accuracy in such conditions is a key enabler for a diverse set of applications: security tracking (the detection and localization of unauthorized persons in high-security areas), medical services (the monitoring of patients), rescue operations (the search for disaster victims in inaccessible areas), logistic (the tracking of goods in warehouses and management chains), and a large set of emerging wireless sensor network (WSN) applications. Nevertheless, the conventional techniques fail to provide satisfactory performance in many scenarios: GPS-based tracking is inaccurate in harsh environments (e.g., indoor and urban canyons) and inertial tracking is inaccurate in long-term operations due to velocity drift.

Depending on the application, the processing of wireless signals at different re-

ceivers allows to infer the position of transmitters, receivers, or others (e.g., devices, objects, or persons). A first classification of localization system can be done by distinguishing between active and passive targets, as well as between active and passive sources.

Active and Passive Target The wireless signals can be directly conveyed between objects (in unknown positions) and anchors (in known positions) or emitted by anchors and backscattered by objects the former is referred to as localization of active objects (tags), while the latter is referred to as localization of passive objects (targets).

A particular case of semi-passive target refers to radio frequency identification (RFID) based on backscatter modulation, which enables both localization and identification of tagged objects. In such a case, the reader is the only active device, thus with capability of transmitting, receiving, and processing the signals. Tags act as passive reflectors only; initially, they are in sleeping mode to save energy, then a wake-up signal is used for waking up all the tags present in the environment monitored by the reader.

Active and Passive Source The source that emits the signal can be active or passive depending on whether it belongs to the localization system or not, respectively. For example, the processing at different receivers of signals transmitted by non-collaborative sources, namely transmitters of opportunity, may be exploited to detect and localize the transmitter itself or a mobile receiver (e.g., passive network localization) or passive scatterers in the monitored environment (e.g., passive radar).

Localization systems with passive sources exploit transmitters of opportunity for stealth and low-cost navigation and tracking [2]. In general, the networked receiving-only nodes receive the signals of opportunity (SOO) directly from the non-collaborative sources or backscattered by the target. Several signal processing techniques are proposed in the literature to estimate the position of the target based on such received waveforms. For example, time difference-of-arrival (TDOA), frequency difference-of-arrival (FDOA) and angle-of-arrival (AOA) metrics are often adopted in this context since no synchronization is guaranteed between receivers and transmitters [3, 4].

Objectives and Dissemination

The main purposes of this thesis are the statistical modeling and algorithm development for design and analysis of different wireless localization systems, with particular

regard to semi-passive and passive systems.

The key contributions of the thesis are:

- derivation of a range information model for design and analysis of wideband ranging systems based on energy detection;
- development of low-complexity ranging algorithms with optimal energy detectors (EDs) for soft-decision and hard-decision localization;
- introduction of blind techniques for the selection of representative observations in sensor radars;
- proposal of a low-complexity scheme for localization in RFID systems based on backscatter modulation and design of Bayesian framework for estimating the order of arrival (OOA) of tagged objects;
- development of a methodology for design and analysis of sensor radars (SRs) by jointly considering (i) network setting, (ii) propagation environment, (iii) waveform processing, (iv) observation selection, and (v) localization algorithm;
- proposal of a Bayesian framework for the passive tracking and velocity estimation of moving targets based on LTE signals of opportunity;

The remainder of the thesis is organized as in the following.

Chapter 2 describes range-based location inference, with particular regard to indoor applications. The signal processing for localization and tracking is discussed and serves for a better understanding of the research activity.

Chapter 3 introduces a tractable model for the range information as a function of wireless environment, signal features, and energy detection techniques. Such a model serves as a cornerstone for the design and analysis of wideband ranging systems. Based on the proposed model, practical soft-decision and hard-decision algorithms are developed. A case study for ranging and localization systems operating in a wireless environment is presented. Sample-level simulations validate the theoretical results.

Chapter 4 presents blind techniques for the selection of representative observations gathered by SRs operating in harsh environments. A methodology for the design and analysis of SRs is developed taking into account the aforementioned impairments and observation selection techniques. Results are obtained for non-coherent ultra-wideband SRs in a typical indoor environment (with obstructions,

multipath, and clutter) to enable a clear understanding of how observation selection improves the localization accuracy.

Chapter 5 analyzes SRs accounting for waveform processing, tracking algorithm, and resource allocation among different task for inferring the position of moving targets. Performance of monostatic and multistatic ultra-wideband SRs with different settings is evaluated in a case study for indoor environments with obstacles, clutter, and multipath. Furthermore, a passive radar system is presented, which exploits long term evolution (LTE) base stations to detect and track moving targets in a monitored environment. Such a system is analyzed based on a Bayesian framework for detection of moving targets and estimation of their position and velocity. A case study is presented accounting for the LTE extended pedestrian model with various settings in terms of network configuration, wireless propagation, and signal processing.

Chapter 6 analyzes the detection of multiple tags employing ultra-wideband (UWB) backscatter modulation and proposes detection schemes that are robust to nonideal conditions. A case study is presented to evaluate the performance of the proposed technique for the detection of multiple tags based on impulsive backscattered signals. Furthermore, the application of such a system for high-accuracy order-of-arrival estimation of goods on conveyor belts is introduced. A tracking technique based on particle filtering is used for order-of-arrival estimation. Results for a case of study show accuracy of the proposed system for various settings.

The results presented in this thesis have been published in the proceedings of international conferences and journals indicated in the author's publication list. Several results have been obtained during a one-year-long research period at the Laboratory for Information and Decision Systems (LIDS) of the Massachusetts Institute of Technology, Cambridge, MA, USA. Furthermore, part of the research activity has been conducted within two research projects, namely SELECT (Smart and Efficient Location, idEntification and Cooperation Techniques) and GRETA (Green Tags). The scopes of the aforementioned projects is described in the following.

SELECT is an European project[1], whose main objectives are: (a) to develop new-generation UWB based, passive, low-cost tag that is compatible with UHF RFID standards; (b) to design an UWB Real Time Location System based on such tags offering up to 15 meters of operational range, with sub-meter location accuracy. The project requirements in terms of ranging accuracy (12 cm of ranging error at a

[1] www.selectwireless.eu

distance of 7.35 meters within 75% confidence) dictated the choice on technologies that have to be used to achieve these goals. Considering the required accuracy, it is necessary to use UWB-IR technology, since it is the only technology that offers the necessary precision level. Moreover, in order to satisfy the low-cost and low power consumption requirements, the tag cannot be equipped with a UWB transmitter, as done in current generation systems, therefore a backscattering modulation approach is adopted. For the sake of fully satisfying the visibility requirement, the tag has been improved with standard RFID UHF capabilities, so that the objects can be tagged with a single SELECT tag in order to be located and tracked when they are inside a SELECT-based facility and to be identified in a conventional UHF RFID system.

GRETA is an Italian project[2], whose main objective is to realize a demonstrator of a wireless ecological system for identification, tracking, and monitoring of mobile subjects adopting zero-power ultra-wide band (UWB) communication techniques, energy harvesting solutions and eco-compatible materials. First of all, the identification of reference applications, requirements and scenarios has lead to designate three possible field of interests: (i) eHealth, for biomedical and hospital scenarios; (ii) ICT for food, for the production and commercial distribution chain; and (iii) Logistic.

Two passive tag architectures (UWB-UHF stand alone tags, UWB as an add on of UHF Gen. 2 Standard tags and active reflector tags) based on UWB backscatter communication have been considered thanks to their extremely low energy consumption and the possibility to adopt energy harvesting techniques via UHF RF signals. In fact the energy necessary for communication is harvested from the interrogation signal, and no radio-frequency (RF) circuits such as amplifiers, oscillators, converters are required in the tag. Thus the main cause of energy consumption is the RF switch and the relative digital control logic, whereas the link budget is bounded only by the interrogator device power constraints. Both the selected architectures present interesting aspects: the high level of innovation for the former and the compatibility with previous standard for the latter. For these reasons both will be investigated by means of a modular approach. The two selected architectures have then been investigated from a communication and technological point-of-view.

[2]www.greentags.eu

Chapter 2

Range-based Localization and Tracking

Wireless localization systems estimate the position of objects based on prior knowledge and on observations (measurements) gathered by a network of sensors deployed in the environment. Figure 2.1 shows an example of network where a number of nodes in known positions (anchors) are employed to estimate the position of a node in unknown position (target or agent). The estimation of target's position is performed by processing the received signal at the different receiving nodes. If the target is dynamic and its trajectory is estimated (usually together with its speed), the system is referred to as tracking system.

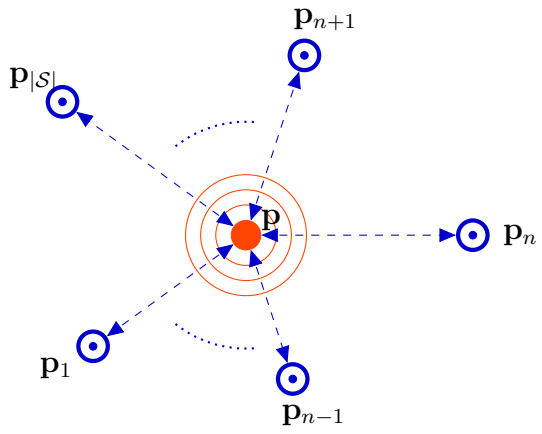

Figure 2.1: Example of a wireless localization system with the target at $\mathbf{p}$ and $|\mathcal{S}|$ nodes at $\mathbf{p}_1, \mathbf{p}_2, ..., \mathbf{p}_{|\mathcal{S}|}$.

The localization and tracking processes typically consist of two phases: (i) a **sensing phase**, during which nodes make measurements; and (ii) a **location inference phase**, during which target position is inferred using an algorithm that incorporates both prior knowledge and measurements. In this thesis, we consider also an **observation selection phase**, which is an intermediate phase where a subset of observations is selected and serves as input for the location inference phase.

2.1 Sensing Phase

Localization techniques can be classified based on measurements between nodes such as range-based, angle-based, and proximity-based. For instance, the position estimate can use an inertial measurement unit (IMU) and a range measurement unit (RMU). Localization accuracy strongly depends on the quality of the measurements, which are affected by impairments such as network topology, multipath propagation, environmental conditions, interference, noise, and clock drift.

Range-based systems (i.e., based on distance estimates) are more suitable for high-definition localization accuracy. In range-based localization, sensors provide range measurements whose reliability depends on the intrinsic properties of the network, such as the sensor positions and wireless medium [5].

Providing accurate ranging in harsh environments (such as indoors) is challenging primarily due to multipath, line-of-sight (LOS) blockage, and excess propagation delays through materials. In this context, time-of-arrival (TOA) estimation of wideband and UWB signals represent an endorsed solution thanks to the robustness to dense propagation environment and interference [6, 7]. In fact, wideband and UWB radios have a relative bandwidth larger than 20% or an absolute bandwidth larger than 500MHz and they offer benefits for both the communication and localization [8–10]. The bandwidth improves reliability and capability of signals to penetrate obstacles. Furthermore, the absolute bandwidth allows the design of high-resolution radars with higher accuracy of distance estimate with respect to more conventional techniques. UWB sensor networks have several application since they combine a good capacity of communication, low power consumption, and low costs enabling detection and localization for environmental monitoring [11]. UWB signals provide fine delay resolution, enabling precise TOA measurements for range estimation between two nodes.

However, the accuracy and reliability of range-based localization techniques typi-

cally degrade in cluttered environments, where multipath, LOS blockage, and excess propagation delays through materials lead to positively-biased range measurements. A method to mitigate such effects is to identify non-line-of-sight (NLOS) situations in a first phase, and consequently adapting localization algorithms in a second phase [12]. NLOS identification techniques are usually based on either distance estimates or characteristics of received waveforms such as delay spread, kurtosis, maximum amplitude (see in [13, 14] techniques and results based on experimentation).

The processing of TOA estimates and the design of techniques for impairments mitigation depend on the topology and configuration of the localization system. In the active case, the TOA estimates correspond to the time taken by the signal to propagate along the direct path from transmitter to receiver. In the passive case, the TOA estimate correspond to the time taken by the signal to propagate along the direct path from the transmitter to the target and the reflected path from the target to the receiver.

2.2 Location Inference Phase

Localization and tracking can be distinguished by considering the first as a static estimation problem (parameter estimation, where the parameter is the target's position) and the second as a dynamic estimation problem (state estimation, where the state is the target's trajectory and/or speed). The purpose of the localization and tracking algorithm is to provide an estimate of tags' position starting from TOA and/or AOA measurements provided by the receiver. From the algorithmic point of view, the estimate of the node position depends on measurements (observations) and prior knowledge.

The estimation of a static parameter can be done by following a Bayesian or non-Bayesian approach. In the first case, the target position $\mathbf{p}$ is considered as a random variable with an associated prior probability distribution function (PDF) $f(\mathbf{p})$. Therefore, a maximum a posteriori probability (MAP) estimator can be employed, where the posterior PDF $f(\mathbf{p}|\mathbf{z})$ is conditioned on the measurements $\mathbf{z}$ and the estimated position is

$$\hat{\mathbf{p}} = \underset{\tilde{\mathbf{p}}\in\mathcal{A}}{\operatorname{argmax}}\, f(\tilde{\mathbf{p}}|\mathbf{z}) = \underset{\tilde{\mathbf{p}}\in\mathcal{A}}{\operatorname{argmax}}\, f(\mathbf{z}|\tilde{\mathbf{p}}) f(\tilde{\mathbf{p}})\,. \tag{2.1}$$

where $\mathcal{A}$ is the locus of point representing the monitored area. In the second case,

the target position is considered as an unknown constant (nonrandom case) with no prior PDF associated. Therefore, a maximum likelihood (ML) estimator can be employed, where the likelihood function is the PDF $f(\mathbf{z}|\tilde{\mathbf{p}})$ of the measurements $\mathbf{z}$ conditioned on $\tilde{\mathbf{p}}$ and

$$\hat{\mathbf{p}} = \underset{\tilde{\mathbf{p}} \in \mathcal{A}}{\operatorname{argmax}} f(\mathbf{z}|\tilde{\mathbf{p}})\,. \tag{2.2}$$

The ML estimator under normal error distribution assumption converges to a least squares (LS) estimator.

The tracking process involves the estimation of position and velocity of the dynamic target. A dynamic system can be fully described by two models: the mobility model $g(\cdot)$, which relates the current state vector to the prior state vector, and the perception model $h(\cdot)$, which relates the observation data to the current state vector as

$$\mathbf{p}_n = g_n(\mathbf{p}_{n-1}, \mathbf{v}_{n-1}) \tag{2.3}$$

$$\mathbf{z}_n = h_n(\mathbf{p}_n, \mathbf{u}_n) \tag{2.4}$$

where $\mathbf{p}_n$ is the state vector at time t_n, $\mathbf{v}_n$ is the process noise vector, $\mathbf{z}_n$ is the measurements collected by sensors at time t_n, and $\mathbf{u}_n$ is the sensor noise. In general, these two equations are nonlinear. The state estimator, also referred to as filter, represents the recursive estimation of the state $\hat{\mathbf{p}}_n$ from the measurements $\mathbf{z}_{(1:n)} = \{\mathbf{z}_1, \mathbf{z}_2, \ldots, \mathbf{z}_n\}$ where $\mathbf{z}_m$ are the measurements obtained at the time indexed by m.

The Bayesian filters rely on the quantification of the posterior PDF, the positional belief, and require the PDF of the current state conditional on the previous state, and the PDF of the observation state conditional on the current state as [15]

$$f(\mathbf{p}_n|\mathbf{z}_1, ..., \mathbf{z}_n) = \frac{f(\mathbf{z}_n|\mathbf{p}_n) f(\mathbf{p}_n|\mathbf{z}_1, ..., \mathbf{z}_{n-1})}{f(\mathbf{z}_n|\mathbf{z}_{n-1})} = C\, f(\mathbf{z}_n|\mathbf{p}_n) f(\mathbf{p}_n|\mathbf{z}_1, ..., \mathbf{z}_{n-1}) \tag{2.5}$$

where C is a normalization constant. Different implementations of the posterior PDF lead to different state estimators. Here, we focus on Kalman Filter (KF) and particle filter (PF), which are largely adopted solutions.

Kalman Filter and Extended Kalman Filter When the mobility and perception models are linear, and noises are Gaussian distributed $\mathbf{v}_n \sim \mathcal{N}(0, \mathbf{Q}_n)$ and $\mathbf{u}_n \sim \mathcal{N}(0, \mathbf{R}_n)$ then the equations reduce to

$$\mathbf{p}_n = \mathbf{F}_n \mathbf{p}_n + \mathbf{v}_{n-1} \tag{2.6}$$

$$\mathbf{z}_n = \mathbf{H}_n \mathbf{p}_n + \mathbf{u}_n \tag{2.7}$$

where $\mathbf{F}_n$ and $\mathbf{H}_n$ are assumed known and named state evolution and measurement matrix, respectively. The KF represents the mathematical solution of this problem, where the prediction phase is given by

$$\begin{aligned} \hat{\mathbf{p}}_{n|n-1} &= \mathbf{F}_n \hat{\mathbf{p}}_{n-1|n-1} \\ \mathbf{P}_{n|n-1} &= \mathbf{F}_n \mathbf{P}_{n-1|n-1} \mathbf{F}_n^{\mathrm{T}} + \mathbf{Q}_n \end{aligned} \tag{2.8}$$

where $\hat{\mathbf{p}}_{n|n-1}$ and $\mathbf{P}_{n|n-1}$ are the a posteriori state and covariance estimates at time n given observations up to n. The update phase is given by

$$\begin{aligned} \hat{\mathbf{p}}_{n-1|n-1} &= \hat{\mathbf{p}}_{n|n-1} + \mathbf{K}_n \left(\mathbf{z}_n - \mathbf{H}_n \hat{\mathbf{p}}_{n|n-1} \right) \\ \mathbf{P}_{n-1|n-1} &= \left(\mathbf{I} - \mathbf{K}_n \mathbf{H}_n \right) \mathbf{P}_{n|n-1} \end{aligned} \tag{2.9}$$

where $\mathbf{K}_n$ is called Kalman gain and is given by

$$\mathbf{K}_n = \mathbf{P}_{n|n-1} \mathbf{H}_n^{\mathrm{T}} \left(\mathbf{H}_n \mathbf{P}_{n|n-1} \mathbf{H}_n^{\mathrm{T}} + \mathbf{R}_n \right)^{-1} . \tag{2.10}$$

The extended Kalman filter (EKF) is a version of the KF that allows non-linear mobility and perception models. In particular, when $g_n(\cdot)$ and $h_n(\cdot)$ are non-linear functions, the mobility and perception matrix are given by

$$\begin{aligned} \mathbf{F}_n &= \left. \frac{\partial g}{\partial \mathbf{p}} \right|_{\hat{\mathbf{p}}_{n|n}} \\ \mathbf{H}_n &= \left. \frac{\partial h}{\partial \mathbf{p}} \right|_{\hat{\mathbf{p}}_{n|n-1}} . \end{aligned} \tag{2.11}$$

Particle Filter The key idea of a PF is to represent the posterior distribution (the belief), by a set of random samples (particles) with associated weights as

$$p(\mathbf{p}_n | \mathbf{z}_1, ..., \mathbf{z}_n) \approx \sum_{i=1}^{N_{\mathrm{par}}} w_{n,i} \delta(\mathbf{p}_n - \mathbf{s}_{n,i}) \tag{2.12}$$

where N_{par} is the number of particles, $\delta(\cdot)$ is the Delta function, $w_{n,i} \geq 0 \ \forall n, i$ is the weight for particle i at time index n, and $\sum_{i=1}^{N_{\mathrm{par}}} w_{n,i} = 1$. The weights are chosen,

for example, using the principle of importance sampling in which a distribution of samples is considered with more dense samples where it is more probable that the object is located. The main important recursive steps for evaluating the ith particle can be summarized as follows

$$\mathbf{s}_{n,i} \sim p(\mathbf{p}_n|\mathbf{p}_{n-1}) \qquad \text{mobility model} \tag{2.13}$$

$$w_{n,i} = w_{n-1,i}\; p(\mathbf{z}_n|\mathbf{s}_{n,i}) \qquad \text{perception model}\,. \tag{2.14}$$

In case of a Gaussian mobility model, the (2.13) becomes

$$p(\mathbf{p}_n|\mathbf{p}_{n-1}) = \frac{1}{\sqrt{2\pi}\sigma_{\mathrm{m}}} e^{-\frac{\|\mathbf{p}_n - \boldsymbol{\mu}_n\|^2}{2\sigma_{\mathrm{m}}^2}} \tag{2.15}$$

where the standard deviation σ_{m} represents the uncertainty on the target movement, and the mean $\boldsymbol{\mu}_n$ depends on both $\mathbf{p}_{n-1}$ and intra-node measurements.
For N independent observations, the perception model in (2.14) is given by

$$p(\mathbf{z}_n|\mathbf{p}_n) = \prod_{i=1}^{N} p(\mathbf{z}_{n,i}|\mathbf{p}_n) \tag{2.16}$$

where $\mathbf{z}_{n,i}$ is the ith measurement at time index n. A perception model with Gaussian distribution is assumed. For example, if the measurement $\mathbf{z}_{n,i}$ is a distance measurement between the ith reader and the tracked tag, the perception model is given by

$$p(\mathbf{z}_{n,i}|\mathbf{p}_n) = \frac{1}{\sqrt{2\pi}\sigma_{\mathrm{p}}} e^{-\frac{\left(\mathbf{z}_{n,i} - \|\mathbf{p}_n - \mathbf{r}_i\|\right)^2}{2\sigma_{\mathrm{p}}^2}} \tag{2.17}$$

where $\mathbf{r}_i$ is the position of the ith reader. The standard deviation σ_{p} depends on both the accuracy of localization technology and signal propagation conditions.

2.3 Location Inference with Observation Selection

A set $\mathbf{z}$ of of N_{meas} observations collected in diverse spatiotemporal conditions is obtained for a target at $\mathbf{p}$. In inference theory, the presence of non-representative and biased observations (also known as non-representative outliers [16]) leads to inaccurate parameter estimation. Therefore, range estimates related to multipath, clutter, and signal obstructions degrade the accuracy of position estimation. Low-complexity techniques are proposed to select a subset $\mathbf{z}_{\mathrm{sel}}$ of $L \leq N_{\mathrm{meas}}$ elements

of the observation vector that contains representative observations for the target position estimation. Such selection techniques are based on signal features that can be extracted in blind conditions (i.e., without prior information). There are several algorithms that differ from how the nodes estimate and how the estimates are propagated in the network. The choice of the localization algorithm is driven by the trade-off between performance and complexity, as well as by prior knowledge of the environment.

The localization complexity in the presence of observation selection, $\mathcal{C}(L, N_{\text{meas}})$, is now determined, where L is the number of selected observations and N_{meas} is the total number of available observations. Such complexity is that of the localization algorithm when all observations available are used ($L = N_{\text{meas}}$), whereas it also depends on the complexity of feature evaluation and observation selection when a subset of the available observations is used.

For example, the estimation of target position via LS algorithm based on range measurements is a NP-hard problem with an exponential complexity on the number of observations $\mathcal{O}\left(N^m\right)$ [17]. In the following, $\mathcal{C}_\ell(N)$ denotes the complexity of the localization algorithm as a function of the number N of processed observations, which is $N = L$ with selection of representative observations and $N = N_{\text{means}}$ without selection. Therefore, the complexity for target localization without ($L = N_{\text{meas}}$) and with ($L < N_{\text{meas}}$) subset selection of representative observations is given by

$$\mathcal{C}(L, N_{\text{meas}}) = \begin{cases} \mathcal{C}_\ell(N_{\text{meas}}) & L = N_{\text{meas}} \\ \mathcal{C}_\ell(L) + \mathcal{C}_{\text{f}}(N_{\text{meas}}) + \mathcal{C}_{\text{s}}(N_{\text{meas}}) & L < N_{\text{meas}} \end{cases} \tag{2.18}$$

where $\mathcal{C}_{\text{f}}(N_{\text{meas}})$ is the complexity of feature evaluation and $\mathcal{C}_{\text{s}}(N_{\text{meas}})$ is the complexity of the observation selection (sorting). The term $\mathcal{C}_{\text{s}}(N_{\text{meas}})$ depends on the sorting algorithm used and is asymptotically quadratic in a worst case analysis $\mathcal{C}_{\text{s}}(N) = \mathcal{O}(N^2)$ [18]. When the term $\mathcal{C}_{\text{f}}(N_{\text{meas}})$ is a linear function with the number of observations, $\mathcal{O}(N_{\text{meas}})$, the comparison between the computational complexity of localization with and without observation selection depends on the complexity of the localization algorithm $\mathcal{C}_\ell(N)$. For example, $\mathcal{C}_\ell(N_{\text{meas}}) = \mathcal{O}\left(N_{\text{meas}}^m\right)$ in the case of a localization algorithm with complexity exponential on the number of observations. In such a case, the selection of representative observations enables significant savings in complexity with $m \geq 2$. A typical value for algorithms operating matrix inversion, such as LS, is $m = 3$.

Chapter 3

Wideband Ranging

Wideband ranging is a key enabler for emerging applications, such as logistic, safety, security, and military, relying on accurate location awareness [5, 19–26]. The localization accuracy of navigation and radar systems is affected by the quality of range information [27–36]. Range information such as range likelihood or range estimate can be extracted from the received signals for soft-decision or hard-decision localization, respectively [9, 37, 38]. The quality of range information depends on network intrinsic properties and signal processing techniques [12, 13, 39–43].

The design and analysis of ranging systems require models for describing range information as a function of the propagation environment, signal features, and detection techniques. A popular class of ranging techniques is based on energy detection, which determines the absence or presence of signals based on the level of energy collected over certain observation intervals [44]. The EDs have been employed in many contexts, including range estimation in positioning systems [45–47], spectrum sensing in cognitive radios [48], and carrier sensing in network access protocols [49, 50] owing to their low-complexity implementation. Energy detection was introduced in [44] to detect unknown deterministic signals in additive white Gaussian noise (AWGN) channels. More recently, the analysis has been extended to detection of random signals in AWGN channels [51–53], random signals in flat fading channels [54–56], and deterministic signals in the presence of interference [57, 58].

Classical ranging techniques based on energy detection provide hard-decision range estimates that are consonant with the TOA of the received signals. The lack of accurate models for range estimates in wireless propagation environments. The range estimate is often modeled as a Gaussian random variable [11, 59–61]. coerces the design of EDs to consider simplified assumptions such as AWGN channels. Such

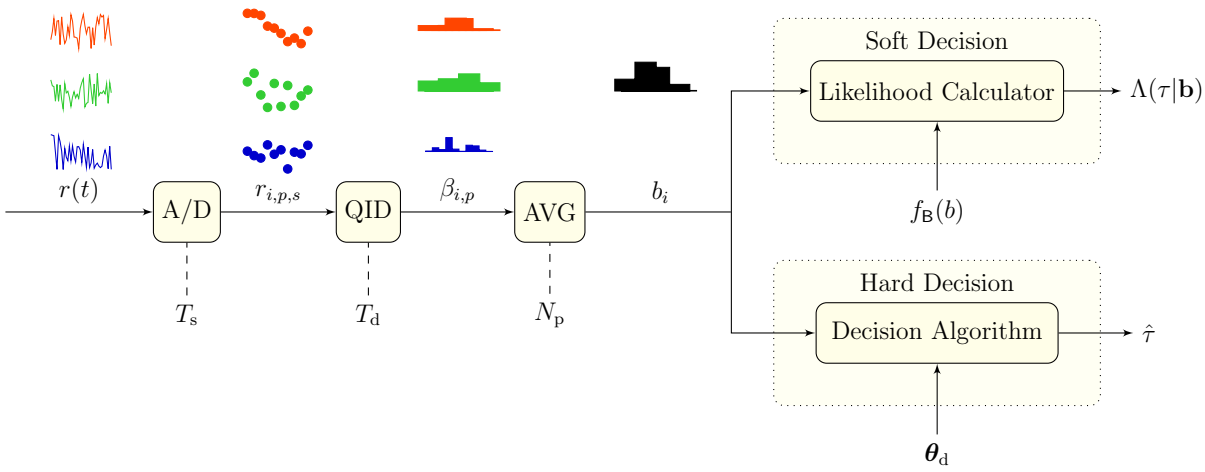

Figure 3.1: Soft-decision and hard-decision energy detection system.

assumptions do not account for multipath fading or obstructed propagation, leading to inaccurate ranging in wireless environments.

A mathematical model is derived, which describes the range information by providing range likelihood and range estimate for soft-decision and hard-decision localization, respectively. The goal is to establish a range information model that accounts for the wireless environment and signal features to facilitate the design and analysis of optimal EDs. The key contributions are as follows:

- Derivation of a range information model for design and analysis of wideband ranging systems based on energy detection;
- Development of low-complexity ranging algorithms with optimal EDs for soft-decision and hard-decision localization;
- Quantification of the benefits to location awareness provided by the proposed range information model in wireless environments.

Notation

For a random variable (RV) X, the x, $f_{\mathsf{X}}(\cdot)$, and $F_{\mathsf{X}}(\cdot)$ denote its realization, distribution function, and cumulative distribution function (CDF), respectively. Let $\mathsf{X} \sim \mathcal{N}(\mu, \sigma^2)$ denote a Gaussian distributed RV with mean μ and variance σ^2. Let $\phi(\cdot)$ and $\Phi(\cdot)$ denote the PDF and CDF of a standard Gaussian RV, respectively. The symbol $\lfloor x \rfloor$ denotes the largest integer less than or equal to x. Let $\mathbf{0}$ be the all-zero vector. The notation $\mathcal{E}^{\mathrm{c}}$ denotes the complement of an event $\mathcal{E}$.

3.1 Ranging System

This section describes the energy detection principle and formulates the statistical model for the energy samples at the ED's output.

3.1.1 Energy Detection

Consider a ranging system composed of a transmitter at position $\mathbf{p}_\mathrm{t}$ that emits N_p copies of a signal $s(t)$ with repetition period T_p, and a receiver at position $\mathbf{p}_\mathrm{r}$. Several techniques are available in the literature to estimate the repetition period of a signal when it is unknown, see e.g., [62]. The aim of the ranging system is to detect the signal $s(t)$ and to estimate its TOA τ with respect to a reference time t_0 from the received signal based on N_p observations each with duration T_obs. Range and TOA are used interchangeably throughout this dissertation since the former is a bijective function of the latter. The reference time t_0 can be the time at which the signal was transmitted (e.g., TOA-based localization or radar systems) or be the time shared among several receivers (e.g., TDOA-based localization systems).

For ranging techniques based on energy detection, energy samples (namely energy bins) are collected, one for each dwell time T_d. After band-pass filtering for noise reduction (and clutter mitigation in case of SR), the received waveforms are non-coherently accumulated for soft-decision and hard-decision processing as illustrated in Figure 3.8. The received signal can be written as

$$r(t) = u(t) + n(t) \tag{3.1}$$

where $u(t)$ is the received probe signal after propagating through a wireless channel with impulse response $h(t;\varsigma)$ and $n(t)$ is the thermal noise component. The received probe signal is a sequence of channel responses to the transmitted signal replicas, the first of which can be written as

$$u(t) = \int h(t;\varsigma)\, s(t-\varsigma)\, d\varsigma\,. \tag{3.2}$$

The received signal is first sampled by an analog-to-digital (A/D) converter with sampling period T_s. At the sampling instant $t_{i,p,s} = i\,T_\mathrm{d} + p\,T_\mathrm{p} + s\,T_\mathrm{s}$, with $i = 0, 1, \ldots, N_\mathrm{b} - 1$ and $p = 0, 1, \ldots, N_\mathrm{p} - 1$, the sample of the received signal is given by

$$r_{i,p,s} = r\left(t_{i,p,s}\right) = u_{i,p,s} + n_{i,p,s} \tag{3.3}$$

where $u_{i,p,s} = u\left(t_{i,p,s}\right)$ and $n_{i,p,s} = n\left(t_{i,p,s}\right)$. After A/D conversion, waveform samples are processed by a quadrature integrate and dump (QID) block that squares and integrates them over a dwell time T_d to obtain $N_\mathrm{b} = \lfloor T_\mathrm{obs}/T_\mathrm{d} \rfloor$ energy bins. The ith energy bin corresponding to the pth observation is given by

$$\beta_{i,p} = \sum_{s=0}^{N_\mathrm{sb}-1} r^2\left(t_{i,p,s}\right) = \sum_{s=0}^{N_\mathrm{sb}-1} \left(u_{i,p,s} + n_{i,p,s}\right)^2 \tag{3.4}$$

where $N_\mathrm{sb} = \lfloor T_\mathrm{d}/T_\mathrm{s} \rfloor$ is the number of signal samples per bin. The energy bins obtained from each observation interval are processed by an averaging (AVG) block over the N_p observations as

$$b_i = \frac{1}{N_\mathrm{p}} \sum_{p=0}^{N_\mathrm{p}-1} \beta_{i,p} \tag{3.5}$$

resulting in a vector of energy bins $\mathbf{b} = [\, b_0, b_1, \ldots, b_{N_\mathrm{b}-1} \,]$. The vector of energy bins at the output of the ED is used as input for soft-decision or hard-decision processing.

The detection of the signal $s(t)$ and the estimation of its TOA τ are based on the energy bin vector $\mathbf{b}$. Classical approaches follow the Bayesian hypothesis testing, involving the comparison of the energy bins with a threshold. Such a threshold is often chosen to achieve a constant false-alarm rate resulting in a certain misdetection rate.

Typically, ranging is based on hard-decision algorithms which provide the TOA estimate from the observed energy bins. If the distribution function of energy bins is known, then soft-decision algorithms can be conceived providing a posterior PDF of the TOA estimates. Models for soft-decision and hard-decision algorithms, which will be provided in Section 3.2, depend on the distribution of the energy samples given in the following.

3.1.2 Energy Samples

Each element b_i of the vector $\mathbf{b}$ is an instantiation of the RV

$$\mathsf{B}_i = \sum_{s=0}^{N_\mathrm{sb}-1} \mathsf{X}_{N_\mathrm{p}}^{(i,s)} \tag{3.6}$$

where

$$\mathsf{X}_n^{(i,s)} = \frac{1}{n} \sum_{p=0}^{n-1} \left(\mathsf{U}_{i,p,s} + \mathsf{N}_{i,p,s}\right)^2 \tag{3.7}$$

is the sample average, in p, of the energy bins. In particular, $\mathsf{U}_{i,p,s}$ and $\mathsf{N}_{i,p,s}$ are independent random samples of the received probe signal and of the thermal noise, respectively. Note that B_i depends on the transmitted signal, thermal noise, true TOA τ, wireless channel, and ED parameters. Let $\boldsymbol{\theta} = [\tau\ \boldsymbol{\theta}_\mathrm{h}\ \boldsymbol{\theta}_\mathrm{d}]$ where $\boldsymbol{\theta}_\mathrm{h}$ and $\boldsymbol{\theta}_\mathrm{d}$ are the vectors of parameters representing the wireless channel and the ED, respectively. The normalized bin $\mathsf{B}_i N_\mathrm{p}/\sigma^2$ conditioned on $\boldsymbol{\theta}$ is distributed as a noncentral chi-squared RV with $N_\mathrm{p}N_\mathrm{sb}$ degrees of freedom, i.e.,

$$\mathsf{B}_i \frac{N_\mathrm{p}}{\sigma^2} \overset{|\boldsymbol{\theta}}{\sim} \chi^2_{N_\mathrm{p}N_\mathrm{sb}}(\lambda_i) \tag{3.8}$$

where λ_i is the noncentrality parameter, which depends on $\boldsymbol{\theta}$, given by [44]

$$\lambda_i = \sum_{p=0}^{N_\mathrm{p}-1} \sum_{s=0}^{N_\mathrm{sb}-1} \frac{u^2_{i,p,s}}{\sigma^2} \tag{3.9}$$

with $u_{i,p,s}$ denoting the instantiation of the RV $\mathsf{U}_{i,p,s}$ and σ^2 denoting the variance of the zero-mean thermal noise. Therefore,

$$f_{\mathsf{B}_i}(b|\boldsymbol{\theta}) = \frac{N_\mathrm{p}}{2\sigma^2} e^{-\frac{bN_\mathrm{p}+\lambda_i\sigma^2}{2\sigma^2}} \left(\frac{bN_\mathrm{p}}{\lambda_i\sigma^2}\right)^{\frac{N_\mathrm{p}N_\mathrm{sb}-2}{4}} I_{\frac{N_\mathrm{p}N_\mathrm{sb}-2}{2}}\left(\sqrt{\frac{\lambda_i b N_\mathrm{p}}{\sigma^2}}\right) \tag{3.10}$$

$$F_{\mathsf{B}_i}(b|\boldsymbol{\theta}) = e^{-\frac{\lambda_i}{2}} \sum_{r=0}^{+\infty} \frac{(\lambda_i/2)^r}{r!} \frac{\gamma\left(\frac{N_\mathrm{p}N_\mathrm{sb}}{2}+r, \frac{bN_\mathrm{p}}{2\sigma^2}\right)}{\Gamma\left(\frac{N_\mathrm{p}N_\mathrm{sb}}{2}+r\right)} \tag{3.11}$$

where $I_a(\cdot)$ is the modified Bessel function of the first kind with order a, $\gamma(\cdot,\cdot)$ denotes the lower incomplete Gamma function, and $\Gamma(\cdot)$ denotes the Gamma function [63].

Remark 1. *In practice, the noise variance can be estimated by observing the energy bins in an absence of the transmitted signal and each λ_i depends on the wireless channel instantiation. Therefore, the derivation of the range estimation error distribution requires averaging the conditional energy bin distribution over all possible wireless channel instantiations [37].*

3.2 Range Information Model

This section offers the range information model by providing the range likelihood and the range estimate, as well as the range error.

3.2.1 Range Likelihood

The range likelihood function is determined from the observation b_i in (3.5) and the distribution of B_i for each energy bin, as shown in Figure 3.8. The RVs B_i's are independent and non-identically distributed with noncentrality parameter depending on $\boldsymbol{\theta}$. The range likelihood function for a given bins observation can be written as

$$\Lambda(\varsigma|\mathbf{b}) = \prod_{i=0}^{N_\mathrm{b}-1} f_{\mathsf{B}_i}(b_i|\varsigma, \boldsymbol{\theta}_\mathrm{h}, \boldsymbol{\theta}_\mathrm{d})\,. \tag{3.12}$$

Remark 2. *The range likelihood function can be used for both soft-decision and hard-decision localization. For soft-decision localization, a localization algorithm can directly process the likelihood functions obtained from one or more receivers to determine the position of a node. For hard-decision localization, a localization algorithm first obtains the TOA estimate by seeking a maximum of the range likelihood function, and then processes such estimates from one or more receivers to determine the position of a node.*

3.2.2 Range Estimate

A widely used approach for ranging is based on hard-decision algorithms that aim to determine the index $\hat{\imath}$ of the first bin containing a portion of the transmitted signal energy. Therefore, the index $\hat{\imath}$ can be thought as the instantiation of a discrete RV I taking value in the set $\mathcal{B} = \{0, 1, \ldots, N_\mathrm{b} - 1\}$.

Let the TOA estimate $\hat{\tau}$ be the instantiation of the RV T with PDF $f_\mathsf{T}(t|\boldsymbol{\theta})$.

The RV T depends on I since $\hat{\tau}$ is chosen from the interval $[\hat{\imath}\,T_\mathrm{d}, (\hat{\imath}+1)\,T_\mathrm{d})$. Consider a bijective function $\hat{\tau} = g(\hat{\imath})$, e.g., the TOA estimate is chosen to be the center of the interval as $g(\hat{\imath}) = \hat{\imath}\,T_\mathrm{d} + T_\mathrm{d}/2$. Therefore, the distribution function $f_\mathsf{T}(t|\boldsymbol{\theta})$ of the TOA estimate is determined by the distribution function $f_\mathsf{I}(i|\boldsymbol{\theta})$ of I. The $f_\mathsf{T}(t|\boldsymbol{\theta})$ depends on $\boldsymbol{\theta}$ since the RV I is a function of both the wireless channel and the ED.

Various hard-decision algorithms have been proposed in the literature [29,37,64]. The most popular hard-decision algorithms are analyzed: threshold crossing search (TCS), maximum bin search (MBS), jump back and search forward (JBSF), and serial backward search (SBS) algorithms. These algorithms involve the comparison of each bin value with a corresponding threshold. Let the threshold crossing event be $\mathcal{C}_\mathrm{th} = \{\exists i \in \mathcal{B} : \mathsf{B}_i > \xi_i\}$ where ξ_i is the threshold for the bin B_i for $i \in \mathcal{B}$. The probability mass function (PMF) of the selected bin index I conditioned on $\mathcal{C}_\mathrm{th}$ and

$$f_{\mathsf{I}}(i|\boldsymbol{\theta}) = \Big[1 - F_{\mathsf{B}_i}(\xi_i|\boldsymbol{\theta})\Big] \prod_{j\in\mathcal{I}_i(i)} F_{\mathsf{B}_j}(\xi_j|\boldsymbol{\theta}) \Big[1 - \prod_{n\in\mathcal{B}} F_{\mathsf{B}_n}(\xi_n|\boldsymbol{\theta})\Big]^{-1} \tag{3.16}$$

$$\begin{aligned} f_{\mathsf{I}}(i|\boldsymbol{\theta}) = &\Big[\int_0^{+\infty} \prod_{j\in\mathcal{B}\setminus\{i\}} F_{\mathsf{B}_j}(b|\boldsymbol{\theta})\, f_{\mathsf{B}_i}(b|\boldsymbol{\theta})\, db - \int_0^{\xi_i} \prod_{j\in\mathcal{B}\setminus\{i\}} F_{\mathsf{B}_j}(\breve{\xi}_j(b)|\boldsymbol{\theta})\, f_{\mathsf{B}_i}(b|\boldsymbol{\theta})\, db\Big] \\ &\times \Big[1 - \prod_{n\in\mathcal{B}} F_{\mathsf{B}_n}(\xi_n|\boldsymbol{\theta})\Big]^{-1} \end{aligned} \tag{3.19}$$

$$\begin{aligned} f_{\mathsf{I}}(i|\boldsymbol{\theta}) = &\Big[\int_0^{+\infty} \prod_{j\in\mathcal{I}_{N_\mathrm{w}}(i)} F_{\mathsf{B}_j}(\breve{\xi}_j(b)|\boldsymbol{\theta}) \prod_{j\in\mathcal{I}^{\mathrm{c}}_{N_\mathrm{w}}(i)\setminus\{i\}} F_{\mathsf{B}_j}(b|\boldsymbol{\theta})\, f_{\mathsf{B}_i}(b|\boldsymbol{\theta})\, db \\ &- \int_0^{\xi_i} \prod_{j\in\mathcal{B}\setminus\{i\}} F_{\mathsf{B}_j}(\breve{\xi}_j(b)|\boldsymbol{\theta})\, f_{\mathsf{B}_i}(b|\boldsymbol{\theta})\, db \\ &+ \sum_{m\in\mathcal{I}_{N_\mathrm{w}}(i+N_\mathrm{w}+1)} \int_{\xi_i}^{+\infty} \prod_{j\in\mathcal{I}_{i-m+N_\mathrm{w}}(i)} F_{\mathsf{B}_j}(\breve{\xi}_j(b)|\boldsymbol{\theta}) \left[F_{\mathsf{B}_i}(b|\boldsymbol{\theta}) - F_{\mathsf{B}_i}(\xi_i|\boldsymbol{\theta})\right] \\ &\times \prod_{j\in\mathcal{I}^{\mathrm{c}}_{i-m+N_\mathrm{w}}(i)\setminus\{i,m\}} F_{\mathsf{B}_j}(b|\boldsymbol{\theta})\, f_{\mathsf{B}_m}(b|\boldsymbol{\theta})\, db\Big] \Big[1 - \prod_{n\in\mathcal{B}} F_{\mathsf{B}_n}(\xi_n|\boldsymbol{\theta})\Big]^{-1} \end{aligned} \tag{3.23}$$

$$\begin{aligned} f_{\mathsf{I}}(i|\boldsymbol{\theta}) = &\Big[\int_0^{+\infty} \breve{F}_{\mathsf{B}_{i-1}}(\breve{\xi}_{i-1}(b)|\boldsymbol{\theta}) \prod_{j\in\mathcal{B}\setminus\{i-1,i\}} F_{\mathsf{B}_j}(b|\boldsymbol{\theta}) f_{\mathsf{B}_i}(b|\boldsymbol{\theta})\, db \\ &- \int_0^{\xi_i} \prod_{j\in\mathcal{B}\setminus\{i\}} F_{\mathsf{B}_j}(\breve{\xi}_j(b)|\boldsymbol{\theta})\, f_{\mathsf{B}_i}(b|\boldsymbol{\theta})\, db \\ &+ \sum_{m\in\mathcal{I}_{N_\mathrm{b}-i-1}(N_\mathrm{b})} \int_{\breve{\xi}_{m,i}}^{+\infty} \breve{F}_{\mathsf{B}_{i-1}}(\breve{\xi}_{i-1}(b)|\boldsymbol{\theta}) \prod_{j\in\mathcal{I}_{m-i}(m)} \left[F_{\mathsf{B}_j}(b|\boldsymbol{\theta}) - F_{\mathsf{B}_j}(\xi_j|\boldsymbol{\theta})\right] \\ &\times \prod_{j\in\mathcal{I}^{\mathrm{c}}_{m-i}(m)\setminus\{i-1,m\}} F_{\mathsf{B}_j}(b|\boldsymbol{\theta})\, f_{\mathsf{B}_m}(b|\boldsymbol{\theta})\, db\Big] \Big[1 - \prod_{n\in\mathcal{B}} F_{\mathsf{B}_n}(\xi_n|\boldsymbol{\theta})\Big]^{-1} \end{aligned} \tag{3.26}$$

$\boldsymbol{\theta}$ can be written as

$$f_{\mathsf{I}}(i|\boldsymbol{\theta}) = \mathbb{P}\left\{\mathcal{S}_i \cap \mathcal{C}_{\mathrm{th}}|\boldsymbol{\theta}\right\} / \mathbb{P}\left\{\mathcal{C}_{\mathrm{th}}|\boldsymbol{\theta}\right\} \tag{3.12}$$

where the event $\mathcal{S}_i \cap \mathcal{C}_{\mathrm{th}}|\boldsymbol{\theta} = \{i \text{ is selected}, \mathcal{C}_{\mathrm{th}}|\boldsymbol{\theta}\}$ and

$$\mathbb{P}\left\{\mathcal{C}_{\mathrm{th}}|\boldsymbol{\theta}\right\} = 1 - \prod_{n\in\mathcal{B}} F_{\mathsf{B}_n}(\xi_n|\boldsymbol{\theta})\,. \tag{3.13}$$

For brevity, $f_{\mathsf{I}}(i|\boldsymbol{\theta})$ will be used to denote $f_{\mathsf{I}}(i|\mathcal{C}_{\mathrm{th}}, \boldsymbol{\theta})$.

Remark 3. *In general, a different threshold ξ_i can be used for each bin index i when it is important to account for the variation among the energy samples.*

Threshold Crossing Search

The TCS algorithm first searches for each bin value b_i that crosses a threshold ξ_i for all $i \in \mathcal{B}$. The algorithm then selects, if $\mathcal{C}_{\text{th}}$ occurs, the bin index $\hat{\imath}$ as the smallest i for which $b_i > \xi_i$. Mathematically,

$$\hat{\imath} \overset{|\mathcal{C}_{\text{th}}}{=} \min\{i \in \mathcal{B} | b_i > \xi_i\} \,. \tag{3.14}$$

The PMF of the selected bin index I conditioned on $\mathcal{C}_{\text{th}}$ and $\boldsymbol{\theta}$ is given by (3.12) with event

$$\mathcal{S}_i \cap \mathcal{C}_{\text{th}} | \boldsymbol{\theta} = \{\mathsf{B}_j \leq \xi_j \, \forall j \in \mathcal{I}_i(i), \mathsf{B}_i > \xi_i | \boldsymbol{\theta}\} \,. \tag{3.15}$$

The index set $\mathcal{I}_{N_{\text{w}}}(m)$ is defined as $\mathcal{I}_{N_{\text{w}}}(m) = \mathcal{B} \cap \{m - N_{\text{w}}, m - N_{\text{w}} + 1, \ldots, m - 1\}$ and its complement over $\mathcal{B}$ as $\mathcal{I}^{\text{c}}_{N_{\text{w}}}(m) = \mathcal{B} \backslash \mathcal{I}_{N_{\text{w}}}(m)$. The set $\mathcal{I}_{N_{\text{w}}}(m)$ is empty for $N_{\text{w}} \leq 0$. This leads to (3.16) shown at the top of the page. The choice of the thresholds ξ_i's affects the accuracy of the TOA estimation, as well as the detection rate and the false-alarm rate.

Maximum Bin Search

The MBS algorithm first searches for the maximum value among all the bins with index $i \in \mathcal{B}$. The algorithm then selects, if $\mathcal{C}_{\text{th}}$ occurs, the bin index $\hat{\imath}$ as the i for which $b_j \leq b_i$ for all $j \neq i$. Mathematically,

$$\hat{\imath} \overset{|\mathcal{C}_{\text{th}}}{=} \underset{i \in \mathcal{B}}{\text{argmax}} \; b_i \,. \tag{3.17}$$

The PMF of the selected bin index I conditioned on $\mathcal{C}_{\text{th}}$ and $\boldsymbol{\theta}$ is given by (3.12) with event

$$\begin{aligned} \mathcal{S}_i \cap \mathcal{C}_{\text{th}} | \boldsymbol{\theta} &= \{i \text{ is selected, } i \text{ is the max, } \mathcal{C}_{\text{th}} | \boldsymbol{\theta}\} \\ &= \{\mathsf{B}_j \leq \mathsf{B}_i \, \forall j \in \mathcal{B} \backslash \{i\} | \boldsymbol{\theta}\} \\ &\quad \backslash \{\mathsf{B}_j \leq \xi_j \, \forall j \in \mathcal{B}, \mathsf{B}_j \leq \mathsf{B}_i \, \forall j \in \mathcal{B} \backslash \{i\} | \boldsymbol{\theta}\} \,. \end{aligned} \tag{3.18}$$

This leads to (3.19) shown at the top of the page, with $\breve{\xi}_j(b) = \min\{\xi_j, b\}$. Note that MBS with thresholds $\xi_j = 0 \, \forall j \in \mathcal{B}$ corresponds to MBS unconditioned on $\mathcal{C}_{\text{th}}$

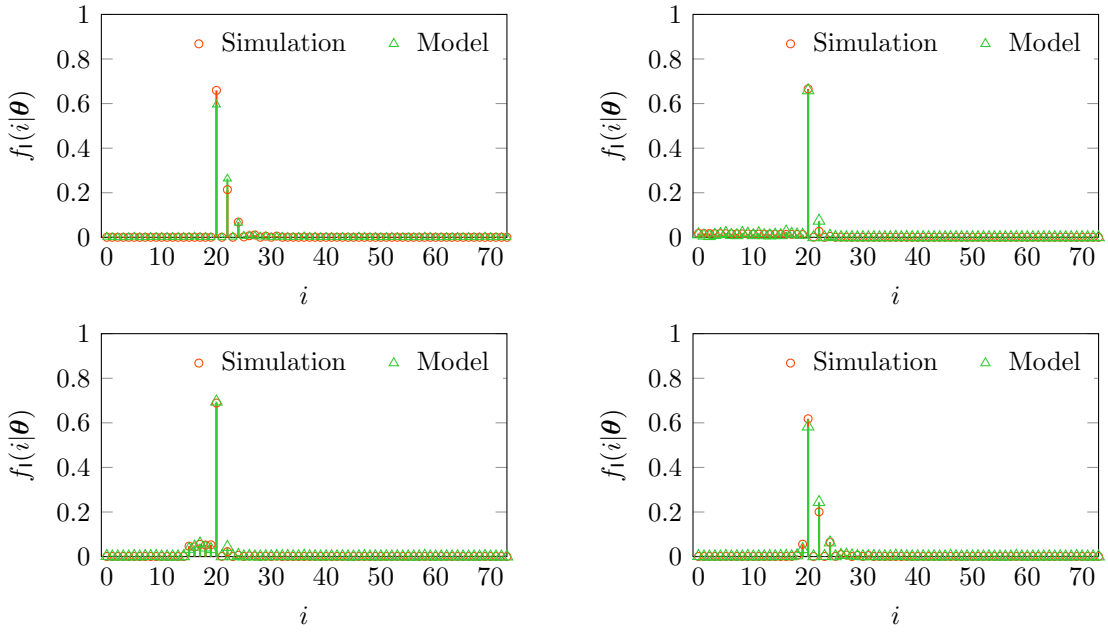

Figure 3.2: Example PMF of the selected bin index for the TCS (top left), MBS (top right), JBSF with $N_{\mathrm{w}} = 5$ (bottom left), and SBS (bottom right) algorithms with $T_{\mathrm{d}} = 2\,\mathrm{ns}$, $N_{\mathrm{p}} = 128$, and $\gamma = -10\,\mathrm{dB}$. The first bin containing the transmitted signal has index $i = 20$.

(i.e., selecting the maximum bin even when none of the bins crosses its threshold). In such a case, (3.19) degenerates to the PMF of the selected bin index for MBS unconditioned on $\mathcal{C}_{\mathrm{th}}$, which is given by

$$f_{\mathsf{I}}(i|\boldsymbol{\theta}) = \int_0^{+\infty} \prod_{j \in \mathcal{B}\setminus\{i\}} F_{\mathsf{B}_j}(b|\boldsymbol{\theta})\, f_{\mathsf{B}_i}(b|\boldsymbol{\theta})\, db\,.$$

Jump Back and Search Forward

The JBSF algorithm first identifies the index m corresponding to the maximum bin value, jumps back to the bin with smallest index in $\mathcal{I}_{N_{\mathrm{w}}}(m)$, and searches forward for each bin value b_i that crosses a threshold ξ_i for all $i \in \mathcal{I}_{N_{\mathrm{w}}}(m)$. Here N_{w} denotes the window length. For example, the window length N_{w} can be chosen according to the channel delay spread and the transmitted signal. The algorithm then selects, if $\mathcal{C}_{\mathrm{th}}$ occurs, the bin index $\hat{\imath}$ as the smallest i for which $b_i > \xi_i$ or as m if none of them crosses the threshold. Mathematically,

$$\hat{\imath} \overset{|\mathcal{C}_{\mathrm{th}}}{=} \min\{\{i \in \mathcal{I}_{N_{\mathrm{w}}}(m) | b_i > \xi_i\} \cup \{m\}\}\,. \tag{3.20}$$

The PMF of the selected bin index I conditioned on $\mathcal{C}_{\text{th}}$ and $\boldsymbol{\theta}$ is given by (3.12) with events

$$\mathcal{S}_i \cap \mathcal{C}_{\text{th}}|\boldsymbol{\theta} = \mathcal{M}_i|\boldsymbol{\theta} \cup \mathcal{M}_i^{\text{c}}|\boldsymbol{\theta} \tag{3.21a}$$

$$\mathcal{M}_i|\boldsymbol{\theta} = \{i \text{ is selected, } i \text{ is the max, } \mathcal{C}_{\text{th}}|\boldsymbol{\theta}\} \tag{3.21b}$$

$$\mathcal{M}_i^{\text{c}}|\boldsymbol{\theta} = \{i \text{ is selected, } i \text{ is not the max, } \mathcal{C}_{\text{th}}|\boldsymbol{\theta}\}\,. \tag{3.21c}$$

In particular,

$$\begin{aligned}\mathcal{M}_i|\boldsymbol{\theta} = \{&\mathsf{B}_j \le \xi_j\,\forall j \in \mathcal{I}_{N_{\text{w}}}(i), \mathsf{B}_j \le \mathsf{B}_i\,\forall j \in \mathcal{B}\backslash\{i\}|\boldsymbol{\theta}\} \\ &\backslash\{\mathsf{B}_j \le \xi_j\,\forall j \in \mathcal{B}, \mathsf{B}_j \le \mathsf{B}_i\,\forall j \in \mathcal{B}\backslash\{i\}|\boldsymbol{\theta}\}\end{aligned} \tag{3.22a}$$

$$\begin{aligned}\mathcal{M}_i^{\text{c}}|\boldsymbol{\theta} = \bigcup_{m\in\mathcal{I}_{N_{\text{w}}}(i+N_{\text{w}}+1)} &\{\mathsf{B}_j \le \xi_j\,\forall j \in \mathcal{I}_{i-m+N_{\text{w}}}(i), \\ &\mathsf{B}_i > \xi_i, \mathsf{B}_j \le \mathsf{B}_m\,\forall j \in \mathcal{B}\backslash\{m\}|\boldsymbol{\theta}\}\,.\end{aligned} \tag{3.22b}$$

This leads to (3.23) shown at the top of previous page. The product is equal to 1 and the sum is equal to 0 if evaluated over an empty index set. Note that JBSF with $N_{\text{w}} = 0$ corresponds to MBS. In such a case, (3.23) degenerates to (3.19).

Serial Backward Search

The SBS algorithm first identifies the index m corresponding to the maximum bin value, and searches backward for each bin value b_i that crosses a threshold ξ_i for all $i \in \mathcal{I}_m(m)$. The algorithm then selects, if $\mathcal{C}_{\text{th}}$ occurs, the bin index $\hat{\imath}$ as the the smallest i for which $b_j > \xi_j$ for all $j \in \mathcal{I}_{m-i}(m)$ or as m if none of them crosses the threshold. Mathematically,

$$\hat{\imath} \overset{|\mathcal{C}_{\text{th}}}{=} \min\{\{i \in \mathcal{I}_m(m)|b_j > \xi_j\,\forall j \in \mathcal{I}_{m-i}(m)\} \cup \{m\}\}\,. \tag{3.24}$$

The PMF of the selected bin index I conditioned on $\mathcal{C}_{\text{th}}$ and $\boldsymbol{\theta}$ is given by (3.12) with the events as in (3.21). In particular,

$$\begin{aligned}\mathcal{M}_i|\boldsymbol{\theta} = \{&\mathsf{B}_{i-1} \le \xi_{i-1} \text{ if } i > 0, \mathsf{B}_j \le \mathsf{B}_i\,\forall j \in \mathcal{B}\backslash\{i\}|\boldsymbol{\theta}\} \\ &\backslash\{\mathsf{B}_j \le \xi_j\,\forall j \in \mathcal{B}, \mathsf{B}_j \le \mathsf{B}_i\,\forall j \in \mathcal{B}\backslash\{i\}|\boldsymbol{\theta}\}\end{aligned} \tag{3.25a}$$

$$\begin{aligned}\mathcal{M}_i^{\text{c}}|\boldsymbol{\theta} = \bigcup_{m\in\mathcal{I}_{N_{\text{b}}-i-1}(N_{\text{b}})} &\{\mathsf{B}_{i-1} \le \xi_{i-1} \text{ if } i > 0, \\ &\mathsf{B}_j > \xi_j\,\forall j \in \mathcal{I}_{m-i}(m), \mathsf{B}_j \le \mathsf{B}_m\,\forall j \in \mathcal{B}\backslash\{m\}|\boldsymbol{\theta}\}\,.\end{aligned} \tag{3.25b}$$

This leads to (3.26) shown at the top of previous page, with

$$\breve{F}_{\mathsf{B}_k}(\cdot|\boldsymbol{\theta}) = \begin{cases} F_{\mathsf{B}_k}(\cdot|\boldsymbol{\theta}) & \text{for } k \in \mathcal{B} \\ 1 & \text{for } k \notin \mathcal{B} \end{cases}$$

and $\breve{\xi}_{m,i} = \max\{\xi_j \, \forall j \in \mathcal{I}_{m-i}(m)\}$.

To illustrate how the hard-decision algorithms operate, consider a simple case of $N_\mathrm{b} = 8$ bins (i.e., $\mathcal{B} = \{0, 1, \ldots, 7\}$) with a vector of bin instantiations and a vector of thresholds given by

$$\mathbf{b} = [0.8, 1.2, 1.3, 2.3, 2.5, 2.8, 2.4, 1.2]$$
$$\boldsymbol{\xi} = [1.3, 1.1, 0.9, 2.5, 1.4, 2.9, 1.9, 1.4]\,.$$

Note that the threshold crossing event is true (bins with index $1, 2, 4$, and 6 cross the corresponding thresholds) and the algorithms select a bin index $\hat{\imath}$ according to (3.14), (3.17), (3.20), and (3.24). In particular, $\hat{\imath} = 1, 5, 2$, and 4 for TCS, MBS, JBSF with $N_\mathrm{w} = 3$, and SBS, respectively.

Remark 4. *Recall that the PMFs $f_{\mathsf{I}}(i|\boldsymbol{\theta})$ for hard-decision algorithms derived above are conditioned on the threshold crossing event $\mathcal{C}_{th}$ and $\boldsymbol{\theta}$. Expressions for the joint PMF of I and $\mathcal{C}_{th}$ conditioned on $\boldsymbol{\theta}$ can be obtained by $\breve{f}_{\mathsf{I}}(i|\boldsymbol{\theta}) = f_{\mathsf{I}}(i|\boldsymbol{\theta}) \left[1 - \prod_{n\in\mathcal{B}} F_{\mathsf{B}_n}(\xi_n|\boldsymbol{\theta})\right]$. The distribution $f_{\mathsf{I}}(i|\boldsymbol{\theta})$ of the selected bin index for numerous other hard-decision algorithms can be derived following a similar approach.*

Figure 3.2 shows examples of PMF $f_{\mathsf{I}}(i|\boldsymbol{\theta})$ for the TCS, MBS, JBSF with $N_\mathrm{w} = 5$, and SBS algorithms with $T_\mathrm{d} = 2$ns, $N_\mathrm{p} = 128$, and $\gamma = -10$dB, according to the IEEE 802.15.4a standard for indoor propagation [65]. It can be observed that the PMFs derived based on the proposed range information model are in agreement with those obtained through sample-level simulations (i.e., simulating the wireless channel and the ED operation). In particular, theory and simulations show the same bin index for which the PMF reaches its maximum value.

3.2.3 Range Error

The distribution of the TOA estimation error is now determined, which depends on the particular hard-decision algorithm. The TOA estimation error $e(\tau) = \hat{\tau} - \tau$ is an instantiation of the RV $\mathsf{E} = \mathsf{T} - \tau$, and thus

$$f_{\mathsf{E}}(e|\boldsymbol{\theta}) = f_{\mathsf{T}}(e + \tau|\boldsymbol{\theta})\,. \tag{3.26}$$

For a given τ, E belongs to a finite set $\mathcal{E}_\tau = \{\mathsf{T} - \tau \text{ s.t. } \mathsf{T} \in g(\mathcal{B})\}$, where $g(\mathcal{B})$ represents a finite set of TOA estimate. In the absence of a prior information on the true TOA, τ can be modeled as a uniform RV over the interval $[0, T_\mathrm{a}]$, where T_a is the maximum possible TOA that depends on the wireless environment. This results in $\mathcal{E}_\tau = [-T_\mathrm{a}, T_\mathrm{obs}]$ with, in general, $0 < T_\mathrm{a} \leq T_\mathrm{obs}$. When the wireless environment is not known, T_a can be chosen as $T_\mathrm{a} = T_\mathrm{obs}$. Therefore,

$$f_{\mathsf{E}}(e|\boldsymbol{\theta}_\mathrm{d}) = \frac{1}{T_\mathrm{a}} \int_0^{T_\mathrm{a}} f_{\mathsf{E}}(e|\boldsymbol{\theta}_\mathrm{d}, \tau)\, d\tau \tag{3.27}$$

where

$$f_{\mathsf{E}}(e|\boldsymbol{\theta}_\mathrm{d}, \tau) = \begin{cases} \left|\frac{d\, g^{-1}(e+\tau)}{d\, e}\right| \; f_{\mathsf{I}}(g^{-1}(e+\tau)|\boldsymbol{\theta}_\mathrm{d}, \tau) & \text{for } e \in \mathcal{E}_\tau \\ 0 & \text{otherwise} \end{cases} \tag{3.28}$$

with $f_{\mathsf{I}}(i|\boldsymbol{\theta}_\mathrm{d}, \tau) = \mathbb{E}_{\boldsymbol{\theta}_\mathrm{h}}\{f_{\mathsf{I}}(i|\boldsymbol{\theta})\}$. For specific hard-decision algorithms, (3.28) can be evaluated by substituting the PDF and CDF of B_i given respectively by (3.10) and (3.11) into the specific conditional PMF $f_{\mathsf{I}}(i|\boldsymbol{\theta})$ derived in Section 3.2.2 and taking the expectation over the vector of noncentrality parameters $\boldsymbol{\lambda} = [\lambda_0, \lambda_1, \ldots, \lambda_{N_\mathrm{b}-1}]$.

Remark 5. *The distribution of the TOA estimate requires both the evaluation of cumbersome expressions and the expectation over all the channel parameters. This calls for a tractable range information model.*

3.3 Tractable Range Information Model

The design of soft-decision and hard-decision algorithms demands tractable expressions for the range information model, which can be obtained by simplifying $f_{\mathsf{B}_j}(b|\boldsymbol{\theta})$ and $F_{\mathsf{B}_j}(b|\boldsymbol{\theta})$. First, recall that the chi-squared RV converges in distribution to a Gaussian RV as the number of degrees of freedom increases. Therefore $\mathsf{B}_i N_\mathrm{p}/\sigma^2$ in (3.8) converges in distribution as

$$\mathsf{B}_i \frac{N_\mathrm{p}}{\sigma^2} \xrightarrow{\mathrm{d}} \tilde{\mathsf{B}}_i \frac{N_\mathrm{p}}{\sigma^2} \overset{|\boldsymbol{\theta}}{\sim} \mathcal{N}(N_\mathrm{p}N_\mathrm{sb} + \lambda_i, 2(N_\mathrm{p}N_\mathrm{sb} + 2\lambda_i)) \tag{3.29}$$

and consequently

$$f_{\mathsf{B}_i}(b|\boldsymbol{\theta}) \simeq \frac{N_\mathrm{p}/\sigma^2}{\sqrt{2(N_\mathrm{p}N_\mathrm{sb} + 2\lambda_i)}}\, \phi\left(\frac{bN_\mathrm{p}/\sigma^2 - N_\mathrm{p}N_\mathrm{sb} - \lambda_i}{\sqrt{2(N_\mathrm{p}N_\mathrm{sb} + 2\lambda_i)}}\right) \tag{3.30}$$

$$F_{\mathsf{B}_i}(b|\boldsymbol{\theta}) \simeq \Phi\left(\frac{bN_\mathrm{p}/\sigma^2 - N_\mathrm{p}N_\mathrm{sb} - \lambda_i}{\sqrt{2(N_\mathrm{p}N_\mathrm{sb} + 2\lambda_i)}}\right). \tag{3.31}$$

The above approximation depends on $N_\mathrm{p}\,N_\mathrm{sb}$ and is accurate for $N_\mathrm{p} \gg 1$ or $T_\mathrm{d} \gg T_\mathrm{s}$. Note that the above distributions depend on the instantiation of the wireless channel through $\boldsymbol{\theta}_\mathrm{h}$ in $\boldsymbol{\theta}$. However, the knowledge of the exact channel instantiation is typically not available.

The range information model is further simplified by considering distributions that depend on channel statistics rather than channel instantiations, i.e., on $\overline{\boldsymbol{\theta}} = [\tau\ \overline{\boldsymbol{\theta}}_\mathrm{h}\ \boldsymbol{\theta}_\mathrm{d}]$ instead of $\boldsymbol{\theta}$, where $\overline{\boldsymbol{\theta}}_\mathrm{h}$ represents the channel statistics. Recall that the sample average $\mathsf{X}_n^{(i,s)}$ in (3.7) depends on $[\tau\ \boldsymbol{\theta}_\mathrm{h}\ \boldsymbol{\theta}_\mathrm{d}]$ through $\mathsf{U}_{i,p,s}$ and on $\boldsymbol{\theta}_\mathrm{d}$ through $\mathsf{N}_{i,p,s}$. Therefore we approximate $\mathsf{X}_n^{(i,s)}$ with $\mathsf{Y}_n^{(i,s)}$ in which $\mathsf{U}_{i,p,s}$ is replaced with a deterministic quantity $U_{i,s}$ that depends on $\overline{\boldsymbol{\theta}}$ as

$$\mathsf{Y}_n^{(i,s)} = \frac{1}{n}\sum_{p=0}^{n-1}\left(U_{i,s} + \mathsf{N}_{i,p,s}\right)^2 . \tag{3.32}$$

A possible choice is $U_{i,s} = \mathbb{E}\left\{\mathsf{U}^\nu\right\}^{1/\nu}$, where $\mathbb{E}\left\{\mathsf{U}^\nu\right\}$ is the νth order moment of U, which is consistent in terms of the unit measure of $U_{i,s}$ and $\mathsf{N}_{i,p,s}$. Also, $\mathbb{E}\left\{\mathsf{U}^\nu\right\}^{1/\nu}$ is monotonically increasing in ν by Lyapunov's inequality. The choice of $U_{i,s}$ is motivated by the following lemma.

Lemma 1. *The sample average* $\mathsf{Z}_n^{(i,s)} \triangleq \mathsf{X}_n^{(i,s)} - \mathsf{Y}_n^{(i,s)}$ *converges almost surely to 0 if and only if* $U_{i,s}^2 = \mathbb{E}\left\{\mathsf{U}^2\right\}$.

Proof. First note that

$$\mathsf{Z}_n^{(i,s,\nu)} = \frac{1}{n}\sum_{p=0}^{n-1}\left[\mathsf{U}_{i,p,s}^2 - U_{i,s}^2 + 2\mathsf{N}_{i,p,s}\left(\mathsf{U}_{i,p,s} - U_{i,s}\right)\right] .$$

Therefore, as n increases, $\mathsf{Z}_n^{(i,s)}$ converges to $\mathbb{E}\left\{\mathsf{U}^2\right\} - U_{i,s}^2$ almost surely by the strong law of large numbers [66–68]. Thus, $\mathsf{X}_n^{(i,s)}$ converges almost surely to $\mathsf{Y}_n^{(i,s)}$ if and only if $U_{i,s}^2 = \mathbb{E}\left\{\mathsf{U}^2\right\}$. □

Lemma 1 suggests

$$\mathsf{B}_i \simeq \frac{1}{N_\mathrm{p}}\sum_{p=0}^{N_\mathrm{p}-1}\sum_{s=0}^{N_\mathrm{sb}-1}\left(\sqrt{\mathbb{E}\left\{\mathsf{U}_{i,p,s}^2\right\}} + \mathsf{N}_{i,p,s}\right)^2 \tag{3.33}$$

implying that the noncentrality parameter for $\mathsf{B}_i N_\mathrm{p}/\sigma^2$ can be written as $\lambda_i \simeq \overline{\lambda}_i$, where

$$\overline{\lambda}_i = \sum_{p=0}^{N_\mathrm{p}-1}\sum_{s=0}^{N_\mathrm{sb}-1}\frac{\mathbb{E}\left\{\mathsf{U}_{i,p,s}^2\right\}}{\sigma^2} . \tag{3.34}$$

Remark 6. *The dependence on wireless channel instantiations can be removed by substituting each noncentrality parameter λ_i, which depends on $\boldsymbol{\theta}$, with its expected value $\overline{\lambda}_i$, which depends on $\overline{\boldsymbol{\theta}}$, in all of the above distributions.*

The impulse response of a wideband wireless channel at time t is commonly described by [69–73]

$$h(t;\varsigma) = \sum_{l=1}^{L(t)} \alpha_l(t)\, \delta(\varsigma - \tau_l(t)) \tag{3.35}$$

where $L(t)$ is the number of multipath components, and $\alpha_l(t)$ and $\tau_l(t)$ are the amplitude gain and the arrival time of the lth path, respectively. The $L(t)$, $\alpha_l(t)$, and $\tau_l(t)$ are considered time-invariant over an observation time.

For a resolvable multipath channel, i.e., the path interarrival time intrinsic to the wireless environment is larger than the temporal duration of the transmitted signal, $\mathbb{E}\left\{\mathsf{U}_{i,p,s}^2\right\}$ in (3.34) can be written as

$$\mathbb{E}\left\{\mathsf{U}_{i,p,s}^2\right\} \simeq \mathbb{E}\Big\{\sum_{l=1}^{L} \alpha_l^2 s^2(t_{i,p,s} - \tau_l)\Big\}. \tag{3.36}$$

Therefore, the calculation of $\overline{\lambda}_i$ requires the averaging with respect to the channel nuisance parameters α_l's and τ_l's in $\boldsymbol{\theta}_{\mathrm{h}}$. The complexity of such calculation depends on the joint distribution of L, α_l's, and τ_l's. However, the resolution of the ED is limited by the dwell time T_{d}. Therefore, the statistics of the energy bins can be determined by considering a tapped-delay-line model [7,73–76]. In particular, $h(t;\varsigma)$ can be replaced by $\breve{h}(t;\varsigma) = \sum_{l=1}^{\breve{L}} \breve{\alpha}_l \delta(\varsigma - \breve{\tau}_l)$, where $\breve{L}$ is a deterministic number of path, $\breve{\tau}_l = \tau + l\Delta$ with Δ deterministic, and $\breve{L}\Delta$ is the approximate dispersion of the channel. For example, Δ can be chosen as the dwell time, the inverse of the bandwidth, or the average interarrival time of the paths. This results in

$$\mathbb{E}\left\{\mathsf{U}_{i,p,s}^2\right\} \simeq \sum_{l=1}^{\breve{L}} \mathbb{E}\left\{\breve{\alpha}_l^2\right\} s^2(t_{i,p,s} - \breve{\tau}_l). \tag{3.37}$$

Substituting (3.37) in (3.34), the expected value of the noncentrality parameter for the ith bin becomes

$$\overline{\lambda}_i = \sum_{p=0}^{N_{\mathrm{p}}-1} \sum_{s=0}^{N_{\mathrm{sb}}-1} \sum_{l=1}^{\breve{L}} \frac{\mathbb{E}\left\{\breve{\alpha}_l^2\right\}}{\sigma^2} s^2(t_{i,p,s} - \breve{\tau}_l). \tag{3.38}$$

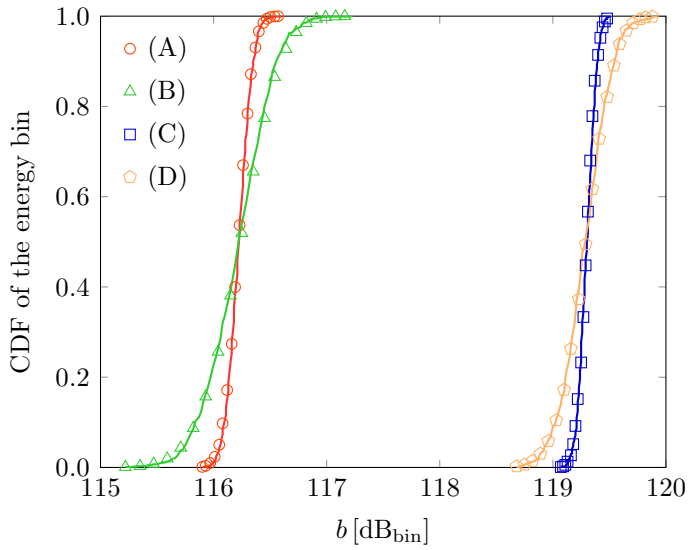

Figure 3.3: Example CDF of the energy bin value for different values of N_p and T_d with $\gamma = -20\,\mathrm{dB}$: (A) $N_\mathrm{p} = 128$, $T_\mathrm{d} = 2\mathrm{ns}$; (B) $N_\mathrm{p} = 16$, $T_\mathrm{d} = 2\mathrm{ns}$; (C) $N_\mathrm{p} = 128$, $T_\mathrm{d} = 4\mathrm{ns}$; (D) $N_\mathrm{p} = 16$, $T_\mathrm{d} = 4\mathrm{ns}$. Simulation results are shown in symbols and theoretical results according to (3.39) are shown in solid lines.

Using (3.38) instead of λ_i in all the above distributions, one can obtain the tractable range information model that depends only on $\overline{\boldsymbol{\theta}}$ instead of $\boldsymbol{\theta}$. For instance, B_i can be approximated by $\overline{\mathsf{B}}_i$ with conditional CDF given by

$$F_{\overline{\mathsf{B}}_i}(b|\overline{\boldsymbol{\theta}}) = \Phi\left(\frac{bN_\mathrm{p}/\sigma^2 - N_\mathrm{p}N_\mathrm{sb} - \overline{\lambda}_i}{\sqrt{2(N_\mathrm{p}N_\mathrm{sb} + 2\overline{\lambda}_i)}}\right) \tag{3.39}$$

which is obtained from (3.31) by replacing λ_i with $\overline{\lambda}_i$.

Figure 3.3 shows the CDF of the energy bin for different numbers of observations and dwell times with received signal-to-noise ratio (SNR) per pulse $\gamma = -20\mathrm{dB}$ according to the IEEE 802.15.4a standard for indoor residential LOS environments [65]. More details about the scenario will be provided in Section 3.3.2 where the case study is presented. It can be observed that the theoretical CDF of the bin value (3.39) accurately describes the empirical CDF obtained by sample-level simulations.

Using the results in this section, tractable expressions of the distribution of the TOA estimation error can be derived for hard-decision algorithms. In particular, substituting the PDF and CDF of B_i given respectively by (3.10) and (3.11) into the

conditional PMF $f_{\mathsf{I}}(i|\boldsymbol{\theta})$ in Section 3.2.2 for specific hard-decision algorithms, and replacing each λ_i with $\overline{\lambda}_i$, (3.28) is simplified into a tractable form.

Remark 7. *The parameters $\overline{\lambda}_i$'s depend on $\overline{\boldsymbol{\theta}}_h$ through $\breve{L}$, the statistics of $\breve{\alpha}_l$, and Δ. The $\overline{\lambda}_i$'s depend on $\boldsymbol{\theta}_d$ through N_{sb} and $t_{i,p,s}$, which further depends on T_d, T_p, and T_s.*

3.3.1 Design of the Energy Detector

This section aims to present the design of energy detection algorithms based on the proposed range information model. Such a model enables us to determine ED parameters (e.g., the choice of the thresholds, window length, and dwell time) according to different optimization criteria and constraints.

The design of ED commonly involves the probability of detection and that of false-alarm. The detection event occurs when, in a presence of the transmitted signal, the presence of the signal is correctly detected. The probability of such an event is given by

$$P_{\mathrm{d}}(\boldsymbol{\theta}_{\mathrm{d}}) = \sum_{i \in \mathcal{B}} \check{f}_{\mathsf{I}}(i|\boldsymbol{\theta}_{\mathrm{d}}, \boldsymbol{\lambda} \neq \mathbf{0}) \,. \tag{3.40}$$

The false-alarm event occurs when, in an absence of the transmitted signal, the presence of the signal is incorrectly detected due to noise. The probability of such an event is given by

$$P_{\mathrm{fa}}(\boldsymbol{\theta}_{\mathrm{d}}) = \sum_{i \in \mathcal{B}} \check{f}_{\mathsf{I}}(i|\boldsymbol{\theta}_{\mathrm{d}}, \boldsymbol{\lambda} = \mathbf{0}) \,. \tag{3.41}$$

For a given minimum tolerable level of detection probability $P_{\mathrm{d}}^{\star}$ or maximum tolerable level of false-alarm probability $P_{\mathrm{fa}}^{\star}$, constraints on parameters value $\boldsymbol{\theta}_{\mathrm{d}}$ can be obtained. For example, $P_{\mathrm{fa}}(\boldsymbol{\theta}_{\mathrm{d}})$ is non-increasing with the threshold ξ and therefore a minimum value ξ_{fa} can be determined for a given $P_{\mathrm{fa}}^{\star}$.

An important metric for ED design is the mean squared error (MSE) of the TOA estimate. When conditioned on the detection of the transmitted signal, the MSE of the TOA estimate is given by

$$\varrho_{\mathrm{t}}(\boldsymbol{\theta}_{\mathrm{d}}) = \int_{-\infty}^{+\infty} e^2 f_{\mathsf{E}}\left(e|\boldsymbol{\theta}_{\mathrm{d}}\right) de \,. \tag{3.42}$$

Recalling that the TOA estimation error belongs to a finite set $\mathcal{E}_\tau$, the MSE of the TOA estimate for hard-decision algorithms can be written as

$$\varrho_{\mathrm{t}}(\boldsymbol{\theta}_{\mathrm{d}}) = \frac{1}{T_{\mathrm{obs}}} \sum_{i=0}^{N_{\mathrm{b}}-1} \int_0^{T_{\mathrm{obs}}} (g(i)-\tau)^2 f_{\mathrm{l}}(i|\boldsymbol{\theta}_{\mathrm{d}}, \tau) d\tau \,. \tag{3.43}$$

The design of an ED minimizing the MSE of the TOA estimate with a guaranteed minimum level of detection probability can be obtained by solving the following constrained optimization problem

$$\hat{\boldsymbol{\theta}}_{\mathrm{d}} = \underset{\left\{\boldsymbol{\theta}_{\mathrm{d}} : P_{\mathrm{d}}(\boldsymbol{\theta}_{\mathrm{d}}) \geq P_{\mathrm{d}}^{\star}\right\}}{\operatorname{argmin}} \varrho_{\mathrm{t}}(\boldsymbol{\theta}_{\mathrm{d}}) \,. \tag{3.44}$$

Instead of guaranteeing a minimum detection probability, the design of an ED can minimize the MSE of the TOA estimate with a guaranteed maximum level of false-alarm probability as

$$\hat{\boldsymbol{\theta}}_{\mathrm{d}} = \underset{\left\{\boldsymbol{\theta}_{\mathrm{d}} : P_{\mathrm{fa}}(\boldsymbol{\theta}_{\mathrm{d}}) \leq P_{\mathrm{fa}}^{\star}\right\}}{\operatorname{argmin}} \varrho_{\mathrm{t}}(\boldsymbol{\theta}_{\mathrm{d}}) \,. \tag{3.45}$$

The design of an ED can also be formulated to maximize the detection probability $P_{\mathrm{d}}(\boldsymbol{\theta}_{\mathrm{d}})$ for a given maximum tolerable MSE $\varrho_{\mathrm{t}}^{\star}$of the TOA estimate, i.e.,

$$\hat{\boldsymbol{\theta}}_{\mathrm{d}} = \underset{\{\boldsymbol{\theta}_{\mathrm{d}} : \varrho_{\mathrm{t}}(\boldsymbol{\theta}_{\mathrm{d}}) \leq \varrho_{\mathrm{t}}^{\star}\}}{\operatorname{argmax}} P_{\mathrm{d}}(\boldsymbol{\theta}_{\mathrm{d}}) \,. \tag{3.46}$$

Alternatively, the ED design can be based on a hybrid objective function where the optimization problem is formulated to minimize a metric involving the MSE of the TOA estimate and a penalty. The mathematical formulation of such an optimization problem can be written as

$$\hat{\boldsymbol{\theta}}_{\mathrm{d}} = \underset{\boldsymbol{\theta}_{\mathrm{d}}}{\operatorname{argmin}}\, \upsilon_{\mathrm{t}}(\boldsymbol{\theta}_{\mathrm{d}}) \tag{3.47}$$

where

$$\upsilon_{\mathrm{t}}(\boldsymbol{\theta}_{\mathrm{d}}) = \varrho_{\mathrm{t}}(\boldsymbol{\theta}_{\mathrm{d}})\, P_{\mathrm{d}}(\boldsymbol{\theta}_{\mathrm{d}}) + \nu(\boldsymbol{\theta}_{\mathrm{d}}) \left[1 - P_{\mathrm{d}}(\boldsymbol{\theta}_{\mathrm{d}})\right] \tag{3.48}$$

is the unconditional MSE of the TOA estimate and $\nu(\boldsymbol{\theta}_{\mathrm{d}})$ is a penalty in an absence of detection. The penalty $\nu(\boldsymbol{\theta}_{\mathrm{d}})$ can be chosen as a function of the detection probability.

The above optimization problems are typical examples for the design of a ranging system. However, the proposed range information model is general and can be used to formulate other optimization problems that arise from energy detection applications.

3.3.2 Results

This section defines the performance metrics, describes the case study scenario, and presents performance results based on the developed theory and sample-level simulations.

Performance Metrics

Performance of the proposed range information model is evaluated in terms of the PMF accuracy, ranging accuracy, and localization accuracy defined as follows.

The following metrics will be used as a measure of the distance between the PMF $f_{\mathsf{I}}(i|\boldsymbol{\theta})$ of the selected bin obtained from the proposed range information model and that obtained through sample-level simulations. Let p_1, p_2 be two possible PMFs representing a RV taking values on a set $\mathcal{X}$, e.g., one approximate and one exact. The Jensen–Shannon divergence (JSD) is defined as [77]

$$\begin{aligned}\mathbb{D}_{\text{JS}}\left\{p_1, p_2\right\} = \frac{1}{2}\sum_{i\in\mathcal{X}} p_1(i)\,\log\left(\frac{2\,p_1(i)}{p_1(i)+p_2(i)}\right) \\ + \frac{1}{2}\sum_{i\in\mathcal{X}} p_2(i)\,\log\left(\frac{2\,p_2(i)}{p_1(i)+p_2(i)}\right).\end{aligned} \tag{3.49}$$

Other important metrics are the root-mean-square error (RMSE), which is defined as

$$\mathbb{D}_{\text{RMSE}}\left\{p_1, p_2\right\} = \left[\frac{1}{|\mathcal{X}|}\sum_{i\in\mathcal{X}} |p_1(i)-p_2(i)|^2\right]^{1/2} \tag{3.50}$$

and the maximum error, which is defined as

$$\mathbb{D}_{\text{ME}}\left\{p_1, p_2\right\} = \max_{i\in\mathcal{X}}\{|p_1(i)-p_2(i)|\}\,. \tag{3.51}$$

The ranging accuracy is determined in terms of CDF of the TOA estimation error $F_{\mathsf{E}}(e|\boldsymbol{\theta}_{\text{d}})$ and in terms of RMSE of the TOA estimate $\rho_{\text{t}}(\boldsymbol{\theta}_{\text{d}}) = \sqrt{\varrho_{\text{t}}(\boldsymbol{\theta}_{\text{d}})}$. The CDF $F_{\mathsf{E}}(e|\boldsymbol{\theta}_{\text{d}})$ and the RMSE $\rho_{\text{t}}(\boldsymbol{\theta}_{\text{d}})$ are obtained starting from (3.27) and (3.42), respectively.

The localization accuracy is determined in terms of the localization error outage (LEO). The LEO is defined as the probability that the localization error is above a maximum tolerable value $\epsilon^{\star}$, i.e.,

$$P_{\text{o}}(\boldsymbol{\theta}_{\text{d}}) = \mathbb{E}_{\boldsymbol{\theta}_{\text{h}}}\big\{\mathbb{1}_{(\epsilon^{\star},+\infty)}\{\epsilon(\mathbf{p}|\boldsymbol{\theta})\}\big\} \tag{3.52}$$

where, for a set $\mathcal{A}$,

$$\mathbb{1}_{\mathcal{A}}\{a\} = \begin{cases} 1 & \text{for } a \in \mathcal{A} \\ 0 & \text{otherwise} \end{cases}$$

and $\epsilon(\mathbf{p}|\boldsymbol{\theta}) = \|\hat{\mathbf{p}}(\boldsymbol{\theta}) - \mathbf{p}\|$ is the absolute value of the localization error, in which $\hat{\mathbf{p}}(\boldsymbol{\theta})$ and $\mathbf{p}$ are the estimated position and the true position, respectively.

Wireless Scenario and Energy Detector Setting

Consider a network of anchors (nodes with known position) aiming to localize agents (nodes in unknown positions) in an indoor environment. Specifically, the network is composed of four anchors located at the corners of a square with side length equal to 10 m. Each anchor emits a sequence of UWB root-raised cosine pulses with pulse repetition period $T_{\text{pr}} = 150\,\text{ns}$. The transmitted power spectral density is compliant with the emission masks according to the following regulations: (a) Japan (Asia Pacific Telecommunity); (b) Europe (European Telecommunications Standards Institute) and Korea (Asia Pacific Telecommunity); (c) USA (Federal Communication Commission); and (d) China (Asia Pacific Telecommunity). The wireless medium follows the IEEE 802.15.4a channel model for UWB indoor residential LOS environments [65] with $T_{\text{a}} = 50\,\text{ns}$.

The received signal is processed based on energy detection with observation time $T_{\text{obs}} = T_{\text{pr}}$. In the case of hard-decision algorithms, $\xi_i = \xi\,\forall i \in \mathcal{B}$ is considered for illustration. The value ξ is commonly chosen by accounting only for the randomness of the noise and discarding that of multipath propagation [78–80]. Alternatively, in [37], a simple criterion to determine a threshold is proposed based on the probability of early detection and on the knowledge of noise power. In contrast, the proposed range information model enables us to choose a threshold that accounts for the randomness of the wireless environments. The received SNR per pulse is $\gamma = E_{\text{p}}/N_0$ where E_{p} is the energy of the received signal pulse and N_0 is the one-sided power spectral density (PSD) of the noise component. The noise has mean zero and variance $\sigma^2 = N_0 W$ where W is the bandwidth of the transmitted signal that depends on the emission masks. Unless otherwise stated, the results in the following are provided for an emission mask as defined by the Federal Communication Commission with bandwidth $W = 7.5\,\text{GHz}$, a number of bins $N_{\text{b}} = 75$, and a dwell time $T_{\text{d}} = 2\,\text{ns}$. The threshold is chosen according to (3.44) as the ξ that minimizes the MSE of the TOA estimate with a guaranteed minimum level of detection probability $P_{\text{d}}^{\star} = 95\%$.

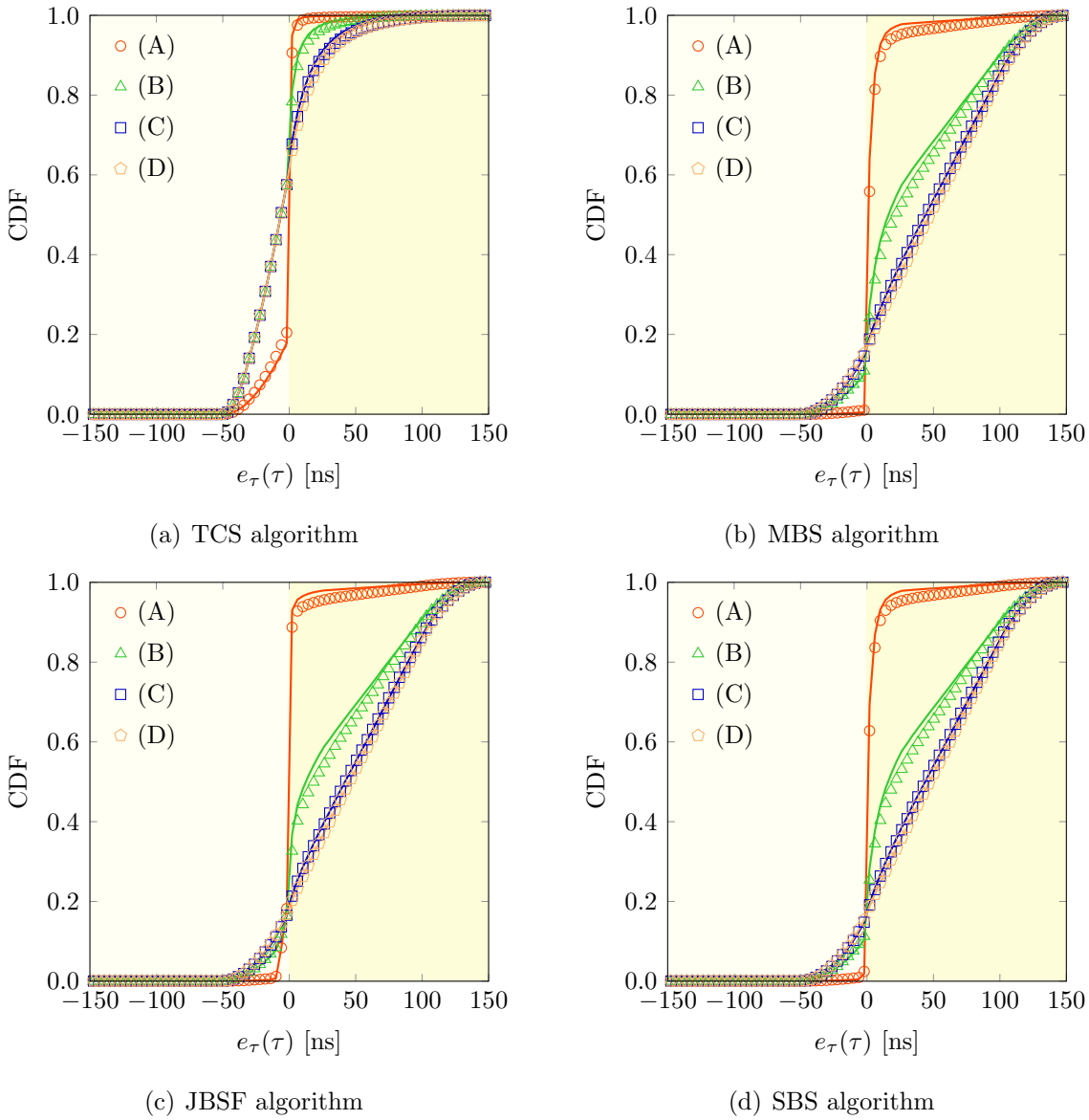

(a) TCS algorithm

(b) MBS algorithm

(c) JBSF algorithm

(d) SBS algorithm

Figure 3.4: Example CDF of the TOA estimation error for the TCS, MBS, JBSF with $N_\mathrm{w} = 5$, and SBS algorithms with different values of N_p and γ: (A) $N_\mathrm{p} = 128$, $\gamma = -10\,\mathrm{dB}$; (B) $N_\mathrm{p} = 16$, $\gamma = -10\,\mathrm{dB}$; (C) $N_\mathrm{p} = 128$, $\gamma = -20\,\mathrm{dB}$; and (D) $N_\mathrm{p} = 16$, $\gamma = -20\,\mathrm{dB}$. Theoretical results are shown in solid lines and simulation results are shown in symbols.

Performance Results

Table 3.1 provides the JSD, RMSE, and maximum error between the PMF $f_{\mathrm{I}}(i|\boldsymbol{\theta})$ of the selected bin obtained from the proposed range information model (i.e., (3.16), (3.19), (3.23), or (3.26)) and that obtained through sample-level simulations for TCS, MBS, JBSF with $N_{\mathrm{w}} = 5$, and SBS algorithms with different values of N_{p} and of γ. It can be noticed that the proposed model for $f_{\mathrm{I}}(i|\boldsymbol{\theta})$ is accurate, having a small distance with respect to the empirical PMF in all the settings.

Figure 3.4 shows the CDF of the TOA estimation error (3.28) for hard-decision algorithms with different values of N_{p} and γ. Two different regions can be discerned for the TOA estimation error: the negative errors (light gray region) due to early detection caused by the noise, and the positive errors (light blue region) due to late detection caused by the wireless channel. It can be observed that the results obtained from the proposed range information model are in agreement with those obtained through sample-level simulations in both regions. It is apparent that the distribution of the TOA estimation error is non Gaussian. Furthermore, the behaviors of the hard-decision algorithms are different in the early detection region, in which the errors are due to false alarms. This behavior is due to the fact that the threshold is chosen to minimize the MSE of the TOA estimate with a guaranteed minimum level of detection probability. Note that, while practical systems typically operate with high N_{p} values, a conservative scenario with small N_{p} values up to 128 is considered here to strain the proposed range information model.

The absolute error of the TOA estimate for $N_{\mathrm{p}} = 128$ and $\gamma = -10\,\mathrm{dB}$ per pulse is evaluated to be below 3.33 ns (corresponding to about 1 m) in 72%, 56%, 73%, and 61% of the instances for TCS, MBS, JBSF with $N_{\mathrm{w}} = 5$, and SBS algorithms, respectively. The absolute error of the TOA estimate is evaluated to be below 5 ns (corresponding to about 1.5 m) in 79%, 79%, 81%, and 80% of the instances for TCS, MBS, JBSF with $N_{\mathrm{w}} = 5$, and SBS algorithms, respectively.

Figure 3.5 shows the unconditional RMSE of the TOA estimate for the TCS algorithm as a function of the threshold-to-noise ratio (TNR) per pulse $\xi/(N_{\mathrm{p}}\,\sigma^2)$ for different values of N_{p} and γ. The unconditional RMSE is defined as $\sqrt{\upsilon_{\mathrm{t}}(\boldsymbol{\theta}_{\mathrm{d}})}$ where $\upsilon_{\mathrm{t}}(\boldsymbol{\theta}_{\mathrm{d}})$ is given in (3.48) with $\nu(\boldsymbol{\theta}_{\mathrm{d}}) = T_{\mathrm{obs}}^2$, which is the maximum possible MSE. It can be seen that the results obtained from the proposed range information model are in agreement with those obtained by sample-level simulations. The accuracy of the proposed model enables us to determine the optimal TNR value that minimizes the RMSE, which is important for ED design. It can also be observed that the minimum

	$N_\mathrm{p} = 16$		$N_\mathrm{p} = 128$	
	$\gamma = -20\,\mathrm{dB}$	$\gamma = -10\,\mathrm{dB}$	$\gamma = -20\,\mathrm{dB}$	$\gamma = -10\,\mathrm{dB}$
TCS	0.015	0.013	0.017	0.009
MBS	0.009	0.013	0.010	0.016
JBSF	0.009	0.012	0.010	0.015
SBS	0.009	0.012	0.010	0.015

	$N_\mathrm{p} = 16$		$N_\mathrm{p} = 128$	
	$\gamma = -20\,\mathrm{dB}$	$\gamma = -10\,\mathrm{dB}$	$\gamma = -20\,\mathrm{dB}$	$\gamma = -10\,\mathrm{dB}$
TCS	0.006	0.007	0.006	0.011
MBS	0.004	0.006	0.004	0.012
JBSF	0.004	0.006	0.004	0.009
SBS	0.004	0.006	0.004	0.010

	$N_\mathrm{p} = 16$		$N_\mathrm{p} = 128$	
	$\gamma = -20\,\mathrm{dB}$	$\gamma = -10\,\mathrm{dB}$	$\gamma = -20\,\mathrm{dB}$	$\gamma = -10\,\mathrm{dB}$
TCS	0.023	0.037	0.028	0.061
MBS	0.010	0.040	0.011	0.089
JBSF	0.010	0.040	0.010	0.054
SBS	0.010	0.038	0.010	0.070

Table 3.1: $\mathbb{D}_\mathrm{JS}\{p_1, p_2\}$ (top), $\mathbb{D}_\mathrm{RMSE}\{p_1, p_2\}$ (middle), and $\mathbb{D}_\mathrm{ME}\{p_1, p_2\}$ (bottom) for theoretical and simulated PMF of the selected bin for hard-decision algorithms.

RMSE decreases with N_p for a given γ. On the other hand, the RMSE varies more rapidly with TNR as N_p increases, revealing that the determination of the optimal threshold is critical for large N_p.

Figure 3.6 shows the unconditional RMSE of the TOA estimate for the TCS algorithm as a function of the TNR per pulse $\xi/(N_\mathrm{p}\,\sigma^2)$ for different emission masks, $N_\mathrm{p} = 16$, and $\gamma = -10\,\mathrm{dB}$. In particular, emission masks that are compliant with the regulations of the following countries are considered: (a) China ($W = 0.6\,\mathrm{GHz}$); (b) Japan ($W = 1.4\,\mathrm{GHz}$); (c) Europe lower band/Korea ($W = 1.7\,\mathrm{GHz}$); and (d) USA ($W = 7.5\,\mathrm{GHz}$). It can be observed that the results obtained from the proposed range information model are in agreement with those obtained through sample-level simulations for all the values of the bandwidth. As shown in Figure 3.5, the optimal TNR that minimizes the RMSE can be obtained from the proposed range information model. Note also that the RMSE varies more rapidly as the bandwidth W increases, revealing that the determination of the optimal threshold is critical for large W.

The localization accuracy of a network in which the agent position is determined according to the ML criterion is now discussed. In particular, the ML criterion selects the agent position $\hat{\mathbf{p}}$ that maximizes the product of range likelihoods, each in the form of (3.54) as a function of the TOA corresponding to the relative position between the agent and each anchor. Figure 3.7 shows the LEO as a function of the maximum tolerable localization error for soft-decision and hard-decision localization with $T_\mathrm{d} = 2\,\mathrm{ns}$, $N_\mathrm{p} = 128$, and different values of the SNR per pulse received at 1 m denoted by γ_0. For hard-decision localization the JBSF algorithm with $N_\mathrm{w} = 2$, and 5 as well as the TCS algorithm are considered; the threshold ξ is chosen according to (3.44) with $P_\mathrm{d}^\star = 95\%$. It can be observed that the LEO obtained from the range information model is in agreement with that obtained through sample-level simulations. The effect of N_w on the LEO is evident, especially for the smaller γ_0. It can be seen that a localization error smaller than 0.09, 1.45, 1.50, and 1.37 meters can be achieved 95% of the time for case (A), (B), (C), and (D), respectively, with $\gamma_0 = 10\,\mathrm{dB}$. Similarly, 0.08, 0.39, 0.39, and 0.40 meters can be achieved under the same settings with $\gamma_0 = 30\,\mathrm{dB}$. The results show that soft-decision localization significantly outperforms hard-decision localization.

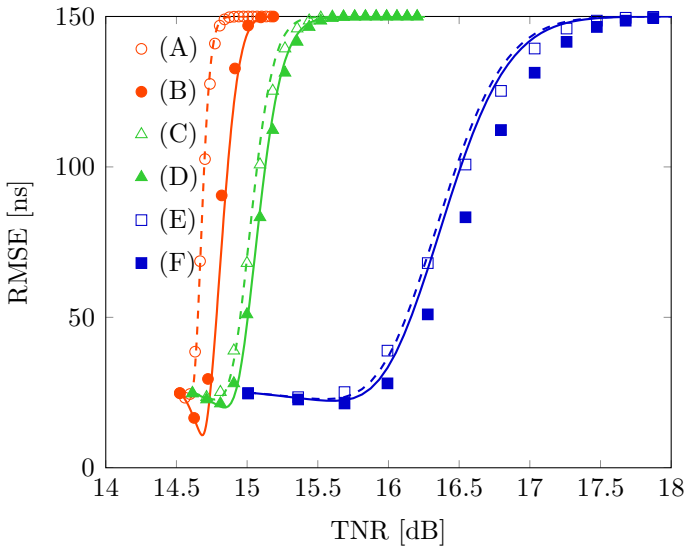

Figure 3.5: RMSE of the TOA estimate as a function of TNR per pulse for different values of N_p and γ: (A) $N_\mathrm{p} = 128$, $\gamma = -20\,\mathrm{dB}$; (B) $N_\mathrm{p} = 128$, $\gamma = -10\,\mathrm{dB}$; and (C) $N_\mathrm{p} = 16$, $\gamma = -20\,\mathrm{dB}$; (D) $N_\mathrm{p} = 16$, $\gamma = -10\,\mathrm{dB}$; (E) $N_\mathrm{p} = 1$, $\gamma = -20\,\mathrm{dB}$; and (F) $N_\mathrm{p} = 1$, $\gamma = -10\,\mathrm{dB}$. Theoretical results are shown in solid lines and simulation results are shown in symbols.

3.4 Range Likelihood based on a Reduced Dataset

In general, the soft-decision approach based on received samples improves the accuracy of the estimate at the cost of increasing the resource utilization for communicating likelihood functions among nodes. In particular, the time complexity due to the communication of likelihood functions among nodes, makes the hard-decision case often preferable in the tradeoff among accuracy and complexity.

Here, soft-decision ranging techniques for wideband localization are presented. The soft-decision ranging is based on range likelihood functions that are determined from a reduced dataset of observations. This reduced dataset is generated by processing the received waveform samples with energy detection techniques. The use of a reduced dataset decreases the amount of resource utilization for commeunicating likelihood functions among nodes. The range likelihood is evaluated by considering two different levels of prior knowledge: (i) approximated likelihood, (ii) empirical likelihood. The first case requires the knowledge of the channel statistic and is based on the tractable range model derived in [81]. The second case requires a measure-

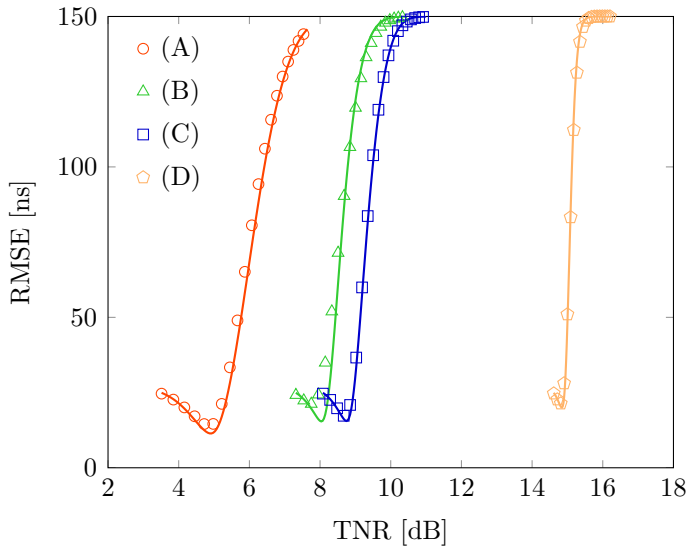

Figure 3.6: RMSE of the TOA estimate as a function of TNR per pulse for $N_{\mathrm{p}} = 16$, $\gamma = -10\,\mathrm{dB}$, and different emission masks: (A) China; (B) Japan; (C) Europe/Korea; and (D) USA. Theoretical results are shown in solid lines and simulation results are shown in symbols.

ment phase in which a reduced dataset is assembled and the empirical distribution of the associated RVs is calculated. The localization performance will be evaluated both via simulation and theoretical results. The key contributions are as follows:

- introduction of soft-decision localization based on a reduced dataset;
- development of low-complexity soft-decision algorithms with different levels of prior knowledge;
- evaluation of the performance for a case study in a realistic scenario.

3.4.1 Soft-Decision Ranging with Reduced Dataset

In this section we introduce two localization algorithms based on soft-decision ranging with reduced dataset: the energy-based soft-decision (ESD) and the threshold-based soft-decision (TSD). A classic approach with hard-decision based on TCS is also presented to serve as a benchmark.

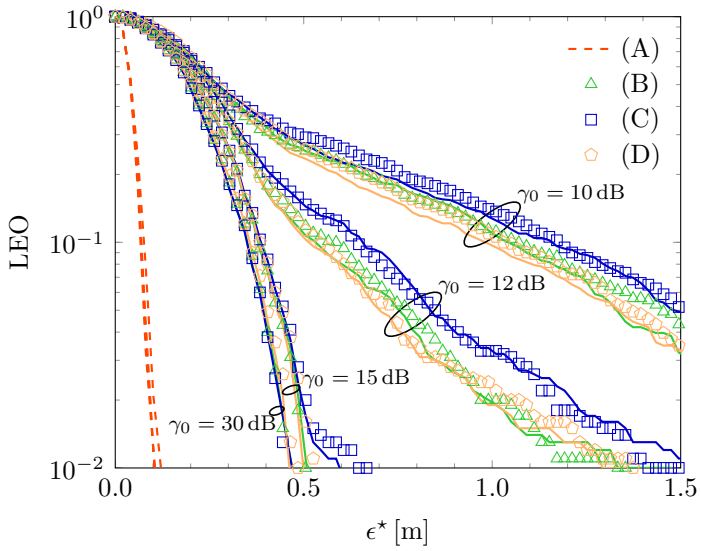

Figure 3.7: LEO as a function of the maximum tolerable localization error for soft-decision and hard-decision localization with $T_\mathrm{d} = 2\,\mathrm{ns}$, $N_\mathrm{p} = 128$, and different values of γ_0: (A) soft decision (dashed curves from left to right are for γ_0 from 30 to 10 dB); (B) JBSF with $N_\mathrm{w} = 5$; (C) JBSF with $N_\mathrm{w} = 2$; and (D) TCS. Theoretical results are shown in solid lines and simulation results are shown in symbols.

Soft and Hard-Decision Ranging

Soft-decision approaches for TOA estimation consider an observation set, usually the samples of the received waveforms, and compute the likelihood function based on statistical models as a function of the wireless channel. Two range likelihood functions are now proposed, which are determined from a reduced dataset $\mathbf{x}$ of variables obtained by processing $r(t)$ as shown in Figure 3.8.

The ESD algorithm is a soft-decision algorithm considering $\mathcal{D} = \mathbf{b}$ as observation set, where B_i with $i = 1, \ldots, N_\mathrm{bin}$. The RVs B_i's are independent and non-identically distributed with noncentrality parameter ang on $\boldsymbol{\theta}$. The range likelihood function can be written as

$$\Lambda_\mathrm{ESD}(\tau|\mathbf{b}) = \prod_{i=0}^{N_\mathrm{b}-1} f_{\mathsf{B}_i}(b_i|\tau, \boldsymbol{\theta}_\mathrm{h}, \boldsymbol{\theta}_\mathrm{d})\,. \tag{3.53}$$

The TSD algorithm is a soft-decision algorithm considering $\mathcal{D} = \{\hat{\imath}\}$ as observation set, where $\hat{\imath} \in \mathcal{B}$ is a selected bin index. In particular, a TCS is first performed, which involve the comparison of each bin value b_i with a corresponding threshold

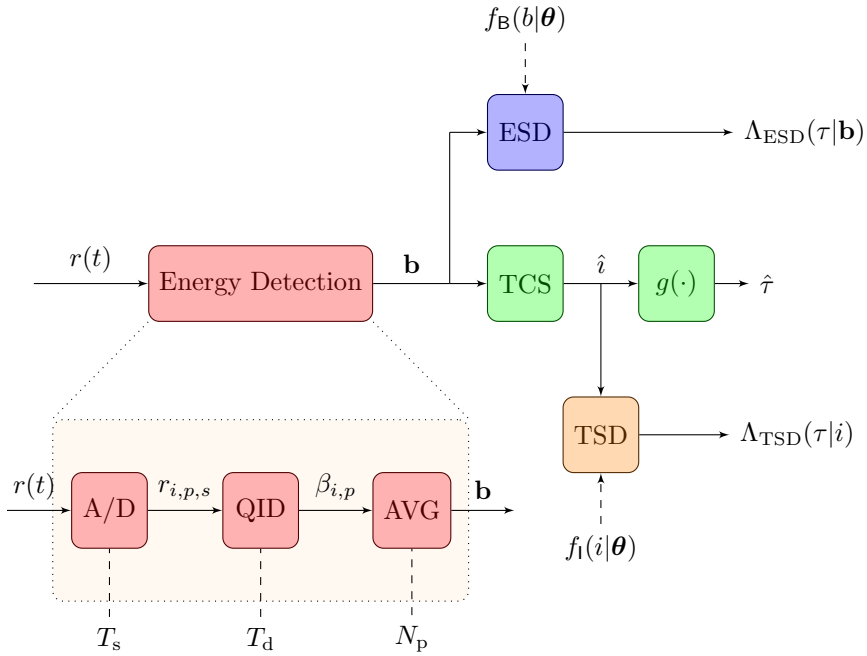

Figure 3.8: Soft-decision and hard-decision energy detection systems.

η_i [29]. Then, the observation set is $\{\hat{\imath}\} = \{\min\{i : b_i > \eta_i\}\}$, that is the first bin crossing a threshold ξ_i, with $\hat{\imath}$ being an outcome of the RV I [81]. The range likelihood function can be written as

$$\Lambda_{\mathrm{TSD}}(\varsigma|\hat{\imath}) = f_{\mathsf{I}}(\hat{\imath}|\varsigma, \boldsymbol{\theta}_{\mathrm{h}}, \boldsymbol{\theta}_{\mathrm{d}})\,. \tag{3.54}$$

where $f_{\mathsf{I}}(\hat{\imath}|\varsigma, \boldsymbol{\theta}_{\mathrm{h}}, \boldsymbol{\theta}_{\mathrm{d}})$ is defined below.

The TCS is considered to compare the proposed soft-decision algorithms with a classical hard-decision algorithm.

3.4.2 Localization via soft and hard-decision

Consider a localization system where a network of N_{a} anchors, with the ath anchor in $\mathbf{p}_a$ and $a \in \mathcal{A} = \{1, \ldots, N_{\mathrm{a}}\}$, are employed to localize a target in position $\mathbf{p}$. Energy detection and hard or soft-decision ranging is performed at each anchor, providing for the ath anchor a vector of energy bins $\mathbf{b}^{(a)} = [b_1^{(a)}, b_2^{(a)}, \ldots b_{N_{\mathrm{b}}}]$ and the selected index $\hat{\imath}$ in the case of TSD and TCS. After soft-decision ranging, a localization algorithm can directly process the likelihood functions obtained from N_{a} anchors to estimate

Algorithm 1 Energy-based Soft-Decision

1: **for** $a \in \mathcal{A}$ **do**
2: $\quad \Lambda^{(a)}_{\mathrm{ESD}}(\tau|\mathbf{b}^{(a)}) = \prod_{i=0}^{N_\mathrm{b}-1} f_{\mathsf{B}_i^{(a)}}(b_i^{(a)}|\tau, \boldsymbol{\theta}_\mathrm{h}, \boldsymbol{\theta}_\mathrm{d})\,.$
3: $\hat{\mathbf{p}} = \mathrm{argmax}_{\mathbf{p}} \prod_{a=1}^{N_\mathrm{a}} \Lambda^{(a)}_{\mathrm{ESD}}(\|\mathbf{p}_a - \mathbf{p}\||\mathbf{b}_a)$

Algorithm 2 Threshold-based Soft-Decision

1: **for** $a \in \mathcal{A}$ **do**
2: $\quad \hat{\imath}_a \leftarrow \min\{i \in \mathcal{B} : b_i^{(a)} > \xi_i\}$
3: $\quad \Lambda^{(a)}_{\mathrm{TSD}}(\tau|\hat{\imath}_a) = f_{\mathsf{I}}(\hat{\imath}_a|\tau, \boldsymbol{\theta}_\mathrm{h}, \boldsymbol{\theta}_\mathrm{d})$
4: $\hat{\mathbf{p}} = \mathrm{argmax}_{\mathbf{p}} \prod_{a=1}^{N_\mathrm{a}} \Lambda^{(a)}_{\mathrm{TSD}}(\|\mathbf{p}_a - \mathbf{p}\||\hat{\imath}_a)$

Algorithm 3 Threshold Crossing Search

1: **for** $a \in \mathcal{A}$ **do**
2: $\quad \hat{\imath}_a \leftarrow \min\{i \in \mathcal{B} : b_{a,i} > \xi_i\}$
3: $\quad \hat{\tau}_a \leftarrow \hat{\imath}_a T_\mathrm{d} + T_\mathrm{d}/2$
4: $\hat{\mathbf{p}} = \mathrm{argmin}_{\mathbf{p}} \sum_{a\in\mathcal{A}} \left(\hat{\tau}_a - \|\mathbf{p}_a - \mathbf{p}\|/c\right)^2$

the position $\mathbf{p}$. For example, a maximum likelihood solution is described in Alg. 1 and Alg. 2 for the ESD and TSD, respectively.

Note that the evaluation of the likelihood function requires the PDF of the energy bins $f_{\mathsf{B}}(b|\tau, \boldsymbol{\theta}_\mathrm{h}, \boldsymbol{\theta}_\mathrm{d})$ and $f_{\mathsf{I}}(\hat{\imath}|\tau, \boldsymbol{\theta}_\mathrm{h}, \boldsymbol{\theta}_\mathrm{d})$ for ESD and TSD, respectively. They can be approximated based on the mathematical model given in [81]. Alternatively, they can be estimated based on measurements. By collecting M outcomes of the variables B or I conditioned on the true TOA τ, the PDF can be approximated with the empirical distributions $\hat{f}^{(M)}_{\mathsf{B}}(b|\tau, \boldsymbol{\theta}_\mathrm{h}, \boldsymbol{\theta}_\mathrm{d})$ or $\hat{f}^{(M)}_{\mathsf{I}}(\hat{\imath}|\tau, \boldsymbol{\theta}_\mathrm{h}, \boldsymbol{\theta}_\mathrm{d})$ obtained from the M measurements.

In the case of hard-decision ranging, a localization algorithm processes the TOA estimates from the N_a anchors. For example, a least square solution is described in Alg. 3 for the TCS.

Remark: Note that the energy detection is distributed at each anchor, whereas the localization process is centralized. Therefore, the dataset size $|\mathcal{D}|$ for the range likelihood is the main parameter influencing the resource utilization for communicating the likelihood functions. In this perspective, the TSD has the minimum dataset size $|\mathcal{D}| = |\{\hat{\imath}_a\}| = 1$ together with the TCS $|\mathcal{D}| = |\{\hat{\tau}_a\}| = 1$. The ESD has dataset size $|\mathcal{D}| = |\mathbf{b}| = N_\mathrm{b}$. However, the original observation dataset is $|\mathcal{D}| \geq N_\mathrm{sb} N_\mathrm{b}$.

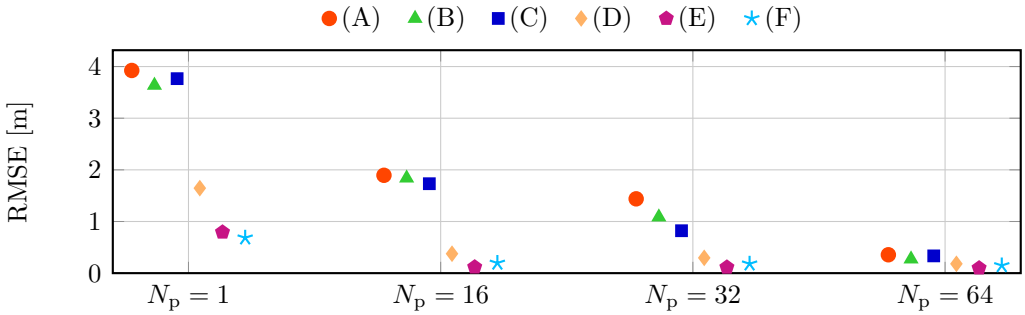

Figure 3.9: RMSE for different number of pulses for : (A) empirical TSD with $M = 5$; (B) empirical TSD with $M = 100$; (C) TSD; (D) empirical ESD with $M = 5$; (E) empirical ESD with $M = 100$; (F) ESD.

3.4.3 Results

This section describes the system settings, defines the performance metrics, and presents performance results based on the developed theory and sample-level simulations.

System Setting

Consider a network of anchors (nodes with known positions) aiming to localize agents (nodes in unknown positions) in an indoor environment. Specifically, the network is composed of four anchors located at the corners of a square with side length equal to 10 m. Each anchor emits a sequence of UWB root-raised cosine pulses with pulse repetition period $T_{\text{pr}} = 150\,\text{ns}$. The transmitted power spectral density is compliant with the emission masks according to the USA regulations (Federal Communication Commission) [82]. The wireless medium follows the IEEE 802.15.4a channel model for UWB indoor residential LOS environments [65] and $T_{\text{a}} = 150\,\text{ns}$.

The received signal is processed based on energy detection with observation time $T_{\text{obs}} = 256\,\text{ns}$. In the case of hard-decision algorithms, $\xi_i = \xi\,\forall i \in \mathcal{B}$ is considered for illustration. The received SNR per pulse is $\gamma = E_{\text{p}}/N_0$ where E_{p} is the energy of the received signal pulse and $N_0 = -110\,\text{dBm/MHz}$ is the one-sided power spectral density of the noise component. The noise has mean zero and variance $\sigma^2 = N_0 W$ where W is the bandwidth of the transmitted signal that is defined by the emission masks. Unless otherwise stated, the results in the following are provided for an emission mask as defined by the Federal Communication Commission with bandwidth $W = 7.5\,\text{GHz}$, the number of bins $N_{\text{b}} = 128$, dwell time $T_{\text{d}} = 2\,\text{ns}$, and number of

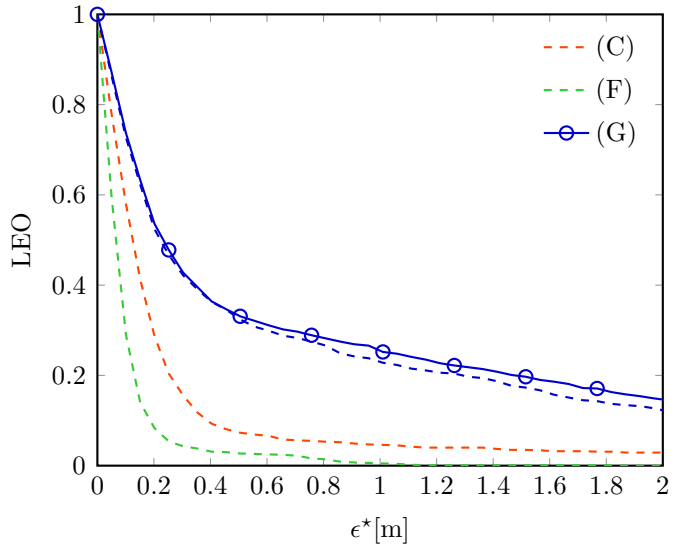

Figure 3.10: LEO as a function of $\epsilon^\star$ with $N_\mathrm{p} = 32$ with: (C) TSD; (F) ESD; and (G) TCS. The dashed blue line is the theoretical result for the TCS according to [81].

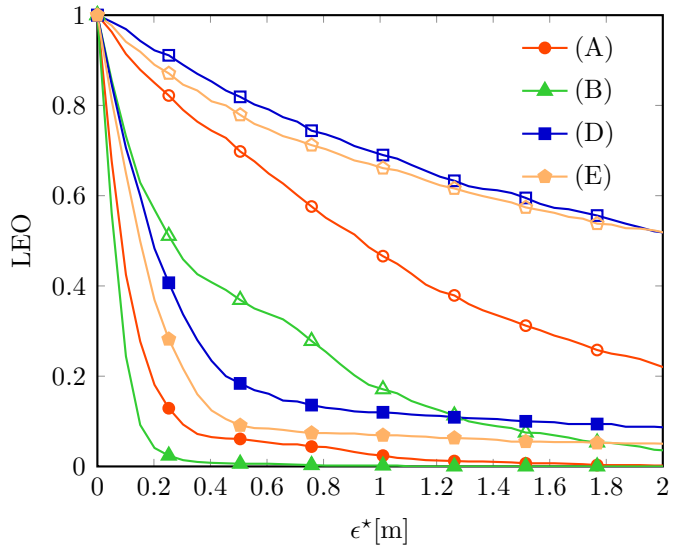

Figure 3.11: LEO as a function of $\epsilon^\star$ with $N_\mathrm{p} = 1$ (empty symbols) and $N_\mathrm{p} = 32$ (filled symbols) with: (A) empirical TSD with and $M = 5$; (B) empirical TSD with $M = 100$; (D) empirical ESD with $M = 5$; and (E) empirical ESD with $M = 100$.

collected pulses $N_\mathrm{p} = 32$.

Localization results are obtained with hard-decision and soft-decision ranging. For the soft-decision case, we consider both the ESD and the TSD algorithms. The energy bin distribution $f_\mathsf{B}(b|\tau, \boldsymbol{\theta}_\mathrm{h}, \boldsymbol{\theta}_\mathrm{d})$ for the ESD and the selected bin distribution $f_\mathsf{I}(b|\tau, \boldsymbol{\theta}_\mathrm{h}, \boldsymbol{\theta}_\mathrm{d})$ for the TSD are obtained with the tractable model in [81] or by a measurement phase where the distributions $\hat{f}_\mathsf{B}^{(M)}(b|\tau, \boldsymbol{\theta}_\mathrm{h}, \boldsymbol{\theta}_\mathrm{d})$ and $\hat{f}_\mathsf{I}^{(M)}(\hat{\imath}|\tau, \boldsymbol{\theta}_\mathrm{h}, \boldsymbol{\theta}_\mathrm{d})$ are obtained as the empirical distribution conditioned on τ for a finite set $\mathcal{T}$ of values and performing M diverse measurements for each value of $\tau \in \mathcal{T}$. In particular, we considered 150 values in $\mathcal{T}$ linearly spaced between 0 and T_a.

Different system settings are considered and referred to as: (A) empirical TSD with $M = 5$; (B) empirical TSD with $M = 100$; (C) TSD; (D) empirical ESD with $M = 5$; (E) empirical ESD with $M = 100$; (F) ESD; and (G) TCS.

Performance Results

Figure 3.9 shows the RMSE for different number of N_p with: (A) empirical TSD with $M = 5$; (B) empirical TSD with $M = 100$; (C) TSD; (D) empirical ESD with $M = 5$; (E) empirical ESD with $M = 100$; and (F) ESD. Results show that when the value of N_p is high, all the algorithms with different complexities have similar performance. Differently, for low values of N_p, the ESD outperforms the TSD for any level of prior knowledge.

Figure 3.10 shows the LEO as a function of $\epsilon^\star$ obtained with the tractable theoretical model and by simulation. The soft-decision ranging improve the performance with respect to the hard-decision. In particular, the localization error is above 1 m in the 0.5% of cases with ESD, in the 5% of cases with the TSD, and in the 25% of cases with the TCS (simulation). It can be observed that the results obtained from the theoretical model are in agreement with those obtained through sample-level simulations for the hard-decision case with TCS.

Figure 3.11 shows the LEO as a function of $\epsilon^\star$ for (A) TSD with $\hat{f}_\mathsf{I}^{(M)}(\hat{\imath}|\tau)$ and $M = 5$; (B) TSD with $\hat{f}_\mathsf{I}^{(M)}(\hat{\imath}|\tau)$ and $M = 100$; (D) ESD with $\hat{f}_\mathsf{B}^{(M)}(b|\tau)$ and $M = 5$; and (E) ESD with $\hat{f}_\mathsf{B}^{(M)}(b|\tau)$ and $M = 100$. It can be observed that the ESD outperforms the TSD and it is also more sensitive to the number of measurements M. For $N_\mathrm{p} = 1$, localization error is above 1 m in the 47% of cases with ESD when $M = 5$ and in the 17% when $M = 100$. Differently, the LEO does not change significantly with M for the TSD, where the localization error is above 1 m in the 69% of cases with the TSD when $M = 5$ and in the 66% when $M = 100$.

Chapter 4

Selection of Representative Observations

Accurate localization via sensor radars is challenging in wireless environments with multipath, clutter, and signal obstructions (for example caused by furniture and walls in indoor scenarios). These conditions can cause observations (e.g., range measurements) that are non-representative of the target object (i.e., non-representative outliers [16]) with heavy impact on the localization accuracy. These conditions can be mitigated by using signals with large bandwidth, exploiting prior knowledge, and selecting representative observations [83–89].

Previous works on selection techniques for sensor radars aim to improve localization accuracy or to reduce signal processing complexity by choosing a subset of active sensors. In [90], the subset of active antennas employed in the localization process is minimized by selecting only those that fulfill the required performance. In [91] and [92], a Kalman filter-based approach for global and local node selection is proposed to increase geolocation accuracy in a distributed network of sensors. The node selection relies on a combinatorial optimization framework and on the use of the Cramèr-Rao bound (CRB), which requires prior knowledge of target position and SNR for each transmitter-target-receiver link.

Sensor radars based on UWB signals [6, 93, 94] can provide accurate localization in harsh propagation environments thanks to their ability to resolve multipath and penetrate obstacles. Specifically, UWB signals provide fine delay resolution, which enables precise TOA measurements for ranging [8, 22, 27, 29, 95–98]. However, the accuracy and reliability of range-based localization typically degrade in wireless environments with multipath, clutter, LOS blockage, and excess propagation delays

through materials [9, 12–14, 59, 99–101]. Sensor radars exploiting the characteristics of UWB signals are presented in [33, 102–106, 108].

Ranging accuracy in sensor radars depends on the capability of exploiting prior knowledge, noise filtering, clutter mitigation, and TOA estimation. A variety of range error models have been adopted in the literature [81].

The fundamental questions for the design of target localization techniques via sensor radars are: (i) What are the intrinsic properties of the radar network dominating its performance in a given operation environment? (ii) How does the quality of the measurements impact the localization accuracy? (iii) How to conceive the network setting, waveform processing, and localization algorithm to mitigate propagation impairments? The answers to these questions enable the design of sensor radars exploiting the intrinsic properties of the network for a new level of localization accuracy even in harsh propagation environments.

Our approach consists in exploiting diversity and selection of measurements to enhance the performance of sensor radars in harsh propagation environments with non-line-of-sight (NLOS) conditions. Diversity is a well known concept used in wireless communications to improve the performance, especially in fading channels (see, e.g., [109–113]). The goal of this work is to provide insights into how the network intrinsic properties, the waveform processing, and the localization algorithm affect detection and localization capabilities of sensor radars, as well as to demonstrate that proper techniques for selecting a subset of observations can improve the localization accuracy despite the lower complexity.

Innovative techniques are presented, which are blind to both channel knowledge and propagation environment for selecting representative observations. Such blind techniques rely on indicators obtained from non-coherent reception and sub-Nyquist sampling of waveforms. A methodology for the design and analysis of SRs is developed by jointly considering network intrinsic properties and signal processing techniques. The key contributions can be summarized as follows:

- introduction of blind techniques for the selection of representative observations in sensor radars;
- development of a methodology for the design and analysis of sensor radars by jointly considering (i) network setting, (ii) propagation environment, (iii) waveform processing, (iv) observation selection, and (v) localization algorithm;
- quantification of the localization accuracy improvement provided by observa-

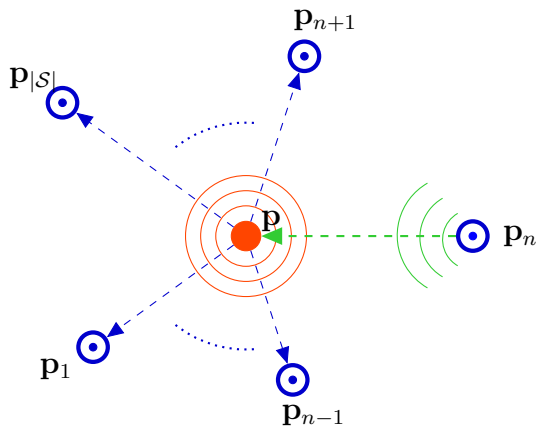

Figure 4.1: Example of a sensor radar configuration with one transmitter at $\mathbf{p}_n$ and $|\mathcal{S}|-1$ receivers at $\mathbf{p}_1, \mathbf{p}_2, ..., \mathbf{p}_{n-1}, \mathbf{p}_{n+1}, \mathbf{p}_{n+2}, ..., \mathbf{p}_{|\mathcal{S}|}$; the target is at $\mathbf{p}$.

tion selection techniques.

The performance evaluation accounts for all the channel impairments such as multipath, clutter, and LOS/NLOS propagation. To understand the key benefits of selecting representative observations, we consider all the relevant aspects of the sensor radar and the propagation environments, neglecting synchronization errors and other secondary aspects that are beyond the scope of this study. Instead of considering a specific range error model, we simulate the entire signal processing chain starting from the received waveforms. As a case study, we consider UWB sensor radars in a typical indoor environment (with LOS and NLOS conditions, clutter, and multipath).

4.1 Sensor Radar Network

The network setting and the propagation environment for the analysis of sensor radars is now described.

4.1.1 Network Setting

Refer to a network of sensors with index set $\mathcal{S}$ and cardinality $|\mathcal{S}|$, where the sensor indexed by $s \in \mathcal{S}$ is in position $\mathbf{p}_s$. The radar configuration is defined by an index subset $\mathcal{T} \subset \mathcal{S}$ of $|\mathcal{T}|$ transmitters and an index subset $\mathcal{R} \subset \mathcal{S}$ of $|\mathcal{R}|$ receivers. The

ith transmitter ($i \in \mathcal{T}$) and the jth receiver ($j \in \mathcal{R}$) are at $\mathbf{p}_i$ and $\mathbf{p}_j$, respectively. Such a radar configuration defines an index set $\mathcal{P}$ of transmitter-receiver pairs with cardinality $|\mathcal{P}| = |\mathcal{T}| \times |\mathcal{R}|$. Specifically, each pair $(i, j) \in \mathcal{P}$ is composed of the ith transmitter emitting a signal and the jth receiver collecting the received signal after backscattering by the target object and wireless propagation. Figure 4.1 shows an example of sensor radar with $\mathcal{P} = \{(n, 1), (n, 2), \ldots, (n, n-1), (n, n+1), \ldots, (n, |\mathcal{S}|)\}$. By processing the received signal for each pair, the TOA is estimated and the transmitter-to-target-to-receiver distance (signal path-length) is determined.

For a target object in position $\mathbf{p}$ and a radar $(i, j) \in \mathcal{P}$, the signal path-length is given by

$$d_{ij}(\mathbf{p}) = d_i(\mathbf{p}) + d_j(\mathbf{p}) = \tau_{ij}(\mathbf{p})\, c \tag{4.1}$$

where $d_i(\mathbf{p})$ and $d_j(\mathbf{p})$ are the ith transmitter-to-target and target-to-jth receiver distances, respectively, c is the speed of light, and $\tau_{ij}(\mathbf{p})$ is the TOA at the jth receiver for a signal emitted by the ith transmitter and backscattered by the target. It is known that the target position $\mathbf{p}$ is given by the intersection of isorange contours (the TOA estimates define circumference or ellipses in the monostatic and bistatic case, respectively) [2]. In general, isorange contours have more points of intersection leading to ambiguities in target location in non-ideal conditions.

The transmitter-receiver pair forms a monostatic or a bistatic radar whether the transmitter and the receiver are co-located ($\mathbf{p}_i = \mathbf{p}_j$) or not ($\mathbf{p}_i \neq \mathbf{p}_j$). Note that bistatic pairs might require accurate phase and time synchronization between transmitter and receiver [2]. In a bistatic radar, each single signal transmission causes the reception of at least two signal replicas in free-space propagation: the direct signal via the transmitted-to-receiver path and the reflected signal via the transmitter-to-target-to-receiver path [114]. Thus, a temporal separation between the two signal replicas is necessary to ensure their resolvability, which results in a minimum resolvable delay for the radar. In a monostatic radar, the same antenna is used for transmission and reception. Thus, a switching time between the transmission and reception phases is present, which results in a blind range for the radar. In the following, $\tau_{\min}$ denotes either the minimum resolvable delay and the blind range for the bistatic or monostatic case, respectively [2].

The TOA $\tau_{ij}(\mathbf{p})$ can be determined and the target detected by the radar $(i, j) \in \mathcal{P}$ if

$$d_{ij}(\mathbf{p}) \geq d^{\star}_{ij} \tag{4.2}$$

where $d^{\star}_{ij} = \|\mathbf{p}_i - \mathbf{p}_j\| + \tau_{\min}\, c$. Then, the target position can be determined by

a localization algorithm that processes the observation vector $\hat{\boldsymbol{\tau}}_{\mathcal{P}}(\mathbf{p})$ with elements $\hat{\tau}_{ij}(\mathbf{p})$ representing the estimated TOA for all the radars $(i,j) \in \mathcal{P}$.

The detection and localization capabilities of a SR depend on its intrinsic properties, the receiver sensitivity, and the received SNRs. Specifically, the received SNR $\gamma_{ij}(\mathbf{p})$ for the radar $(i,j) \in \mathcal{P}$ and target at $\mathbf{p}$ is given by

$$\gamma_{ij}(\mathbf{p}) = \frac{P_{\mathrm{R},ij}(\mathbf{p})}{f_{\mathrm{pr}} N_0} \tag{4.3}$$

where $P_{\mathrm{R},ij}(\mathbf{p})$ is the received power referred to a pulse repetition frequency (PRF) f_{pr} and N_0 is the one-sided PSD of the noise. Target detection and TOA estimation benefit from gathering the energy of multiple backscattered signals. This gathering occurs by processing received signals collected from the transmission of N_{p} signals.

A minimum received SNR $\gamma^\star$ must be guaranteed to fulfill detection requirements. From (5.1), this requirement corresponds to a minimum received power $P_{\mathrm{R}}^\star$ as

$$P_{\mathrm{R},ij}(\mathbf{p}) \geq P_{\mathrm{R}}^\star \,. \tag{4.4}$$

The locus of points satisfying the minimum SNR requirement, in a bidimensional scenario with free-space propagation, corresponds to that inside a circumference (namely maximum circumference) for monostatic radars, and that inside a Cassini oval (namely maximum Cassini oval) for bistatic radars [114]. In NLOS conditions, the area covered is irregular and depends on the obstructions of signal propagation.

4.1.2 Propagation Environment

The power received in a band $[f_{\mathrm{L}}, f_{\mathrm{U}}]$ from the ith transmitter-to-target-to-jth receiver path is given by

$$P_{\mathrm{R},ij}(\mathbf{p}) = \int_{f_{\mathrm{L}}}^{f_{\mathrm{U}}} R_{ij}(f,\mathbf{p})\, df \tag{4.5}$$

where $R_{ij}(f,\mathbf{p})$ is the one-sided PSD of the received signal.

In free-space propagation (i.e., LOS conditions), the signal is attenuated due to the path-loss. In obstructed propagation (i.e., NLOS conditions), in addition to the path-loss the signal is also attenuated and time-delayed by obstructions depending on the material characteristics such as the relative permittivity and attenuation coefficient. The obstruction-loss $L_{ij}(f,\mathbf{p})$ accounts for such effects on the received signal PSD. In a general case, the received signal PSD is affected by path-loss and

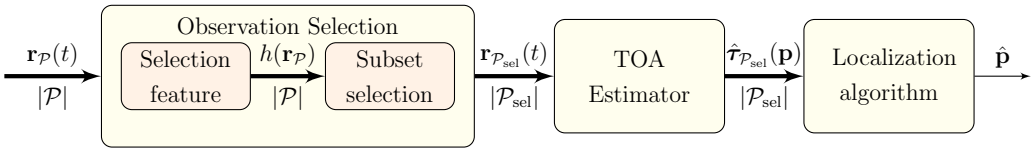

Figure 4.2: Sensing and processing in SRs for localization based on observation selection.

obstruction-loss as

$$R_{ij}(f,\mathbf{p}) = \frac{\overset{\circ}{R}_{ij}(f,\mathbf{p})}{L_{ij}(f,\mathbf{p})} \tag{4.6}$$

where $\overset{\circ}{R}_{ij}(f,\mathbf{p})$ is the received signal PSD in LOS conditions.

In the case of UWB signals, the path-loss is modeled according to the IEEE 802.15.4a standard [65]. In particular, the one-sided PSD of the signal received for the radar $(i,j) \in \mathcal{P}$ and target at $\mathbf{p}$ in the absence of signal obstructions is given by

$$\overset{\circ}{R}_{ij}(f,\mathbf{p}) = \frac{T_i(f)\eta_i(f,\mathbf{\Theta}_i)\eta_j(f,\mathbf{\Theta}_j)\Sigma(f,\mathbf{\Theta}_i,\mathbf{\Theta}_j)}{(4\pi)^3(f_0 d_0/c)^2 \ell_{ij}^{\beta}(\mathbf{p})(f/f_0)^{2\kappa+2}} \tag{4.7}$$

where $T_i(f)$ is the transmitted signal PSD that feeds the transmitting antenna; d_0 is the reference distance and f_0 the center frequency; $\eta_i(f,\mathbf{\Theta}_i)$ and $\eta_j(f,\mathbf{\Theta}_j)$ are the transmitting and receiving antenna efficiencies, respectively; $\mathbf{\Theta}_i$ and $\mathbf{\Theta}_j$ are the solid angles between ith transmitter-target and target-jth receiver, respectively; $\Sigma(f,\mathbf{\Theta}_i,\mathbf{\Theta}_j)$ is the radar cross section (RCS) of the target; and $\ell_{ij}(\mathbf{p}) = d_i(\mathbf{p})d_j(\mathbf{p})/{d_0}^2$. The path-loss exponents β and κ provide the path-loss dependence on distance and frequency, respectively. In a typical indoor environment the presence of walls determines an NLOS condition with obstruction-loss (in dB) given by [115]

$$10\log_{10} L_{ij}(f,\mathbf{p}) = \sum_{w=1}^{W_{ij}(\mathbf{p})} n_{ij}^{(w)}(\mathbf{p})\, X^{(w)}(f) \tag{4.8}$$

where $W_{ij}(\mathbf{p})$ is the number of wall-types met by the signal (incident and scattered), $n_{ij}^{(w)}(\mathbf{p})$ is the number of walls of type w, and $X^{(w)}(f)$ is the frequency-dependent loss induced by a wall of type w. Therefore, the total loss is the sum of path-loss and obstruction-loss located along the propagation paths. Note that $L_{ij}(f,\mathbf{p}) = 1$ in free-space propagation.

Together with the obstruction-loss, the presence of obstacles and walls obstructing the signal path results in an excess delay for the TOA, which causes a positive bias on

the TOA estimate. For example, a set of measurements was performed to characterize the excess delay on UWB signals due to the presence of concrete walls in a typical office building [13], showing that the TOA estimate bias is $\beta_{ij}(\mathbf{p}) \simeq \Delta/c$, where Δ is the total thickness of the wall.

The accuracy of target location inference relies on the quality of TOA estimates composing the observation vector $\hat{\boldsymbol{\tau}}_{\mathcal{P}}(\mathbf{p})$, which depends on the intrinsic properties of the sensor radar. The processing of signals received in LOS conditions might result in imperfect TOA estimation $\hat{\tau}_{ij}(\mathbf{p})$, therefore in an imperfect signal path-length estimation $\hat{d}_{ij}(\mathbf{p}) = \hat{\tau}_{ij}(\mathbf{p})\, c$, due to non-ideal propagation (e.g., multipath, clutter, noise). The processing of signals received in NLOS conditions might result in an inaccurate TOA estimates due to excess delay and obstruction-loss. Therefore, in NLOS conditions the TOA estimates are more likely non-representative observations of the target. Hence, given an observation vector obtained from diverse radars in the network, the localization accuracy can be enhanced by processing a subset of representative observations of the target. Section 4.3 will present the processing techniques for the selection of representative observations in sensor radars.

4.2 Observation Selection Methods

Blind and low-complexity techniques are now proposed, which exploit diversity and provide selection of observations to alleviate harsh propagation impairments and improve localization performance.

Figure 4.2 shows the block scheme for target localization starting from the set of received signals $\mathbf{v}_{\mathcal{P}}(t) = \{v_{ij}(t) : (i,j) \in \mathcal{P}\}$. For each signal after pre-filtering and clutter removal $r_{ij}(t)$, a feature $h(r_{ij})$ is extracted. Then, a subset of cardinality $L \leq N_{\text{obs}}$ of vectors $\boldsymbol{r}_{\mathcal{P}_{\text{sel}}}(t)$ is selected based on such a feature. The TOA estimator at each receiver determines $\hat{\tau}_{ij}$ for the signal $r_{ij}(t)$ if selected, i.e., $(i,j) \in \mathcal{P}_{\text{sel}}$.

The choice of the feature is crucial for the sensor radar's ability to select observations that are representative for target location inference. Therefore, such a choice has to be based on the relation between the feature $h(r_{ij})$ and the range error $e_{ij} = c\,|\hat{\tau}_{ij}(\mathbf{p}) - \tau_{ij}(\mathbf{p})|$. Consider a decision vector $\overline{\boldsymbol{\epsilon}}_{ij} = [\overline{\epsilon}_{ij}^{(0)}, \overline{\epsilon}_{ij}^{(1)}, \ldots, \overline{\epsilon}_{ij}^{(N_{\text{b}}-1)}]$ of N_{b} signal indicator samples for the pair $(i,j) \in \mathcal{P}$ (e.g., with an energy detector the $\overline{\epsilon}_{ij}^{(q)}$ is related to the energy of samples within the qth time interval) then $h(r_{ij}) = h(\overline{\boldsymbol{\epsilon}}_{ij})$. Since the range error depends on the true TOA, the ideal selection would be based on the centrality of $\overline{\epsilon}_{ij}^{(q)}$ distribution with respect to $\tau_{ij}(\mathbf{p})$. Unfortunately, the true

TOA is not known in a blind context. Different features are now considered and are related to the amplitude and temporal distribution of the decision vector $\overline{\boldsymbol{\epsilon}}_{ij}$ for selecting the observations that are most likely representative of the target (i.e., less affected by multipath, noise, and obstruction-loss).

To evaluate the temporal dispersion of $\overline{\boldsymbol{\epsilon}}_{ij}$ over the observation time, first normalize its elements, within each decision vector, as

$$f_{ij}(q) = \frac{\overline{\epsilon}_{ij}^{(q)}}{\sum_{q=1}^{N_\mathrm{b}} \overline{\epsilon}_{ij}^{(q)}} \tag{4.9}$$

where $f_{ij}(q)$ represents the sampling probability that the true TOA belongs to the qth time interval given the vector $\overline{\boldsymbol{\epsilon}}_{ij}$. Note that, in the absence of prior knowledge, we consider the true TOA included in the maximum element of $\overline{\boldsymbol{\epsilon}}_{ij}$ with highest probability. Define the cumulative distribution function, the first moment, and the nth central moment of $f_{ij}(q)$, respectively, as

$$F_{ij}(x) = \sum_{q \le x} f_{ij}(q) \tag{4.10}$$

$$\overline{\mu}_{ij} = \sum_{q=1}^{N_\mathrm{b}} q\, f_{ij}(q) \tag{4.11}$$

$$\mu_{ij}^{(n)} = \sum_{q=1}^{N_\mathrm{b}} (q - \overline{\mu}_{ij})^n\, f_{ij}(q)\,. \tag{4.12}$$

From (4.10), (4.11), and (4.12), the temporal dispersion of the signal indicator samples can be evaluated by considering variance σ_{ij}^2, interquartile range IQR_{ij}, kurtosis κ_{ij}, and skewness χ_{ij}, which are respectively given by

$$\sigma_{ij}^2 = \mu_{ij}^{(2)} \tag{4.13}$$

$$\mathsf{IQR}_{ij} = F_{ij}^{-1}(0.75) - F_{ij}^{-1}(0.25) \tag{4.14}$$

$$\kappa_{ij} = \frac{\mu_{ij}^{(4)}}{\left(\mu_{ij}^{(2)}\right)^2} \tag{4.15}$$

$$\chi_{ij} = \frac{\mu_{ij}^{(3)}}{\left(\sqrt{\mu_{ij}^{(2)}}\right)^3}\,. \tag{4.16}$$

To evaluate the amplitude dispersion of $\overline{\boldsymbol{\epsilon}}_{ij}$, consider the maximum value M_{ij}, sample variance s_{ij}^2, sample range r_{ij}, and sample skewness c_{ij}, which are respectively given

by

$$\mathsf{M}_{ij} = \max_q \overline{\epsilon}_{ij}^{(q)} \tag{4.17}$$

$$\mathsf{s}_{ij}^2 = \frac{1}{N_\mathrm{b}} \sum_{q=1}^{N_\mathrm{b}} \left[\overline{\epsilon}_{ij}^{(q)} - \left(\frac{1}{N_\mathrm{b}} \sum_{q=1}^{N_\mathrm{b}} \overline{\epsilon}_{ij}^{(q)} \right) \right]^2 \tag{4.18}$$

$$\mathsf{r}_{ij} = \left| \max_q \overline{\epsilon}_{ij}^{(q)} - \min_q \overline{\epsilon}_{ij}^{(q)} \right| \tag{4.19}$$

$$\mathsf{c}_{ij} = \frac{\sum_{q=1}^{N_\mathrm{b}} \left[\overline{\epsilon}_{ij}^{(q)} - \frac{1}{N_\mathrm{b}} \left(\sum_{q=1}^{N_\mathrm{b}} \overline{\epsilon}_{ij}^{(q)} \right) \right]^3}{N_\mathrm{b} \left(\mathsf{s}_{ij}^2 \right)^{3/2}}. \tag{4.20}$$

The relation between a feature $h(\overline{\boldsymbol{\epsilon}}_{ij}) \in \left\{ \sigma_{ij}^2, \mathsf{IQR}_{ij}, \kappa_{ij}, \chi_{ij}, \mathsf{s}_{ij}^2, \mathsf{M}_{ij}, \mathsf{r}_{ij}, \mathsf{c}_{ij} \right\}$ and the range error e_{ij} can be evaluated through the correlation $\rho(h(\overline{\boldsymbol{\epsilon}}_{ij}), \mathsf{e}_{ij})$. Such correlation is determined via both the Spearman and the Pearson correlation coefficients, which indicates whether a monotone relation between the two variables exists [116]. Specifically, the Pearson correlation coefficient for N observations of two variables x and y is given by

$$\rho(x, y) = \frac{\sum_{i=1}^{N} (x_i - \overline{x})(y_i - \overline{y})}{\sqrt{\sum_{i=1}^{N} (x_i - \overline{x})^2 (y_i - \overline{y})^2}} \tag{4.21}$$

where x_i and y_i, with $i = 1, ..., N$, are observations of x and y, respectively; and $\overline{x}$ and $\overline{y}$ are the average values of the observation sample $\{x_i\}_{i=1}^N$ and $\{y_i\}_{i=1}^N$, respectively. The Spearman correlation coefficient is determined similarly to (4.21) by using the ranked variables in place of the original ones. Ranking is performed by sorting the observations in ascending order and associating them to the corresponding ordinal number. Both correlation coefficients take values in $[-1, 1]$, where the value $\rho(h(\overline{\boldsymbol{\epsilon}}_{ij}), \mathsf{e}_{ij}) = 0$ indicates that the two variables are uncorrelated, whereas positive or negative values indicate that any monotone relation between the two variables is non-decreasing or non-increasing, respectively. The statistical significance of such correlation coefficients can be tested based on the sample size and the resulting correlation values providing a p-value, where p represents the probability of obtaining the same correlation coefficient with two independent variables [117].

Consider for example the cases $h(\overline{\boldsymbol{\epsilon}}_{ij}) = \sigma_{ij}^2$, $h(\overline{\boldsymbol{\epsilon}}_{ij}) = \chi_{ij}$, and $h(\overline{\boldsymbol{\epsilon}}_{ij}) = \mathsf{c}_{ij}$. Specifically, low or high values of the variance σ_{ij}^2 are obtained with narrow or wide sampling distribution of the time interval containing the true TOA, respectively.

Therefore, lower values of σ_{ij}^2 are expected for large values of SNR corresponding to smaller range errors. Differently, positive or negative values of skewness χ_{ij} are obtained when the sampling distribution is right-side or left-side tailed, respectively. In particular, positive values are due to the shape of the channel impulse response, whose right-side tail is given by the delay spread of the channel. The channel impulse response guides the shape of $f_{ij}(q)$ for large SNR values, while it has a lower impact for small SNR values. Therefore, higher values of χ_{ij} are expected for smaller range errors. Finally, low or high values of sample skewness are obtained when there are many or few elements with large values within the decision vector $\overline{\boldsymbol{\epsilon}}_{ij}$, respectively. Large-value indicator samples are more likely to be associated with the target for large SNR values, when the energy due to the target is easily discernible from the noise floor. Therefore, higher values of c_{ij} are expected for smaller range errors.

The observations $\hat{\boldsymbol{\tau}}_{\mathcal{P}}(\mathbf{p})$ are sorted based on the features $h(\overline{\boldsymbol{\epsilon}}_{\mathcal{P}})$ in increasing or decreasing order, depending on whether the relation between $h(\overline{\boldsymbol{\epsilon}}_{ij})$ and e_{ij} is monotonically non-increasing or non-decreasing, respectively. The features $h(\overline{\boldsymbol{\epsilon}}_{\mathcal{P}})$ are calculated based on the vector $\overline{\boldsymbol{\epsilon}}_{\mathcal{P}}$, that contains all the decision vectors $\overline{\boldsymbol{\epsilon}}_{ij}$ with $(i,j) \in \mathcal{P}$. Then, the subset $\hat{\boldsymbol{\tau}}_{\mathcal{P}_{\text{sel}}}(\mathbf{p})$ of $L = |\mathcal{P}_{\text{sel}}| \leq N_{\text{obs}}$ selected observations is composed by the first L sorted observations and further processed by the localization algorithm.

From (2.18), the comparison between the computational complexity of localization with and without observation selection depends on the complexity of the localization algorithm $\mathcal{C}_{\text{l}}(N)$. Note that the term $\mathcal{C}_{\text{f}}(N_{\text{meas}})$ is a linear function with the number of observations $\mathcal{O}(N_{\text{meas}})$ for all the aforementioned features, except for the IQR_{ij} that requires function inversion. Therefore, the selection of representative observations enables significant savings in complexity when $m \geq 2$.

The extraction of the aforementioned features will be detailed in the following for a case of wide usage based on sub-Nyquist processing with energy detection.

4.3 Observation Processing

The signal pre-processing techniques and TOA estimation is now described.

4.3.1 Pre-filtering and Clutter Removal

The out-of-band noise can be mitigated by means of a band-pass zonal filter (BPZF), which consists of a band-pass filter having the same center frequency and bandwidth

of the transmitted signal. The output of the BPZF, corresponding to the transmission of N_p pulses, is given by

$$\tilde{v}_{ij}(t) = \sum_{p=0}^{N_\mathrm{p}-1} \sum_{l=1}^{L_\mathrm{p}} \alpha_{ij}^{(l)}\, s(t - p\,T_\mathrm{g} - \tau_{ij}^{(l)}) + w_{ij}(t) \tag{4.22}$$

where $s(t)$ is the output of the BPZF corresponding to a single pulse at its input, L_p is the number of received multipath components due to target backscattering (with lth component having gain $\alpha_{ij}^{(l)}$ and delay $\tau_{ij}^{(l)}$), and $T_\mathrm{g} \triangleq 1/f_\mathrm{pr}$. The term $w_{ij}(t)$ includes the filtered components of noise and clutter.

There are various techniques for clutter removal, based on the operation environment. In case of static clutter, two classical techniques are the empty-room technique and the frame-to-frame technique. The empty-room technique consists in a setup phase where a signal, namely reference signal, is received and recorded at each radar in the absence of target object [118]. Such a reference signal is recorded off-line from a high number of transmitted pulses, therefore including the time-invariant clutter. Then, the reference signal is subtracted from the signal received in the presence of target objects to mitigate static clutter. The frame-to-frame technique exploits the amplitude and phase variations of backscattered signals due to the target mobility for discerning the time-invariant clutter from the moving target [104]. In the case of non-static clutter, both clutter removal techniques present a residual clutter in the waveforms at the input of the TOA estimator.

4.3.2 Time-of-Arrival and Position Estimation

A variety of TOA estimators is present in the literature; those based on energy detection received attention because they are based on non-coherent signal reception and sub-Nyquist sampling. In particular, with energy detection the TOA estimates are determined based on energy values collected in time intervals (energy bins) [29].

The signal at the input of the TOA estimator, after pre-filtering and clutter removal, is given by

$$r_{ij}(t) = \sum_{p=0}^{N_\mathrm{p}-1} \sum_{l=1}^{L_\mathrm{p}} \alpha_{ij}^{(l)}\, s(t - p\,T_\mathrm{g} - \tau_{ij}^{(l)}) + n_{ij}(t) \tag{4.23}$$

where $n_{ij}(t)$ includes the filtered noise and the residual clutter.

After perfect clutter removal, multipath propagation in (5.2) accounts for the paths scattered by the target, and these paths arrive at the receiver after reflections. In the absence of prior information, we consider the true $\tau_{ij}(\mathbf{p})$ uniformly distributed in the interval $[0, T_{\mathrm{a}}]$, where the maximum possible delay T_{a} depends on the propagation environment. The PRF is chosen to satisfy $T_{\mathrm{g}} > T_{\mathrm{a}}$.

A decision vector based on energy bins is obtained as $\overline{\boldsymbol{\epsilon}}_{ij} = [\overline{\epsilon}_{ij}^{(0)}, \overline{\epsilon}_{ij}^{(1)}, \ldots, \overline{\epsilon}_{ij}^{(N_{\mathrm{b}}-1)}]$, where the qth element $\overline{\epsilon}_{ij}^{(q)}$ is determined, for example, by averaging over the N_{p} received signals [29] as described in 3.1.1. In particular, an hard-decision TCS algorithm is considered. For the radar $(i, j) \in \mathcal{P}$ and target at $\mathbf{p}$, the estimated TOA $\hat{\tau}_{ij}(\mathbf{p})$ is chosen as the central value of the corresponding dwell interval for the first element of the energy vector above the threshold ξ_{ij}.

The amplitude and temporal distributions of the elements $\overline{\epsilon}_{ij}^{(q)}$ depend on the true TOA $\tau_{ij}(\mathbf{p})$ and the received SNR $\gamma_{ij}(\mathbf{p})$, which are affected by propagation conditions (i.e., noise, path-loss, obstruction-loss). Figure 4.3 shows three examples of energy vectors $\overline{\epsilon}_{ij}^{(q)}$ as a function of q for different signal path-lengths and total thickness of the crossed walls. Note that the true TOA $\tau_{ij}(\mathbf{p})$, which is dependent on both signal path-length and obstructions, guides the centrality of distribution of $\overline{\epsilon}_{ij}^{(q)}$, while the SNR, which is dependent on path-loss and obstruction-loss, guides the amplitude and temporal dispersion of $\overline{\epsilon}_{ij}^{(q)}$. Decisions provided by comparison with a threshold in the case of disperse distribution of energy bins are more vulnerable to non-representative elements of the observation vector. Hence, $\hat{\tau}_{ij}(\mathbf{p})$ is most likely due to a non-representative observation of the target when the values $\overline{\epsilon}_{ij}^{(q)}$ have a flat distribution with values close to the noise floor.

4.4 Case Study

A case study for a network of UWB sensor radars is presented, which operates in an indoor environment and that exploits the selection of representative observations. The operation environment, the signal processing techniques, and the numerical results are described in the following subsections.

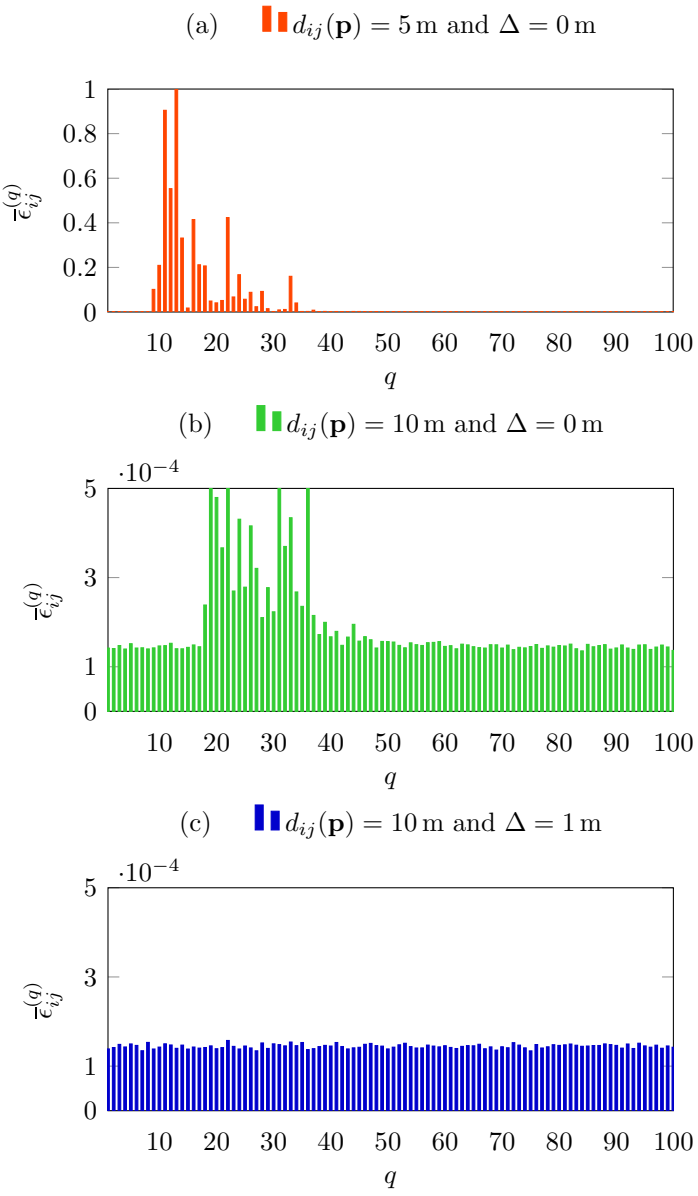

Figure 4.3: Energy vectors for different values of signal path-length $d_{ij}(\mathbf{p})$ and total wall thickness Δ. Energy values are normalized to the maximum of the vector in (a). Results are obtained with an ED setting and channel model used in the case study.

4.4.1 Operation Environment

Scenario

Figure 4.4 shows the operation environment of $10\,\mathrm{m} \times 10\,\mathrm{m}$ with walls, in which $N_\mathrm{S} = |\mathcal{S}| = 12$ UWB sensors are placed. Results are compared to those obtained

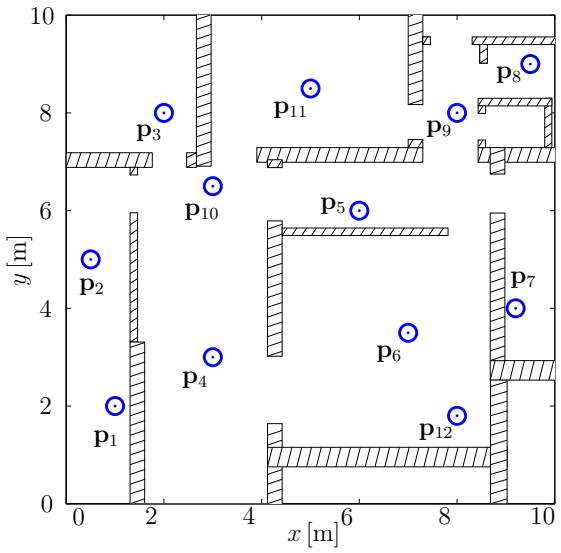

Figure 4.4: Operation environment with sensor radars and walls. Sensor position coordinates are: $\mathbf{p}_1 = (1, 2)$, $\mathbf{p}_2 = (0.5, 5)$, $\mathbf{p}_3 = (2, 8)$, $\mathbf{p}_4 = (3, 3)$, $\mathbf{p}_5 = (6, 6)$, $\mathbf{p}_6 = (7, 3.5)$, $\mathbf{p}_7 = (9.2, 4)$, $\mathbf{p}_8 = (9.5, 8)$, $\mathbf{p}_9 = (8, 8)$, $\mathbf{p}_{10} = (3, 6.5)$, $\mathbf{p}_{11} = (5, 8.5)$, $\mathbf{p}_{12} = (8, 1.8)$, in meters.

in the absence of walls. In the operation environment, the maximum TOA value is $T_\mathrm{a} = 94.2\,\mathrm{ns}$ (corresponding to the TOA of a signal traveling over a distance of twice a diagonal line). The network of sensor radars varies its configuration during the localization process. Specifically, we consider $N_\mathrm{S} - 1$ multistatic configurations with a single transmitter and multiple receivers. At the nth configuration, there is one transmitter at $\mathbf{p}_n$ and the $N_\mathrm{S} - n$ receivers in positions $\{\mathbf{p}_{n+1}, \mathbf{p}_{n+2}, ..., \mathbf{p}_{N_\mathrm{S}}\}$. In reciprocal channels, the choice of these multistatic configurations ensures diverse propagation paths for received signals $r_{ij}(t)$ with a single observation per sensor pair. The total number of observations is $N_\mathrm{meas} = N_\mathrm{S}(N_\mathrm{S} - 1)/2$ (i.e., $N_\mathrm{meas} = 66$ for $N_\mathrm{S} = 12$).

The impulse radio UWB sensor radars transmit a sequence of root raised cosine (RRC) pulses compliant with the European lower band with $\mathsf{PRF} = 5\,\mathrm{MHz}$. The antennas are omnidirectional and the one-sided noise power spectral density is $N_0 = -200\,\mathrm{dBW/Hz}$ (e.g., noise figure $F = 6\,\mathrm{dB}$ and antenna noise temperature $290\,\mathrm{K}$).

Multipath and clutter

Multipath propagation for the direct signal (from transmitter to target) and backscattered signal (from target to receiver) are modeled according to IEEE 802.15.4a [119] for a residential LOS environment. The NLOS conditions caused by walls generate obstruction-loss and excess delay, which are taken into account as described in Section 4.1.2. For each TOA estimation, the presence of 100 clutter objects uniformly distributed in the operation environment is considered. Such clutter is static, with RCS for each object obtained as a realization of a Swerling type-V RCS (i.e., a Chi-squared RV with four degrees of freedom).

Target

A Swerling type-III RCS Σ is considered for the target, which models a human body with random RCS distributed as a Chi-squared RV with four degrees of freedom, constant during a scan (i.e., the transmission of N_{p} pulses necessary for the TOA estimation process) and independent from scan to scan [2]. The average RCS is $\mathbb{E}\{\Sigma\} = 1\,\mathrm{m}^2$, which is typical for the human body [120].

4.4.2 Signal processing and Localization Algorithm

The energy vector $\overline{\boldsymbol{\epsilon}}_{ij}$ for each radar $(i,j) \in \mathcal{P}_{\mathrm{sel}}$ is obtained via an ED with dwell time $T_{\mathrm{dwell}} = 2\,\mathrm{ns}$ and observation time $T_{\mathrm{g}} = 200\,\mathrm{ns}$. Then, a TOA estimate $\hat{\tau}_{ij}(\mathbf{p})$ is determined through comparison with a threshold ξ_{ij}, which is chosen to obtain a constant probability of the event that an only-noise energy bin is above the threshold. Therefore, $\mathbb{P}\{\overline{\epsilon} > \xi_{ij}\} = 10^{-3}$ when $\overline{\epsilon}$ is an only-noise bin (e.g., corresponding to an absence of the target). The static clutter is mitigated via an empty-room algorithm with reference signal obtained by averaging 100 received waveforms in an absence of the target [104].

The performance of the SR is evaluated when L observations are selected based on the eight different features presented in Section 4.3, i.e.,

$$h(\overline{\boldsymbol{\epsilon}}_{ij}) \in \left\{\sigma_{ij}^2, \mathsf{IQR}_{ij}, \kappa_{ij}, \chi_{ij}, \mathsf{s}_{ij}^2, \mathsf{M}_{ij}, \mathsf{r}_{ij}, \mathsf{c}_{ij}\right\} \tag{4.24}$$

for $(i,j) \in \mathcal{P}_{\mathrm{sel}}$. To evaluate the benefits offered by selecting representative observations using the proposed features, a case in which L observations are randomly chosen is also presented for comparison. In addition, a non-blind case is presented as

a benchmark where the L energy vectors are chosen as those leading to the minimum range errors by using

$$h(\overline{\boldsymbol{\epsilon}}_{ij}) = \mathsf{e}_{ij} = c\,|\hat{\tau}_{ij}(\mathbf{p}) - \tau_{ij}(\mathbf{p})| \tag{4.25}$$

There, localization is performed based on the selected observations for 1000 target positions uniformly distributed in the environment of Figure 4.4 with and without walls.

4.4.3 Numerical Results

The results related to the choice of observation selection features and to the localization accuracy are now presented.

Observation selection features

Figures 4.5 and 4.6 show the variance σ_{ij} and kurtosis κ_{ij}, respectively, for two bistatic radars in the network (transmitter indexed by $i = 6$ and receiver indexed by $j = 10$ or 12). One thousand target positions uniformly distributed in the environment with walls are considered. It can be observed how the feature varies with the signal propagation conditions (i.e., target in LOS or NLOS conditions with both transmitter and receiver). In particular, Figure 4.5 shows that high values of variance σ_{ij} are obtained when the target is in LOS conditions with both transmitter and receiver (i.e., Figure 4.5(b)) or in light NLOS conditions (i.e., Figure 4.5(a)). NLOS conditions are referred to as light or heavy when one or more walls are present in the signal propagation path, respectively. Figure 4.6 shows that high values of kurtosis can be obtained not only in LOS and light NLOS conditions, but also in heavy NLOS conditions (e.g., for targets in the bottom right corner of the environment). These results indicate that using the variance as feature enables a more accurate selection of representative observations than using the kurtosis. Therefore, we expect a correlation $|\rho(\sigma_{ij}, \mathsf{e}_{ij})|$ higher than $|\rho(\kappa_{ij}, \mathsf{e}_{ij})|$.

To understand the ability of the features proposed in Section 4.2 to indicate representative observations, Figure 4.7 shows the Spearman and Pearson correlation between each feature $h(\overline{\boldsymbol{\epsilon}}_{ij})$ and the range error e_{ij}. The non-blind case with $h(\overline{\boldsymbol{\epsilon}}_{ij}) = \mathsf{e}_{ij}$ used as a benchmark is also presented. Correlation is obtained by considering a data set of $1000 \times N_{\text{meas}}$ energy vectors (i.e., one energy vector per transmitter-receiver pair, for each of the 1000 uniformly distributed target positions). The p-value

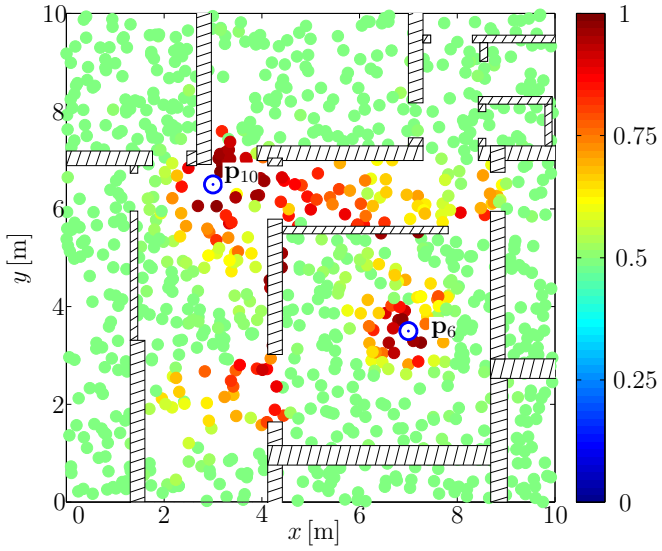

(a) Sensor radar $(\mathbf{p}_6, \mathbf{p}_{10})$.

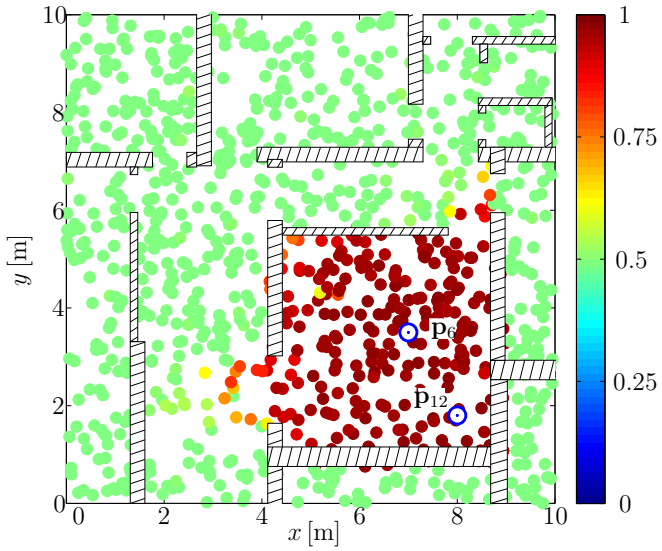

(b) Sensor radar $(\mathbf{p}_6, \mathbf{p}_{12})$.

Figure 4.5: Color map of variance σ_{ij}^2 with $i = 6$ and $j = 10, 12$, for 1000 target positions uniformly distributed in the environment. The value of σ_{ij}^2 is normalized to the maximum value in the environment.

is lower than 10^{-5} for all the features according to both Spearman and Pearson's correlations, which indicates that the correlation is statistically significant [117]. Specifically, low or high values of $|\rho(h(\overline{\boldsymbol{\epsilon}}_{ij}), \mathbf{e}_{ij})|$ indicate a weak or strong capability

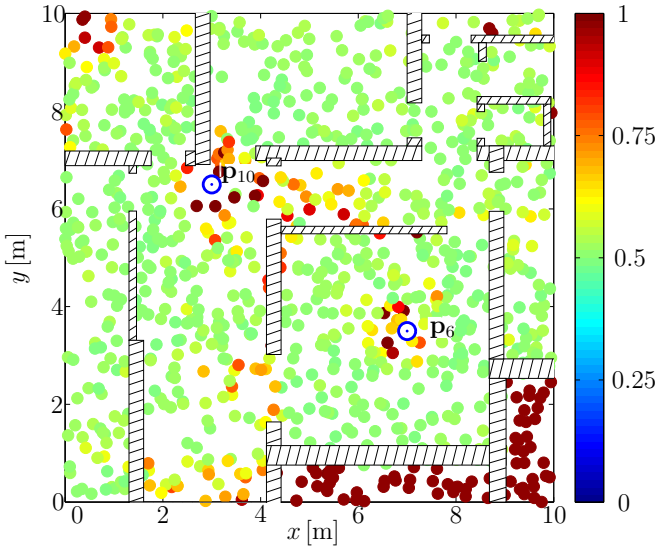

(a) Sensor radar $(\mathbf{p}_6, \mathbf{p}_{10})$.

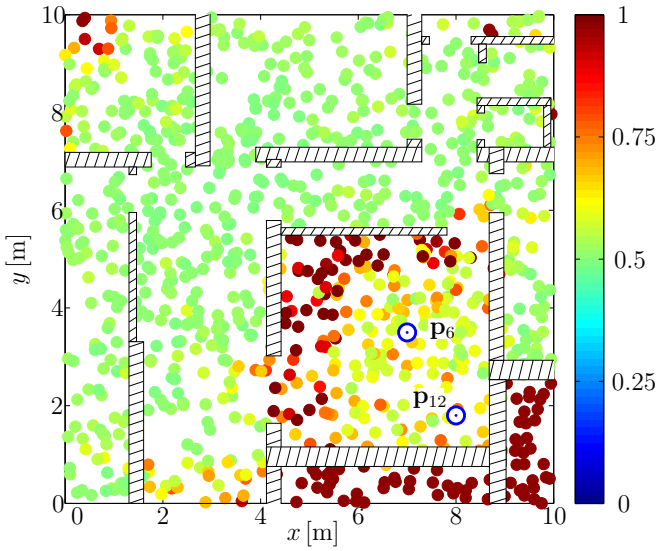

(b) Sensor radar $(\mathbf{p}_6, \mathbf{p}_{12})$.

Figure 4.6: Color map of kurtosis κ_{ij}^2 with $i = 6$ and $j = 10, 12$, for 1000 target positions uniformly distributed in the environment. The value of κ_{ij}^2 is normalized to the maximum value in the environment.

of selecting representative observations using the feature $h(\overline{\boldsymbol{\epsilon}}_{ij})$, respectively. The positive or negative sign of $\rho(h(\overline{\boldsymbol{\epsilon}}_{ij}), \mathsf{e}_{ij})$ indicates that the lower values of $h(\overline{\boldsymbol{\epsilon}}_{ij})$ are most likely to provide smaller or larger range errors, respectively. Therefore, the

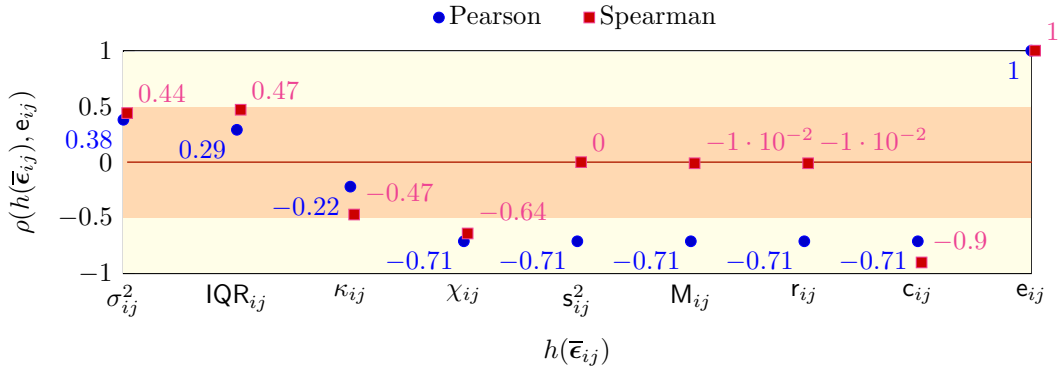

Figure 4.7: Pearson and Spearman correlation coefficients between each considered feature and the range error. Green and red regions represent index values of either strong or weak correlation, respectively. The red line represent the case of uncorrelation between the two variables.

subset of representative observations leading to the lower or higher values of $h(\overline{\boldsymbol{\epsilon}}_{ij})$ is selected if the sign of $\rho(h(\overline{\boldsymbol{\epsilon}}_{ij}), \mathsf{e}_{ij})$ is positive or negative, respectively. Note that the correlation for the feature $h(\overline{\boldsymbol{\epsilon}}_{ij}) = \sigma^2_{ij}$ is 0.38 with Pearson's method and 0.44 with Spearman's method; the correlation for the feature $h(\overline{\boldsymbol{\epsilon}}_{ij}) = \chi_{ij}$ is -0.71 with Pearson's method and -0.64 with Spearman's method; and the correlation for the feature $h(\overline{\boldsymbol{\epsilon}}_{ij}) = \mathsf{c}_{ij}$ is -0.71 with Pearson's method and -0.90 with Spearman's method. Therefore, the selection of representative observations leading to the lower variance, the higher skewness, or high sample skewness most likely provides small range errors.

Based on these results we evaluate the effects of observation selection on the localization performance for these three features, which present large values of correlation together with linear computational complexity.

Localization performance

Figure 4.8 shows the LEO at $e_{\text{th}} = 1\,\text{m}$ as a function of the number of selected observations L for $h(\overline{\boldsymbol{\epsilon}}_{ij}) = \sigma^2_{ij}, \kappa_{ij}$, and M_{ij}. To better understand the importance of the observation selection features on localization accuracy, the results are also obtained by considering a random selection of the L observations. The non-blind case $h(\overline{\boldsymbol{\epsilon}}_{ij}) = \mathsf{e}_{ij}$ serves as a benchmark. In the absence of walls (LOS conditions), all selection features provide a LEO that decreases with the number of selected observations. This is expected from the absence of obstruction-loss and excess delay.

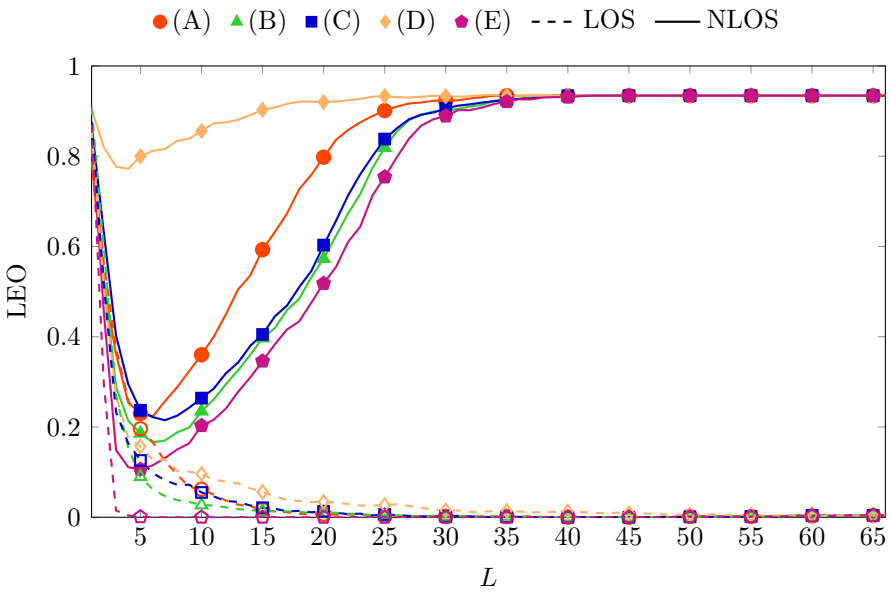

Figure 4.8: LEO as a function of $L = 1, 2, ..., N_{\text{meas}}$ for $e_{\text{th}} = 1\,\text{m}$, with (solid) and without (dashed) walls, for the cases (A) $h(\overline{\boldsymbol{\epsilon}}_{ij}) = \sigma_{ij}^2$, (B) $h(\overline{\boldsymbol{\epsilon}}_{ij}) = \kappa_{ij}$, and (C) $h(\overline{\boldsymbol{\epsilon}}_{ij}) = \mathsf{M}_{ij}$. The case (D) represents the random choice of L observations. The case (E) refers to the non-blind case $h(\overline{\boldsymbol{\epsilon}}_{ij}) = \mathsf{e}_{ij}$.

However, note that $L = 5$ observations, even randomly chosen, are sufficient to have a localization error $e_{\text{p}}(\mathbf{p}) < 1\,\text{m}$ in 80% of cases despite only $L = 5$ TOA estimates out of 66 are processed. This significantly reduces localization complexity, which is a quadratic function of the number of estimates that are processed. The worse performance levels for $L < 5$ are mainly due to ambiguities (e.g., ghost targets [2]) given by the intersection of L isorange contours (ellipses in two dimensions) leading to more than a single point in the absence of prior information (e.g., information on the environment). In the presence of walls (NLOS conditions) the LEO presents a minimum for all the selection features with $L = 5$ or 6. Here, the effect of selection is clear since in the case with $L = 5$ the localization error is $e_{\text{p}}(\mathbf{p}) < 1\,\text{m}$ in 20% of cases for random observation choice and in 77%, 80%, and 76% of cases for $h(\overline{\boldsymbol{\epsilon}}_{ij}) = \sigma_{ij}^2, \chi_{ij}$, and c_{ij}, respectively. Note also that the localization error is $e_{\text{p}}(\mathbf{p}) < 1\,\text{m}$ in only 7% of cases when no selection is performed (i.e., all the $L = N_{\text{meas}} = 66$ observations are processed). Therefore, the performance improvement offered by the proposed method for this selection of representative observations is remarkable.

Figure 4.9 shows the LEO as a function of e_{th} for $L = 5$ selected observations using the features considered in Figure 4.8. In the absence of walls (Figure 4.9(a)), the

localization error in 80% of cases is below 0.08 m for the non-blind case $h(\overline{\boldsymbol{\epsilon}}_{ij}) = \mathsf{e}_{ij}$, 0.98 m for $h(\overline{\boldsymbol{\epsilon}}_{ij}) = \sigma^2_{ij}$, 0.72 m for $h(\overline{\boldsymbol{\epsilon}}_{ij}) = \chi_{ij}$, 0.74 m for $h(\overline{\boldsymbol{\epsilon}}_{ij}) = \mathsf{c}_{ij}$, and 0.84 m for the random observation selection. Note that, the random choice shows similar performance to the other selection techniques in the absence of obstructions. This is due to the fact that range measurements almost have the same representativeness in the absence of obstruction-loss and excess delay. In the presence of walls (Figure 4.9(b)), the localization error in 80% of cases is below 0.42 m for the non-blind case $h(\overline{\boldsymbol{\epsilon}}_{ij}) = \mathsf{e}_{ij}$, 1.1 m for $h(\overline{\boldsymbol{\epsilon}}_{ij}) = \sigma^2_{ij}$, 0.96 m for $h(\overline{\boldsymbol{\epsilon}}_{ij}) = \mathsf{k}_{ij}$, and 1 m for $h(\overline{\boldsymbol{\epsilon}}_{ij}) = \mathsf{c}_{ij}$. Note that the localization error is above 3 m in 49% of cases when the subset of observations is randomly selected. This highlights that, together with complexity reduction, the processing of a small subset of properly selected representative observations significantly improves the localization performance. It is remarkable that proper observation selection can provide localization performance close to that in the absence of walls.

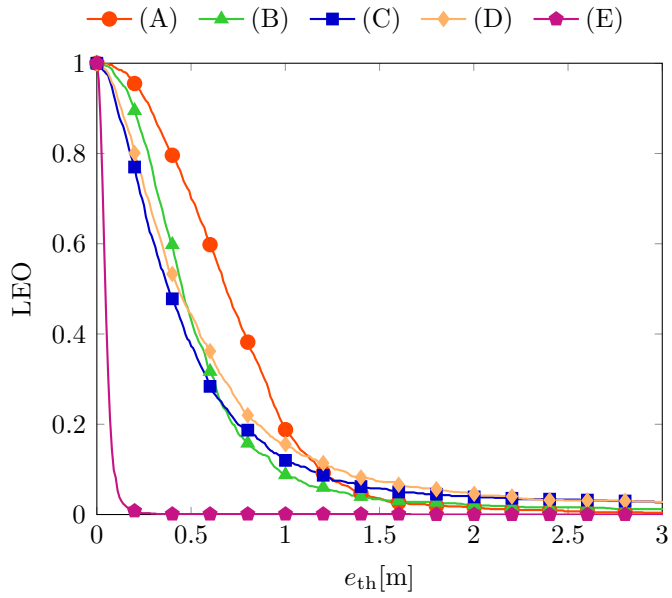

(a) Without walls.

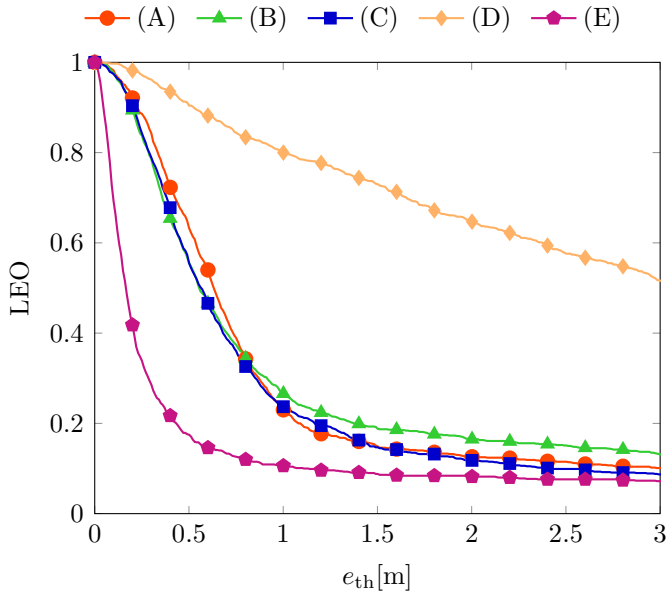

(b) With walls.

Figure 4.9: LEO as a function of e_{th}, with $L = 5$ and $N_{\text{meas}} = 66$, for the cases (A) $h(\overline{\boldsymbol{\epsilon}}_{ij}) = \sigma_{ij}^2$, (B) $h(\overline{\boldsymbol{\epsilon}}_{ij}) = \kappa_{ij}$, (C) $h(\overline{\boldsymbol{\epsilon}}_{ij}) = \mathsf{M}_{ij}$. The case (D) represents the random choice of L observations. The case (E) refers to the non-blind cases, where $h(\overline{\boldsymbol{\epsilon}}_{ij}) = e_{ij}^2$.

Chapter 5

Passive Tracking

5.1 Tracking with Sensor Radar Networks

Tracking of moving targets (objects, persons, and vehicles) enables several applications in military, security, and safety sectors. While active tracking relies on targets that emit signals, passive tracking via SRs relies on a network of sensors that emit radar signals and receive them after backscattering from the target [5, 61, 121]. The inference of target position, which is based on the joint processing of received waveforms and prior knowledge, is particularly challenging in indoor environments, where multipath, clutter, and NLOS conditions affect the received waveforms.

The literature considers SRs to be a low-power and low-complexity solution for accurate detection and tracking of moving targets. Recently, UWB SRs have gained interest owing to their ability to resolve multipaths and penetrate obstacles [9,22,93]. It has been shown that UWB SRs can provide submeter tracking accuracy even in harsh indoor environments [32, 118, 122].

The fundamental question related to passive tracking via SRs under complexity constraints is the following: how to design the network (e.g., sensor positions and radar configurations) and to allocate the processing (e.g., ranging and tracking) resources for different tasks? The answers to this question will provide insights into the efficient design of high accuracy SRs. The goal of this letter is to illustrate the SR performance improvement that can be obtained by properly designing the radar network and allocating the processing resources. Previous works on SRs separately investigated the following aspects: sensor positions [123], wireless propagation [124], ranging techniques [29], and tracking algorithms [15]. Our view is that the joint design of radar network, waveform processing, and tracking algorithm can significantly

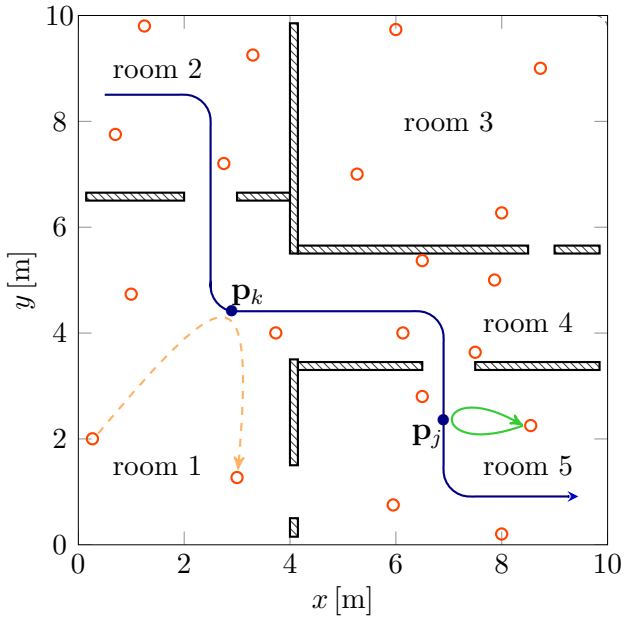

Figure 5.1: An example of SR deployment (red circles) and of a target trajectory (solid blue line). The blue dots indicate target positions at time indexes k and j. Continuous green and dashed brown arrows exemplify a transmitter-target-receiver radar signal for monostatic and multistatic configuration, respectively.

improve the SR performance.

This letter explores SRs by considering network configuration, propagation impairments, as well as ranging and tracking techniques. A case study in indoor environments is provided (with obstructions, clutter, and multipath) and the performance (tracking error and outage) of monostatic and multistatic UWB SRs for different settings is quantified. The case study provides insights into the joint design of networking and processing for SRs operating in challenging environments.

5.1.1 Networking and Propagation

Consider an SR (see e.g., Figure 5.1) composed of N_s sensors, of which N_t serve as transmitters and N_r serve as receivers.[1] The radar configuration is monostatic or multistatic depending on whether transmitters and receivers are co-located or not.

The radar configuration determines the index set $\mathcal{P}$ of transmitter-receiver pairs,

[1] The discrimination among different transmitted UWB signals can be performed by timehopping (TH) and/or direct-sequence (DS) codes [93].

where each $(i,j) \in \mathcal{P}$ denotes the ith transmitter emitting radar signals and the jth receiver collecting them after backscattering from the target. For a target position $\mathbf{p} \in \mathbb{R}^d$ at time k, the signal path-length is given by $d_{ij}(\mathbf{p})$, which is the distance from the ith transmitter to the target to the jth receiver. The range estimate results in $\hat{d}_{ij}(\mathbf{p}) = \hat{\tau}_{ij}\mathbf{p}\, c$, where c is the speed of light and $\hat{\tau}_{ij}\mathbf{p}$ is the estimated TOA of a backscattered signal, at the jth receiver, emitted by the ith transmitter [2]. The delay $\tau_{\min}$ is the minimum resolvable delay for the multistatic case and as the blind temporal range for the monostatic case.[2]

The accuracy of TOA estimation depends on radar signal propagation, which is affected by multipath, clutter, and obstructions. Specifically, when the target is at $\mathbf{p}$, the received SNR is given by

$$\gamma_{ij}(\mathbf{p}) = P_{\mathrm{R},ij}(\mathbf{p})\, T_{\mathrm{g}}/N_0 \tag{5.1}$$

where $P_{\mathrm{R},ij}(\mathbf{p})$ is the received power per pulse, T_{g} is the pulse repetition period (PRP), and N_0 is the one-sided PSD of the noise. The TOA can be estimated if the received SNR is above a value $\gamma^\star$, which corresponds to the minimum required received power per pulse $P_{\mathrm{R}}^\star$.[3]

For UWB signals propagating in indoor environments, we determine the received power as in [122] and model the obstruction-loss accounting for the number and the type (i.e., electromagnetic characteristics) of obstructions in the transmitter-to-target-to-receiver path, as in [115]. Note that the presence of objects and walls obstructing the signal path also causes an excess delay in the TOA estimates. These effects are quantified based on experimentations performed in a typical building [13]. In particular, the walls cause a positive bias $\mu_{ij}(\mathbf{p}) \simeq \Delta/c$ on the TOA estimate, where Δ is the aggregate thickness of the walls.

5.1.2 Signal Processing

The signal processing to infer target positions is now described. First, received radar waveforms are processed to determine transmitter-target-receiver distances based on TOA estimation. Then, such radar ranging information is used to infer target positions based on the tracking algorithm.

[2]The $\tau_{\min}$ is determined by the relative delay between the backscattered signal and the direct signal for multistatic configuration, and by the switching time between transmitting and receiving modes for monostatic configuration.

[3]The target in $\mathbf{p}$ is considered as detected if $\exists (i,j) \in \mathcal{P}$ s.t. $P_{\mathrm{R},ij}(\mathbf{p}) > P_{\mathrm{R}}^\star$ (i.e., at least one TOA estimation can be performed).

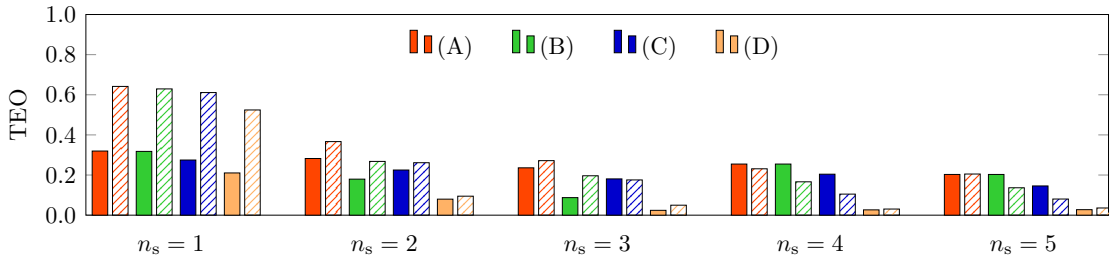

Figure 5.2: TEO for $e_{\text{th}} = 1\text{m}$, $T_{\text{d}} = 2\,\text{ns}$, and varying number of sensors per room n_{s}. The processing configurations A, B, C, D are considered for monostatic (uniform pattern) and multistatic (dashed pattern) networking.

5.1.3 TOA Estimation

The TOA estimation based on an ED is now considered, which is amenable to efficient low-complexity implementation for UWB ranging [29]. Before energy detection, received waveforms are processed by a band-pass filter and clutter mitigation techniques. The signal at the input of the ED is

$$v_{ij}(t) = \sum_{p=0}^{N_{\text{p}}-1} \sum_{l=1}^{L_{\text{p}}} \alpha_{ij}^{(l)}\, s(t - p\,T_{\text{g}} - \tau_{ij}^{(l)}) + n_{ij}(t) \tag{5.2}$$

where N_{p} is the number of transmitted pulses, L_{p} is the number of multipath components (with amplitude $\alpha_{ij}^{(l)}$ and delay $\tau_{ij}^{(l)}$ for the lth component), $s(t)$ is the filtered pulse shape, and $n_{ij}(t)$ is the filtered noise. The TOA to be estimated is that of the first path (i.e., $\tau_{ij}(\mathbf{p}) = \tau_{ij}^{(1)}$).[4] Target detection and TOA estimation are performed by collecting $N_{\text{bin}} = \lfloor T_{\text{g}}/T_{\text{d}} \rfloor$ energy bins, where T_{d} is the dwell time, as described in 3.1.1.[5] Then, the decision vector $\overline{\boldsymbol{\epsilon}}_{ij} = \left(\overline{\epsilon}_{ij}^{(0)}, \overline{\epsilon}_{ij}^{(1)}, \ldots, \overline{\epsilon}_{ij}^{(N_{\text{bin}}-1)}\right)$ is obtained by averaging each energy bin over the N_{p} transmitted pulses. Each $\overline{\epsilon}_{ij}^{(q)}$ is then compared with a threshold ξ_{ij}, and the first crossing event provides the TOA estimate [29, 98].

5.1.4 Tracking Algorithm

The tracking algorithm infers the target position $\mathbf{p}_k$ at each time index k (i.e., the current state vector) from a set of TOA estimates (i.e., observations), a mobility

[4] The value $\tau_{ij}^{(1)}$ is in the range $[\tau_{\min}, T_{\text{a}}]$, where T_{a} is the greatest possible TOA value in the environment and T_{g} is chosen such that $T_{\text{g}} > T_{\text{a}}$.

[5] The notation $\lfloor x \rfloor$ denotes the largest integer not greater than x.

model (i.e., relation between the current and the prior state vectors), and a perception model (i.e., relation between the observations and the current state vector [5]. Following a Bayesian approach, the position estimate $\hat{\mathbf{p}}_k$ is determined as the value that maximizes the positional belief $b(\mathbf{p}_k) = p(\mathbf{p}_k|\hat{\boldsymbol{\tau}}_{\mathcal{P}_{\text{sel}}}(\mathbf{p}_{1:k}))$, which is the posterior distribution of the state vector, conditioned on a subset of observations $\hat{\boldsymbol{\tau}}_{\mathcal{P}_{\text{sel}}}(\mathbf{p}_{1:k})$ with $\mathcal{P}_{\text{sel}} \subseteq \mathcal{P}$, i.e. $\hat{\mathbf{p}}_k = \text{argmax}_{\mathbf{p}_k}\, b(\mathbf{p}_k)$.[6] In particular, the positional belief is

$$b(\mathbf{p}_k) \propto p\left(\hat{\boldsymbol{\tau}}_{\mathcal{P}_{\text{sel}}}(\mathbf{p}_{1:k})|\mathbf{p}_k\right) \times p\left(\mathbf{p}_k|\hat{\boldsymbol{\tau}}_{\mathcal{P}_{\text{sel}}}(\mathbf{p}_{1:k-1})\right) \tag{5.3}$$

where the first term is the perception model and

$$p\left(\mathbf{p}_k|\hat{\boldsymbol{\tau}}_{\mathcal{P}_{\text{sel}}}(\mathbf{p}_{1:k-1})\right) = \int p(\mathbf{p}_k|\mathbf{p}_{k-1})\, p\left(\mathbf{p}_{k-1}|\hat{\boldsymbol{\tau}}_{\mathcal{P}_{\text{sel}}}(\mathbf{p}_{1:k-1})\right) \tag{5.4}$$

marginalizes the mobility model $p(\mathbf{p}_k|\mathbf{p}_{k-1})$ with respect to $\mathbf{p}_{k-1}$. The subset of selected observations $\mathcal{P}_{\text{sel}}$ is chosen based on a selection criterion [125]. Specifically, in the case study we select the $|\mathcal{P}_{\text{sel}}| = 3$ observations that provided the maximum received power, i.e., $\min\{P_{\text{R},\mathcal{P}_{\text{sel}}}\} \geq \max\{P_{\text{R},\mathcal{P}\setminus\mathcal{P}_{\text{sel}}}\}$.

Among the common implementations of Bayesian algorithms presented in2.3, we consider the PF algorithm, which can outperform EKF in non-Gaussian noisy observations [15].[7] In particular, the positional belief at time k is represented by a set of N_{par} random samples (particles) at $\{\mathbf{p}_k^{(n)}\}$, with $n = 1, 2, ..., N_{\text{par}}$. The mobility and perception models are used to predict, update, and resample the positional belief at each k. In particular, a Gaussian mobility model is given by $\mathbf{p}_k^{(n)}|\mathbf{p}_{k-1}^{(n)} \sim \mathcal{N}(\boldsymbol{\mu}_k^{(n)}, \sigma_{\text{m},k}^2\, \mathbf{I})$, where $\mathbf{I}$ is the identity matrix and $\sigma_{\text{m},k}^2$ depends on the target mobility.[8] The mean $\hat{\boldsymbol{\mu}}_k^{(n)}$ is determined based on previous position estimates as $\hat{\boldsymbol{\mu}}_k^{(n)} = \mathbf{p}_{k-1}^{(n)} + \hat{\mathbf{v}}_k\, T_{\text{L}}$, where $\hat{\mathbf{v}}_k$ is the average speed calculated over N_{w} previous positions, and T_{L} is the time between two position estimations. A perception model for particles with independent and gaussian-distributed observations, is considered with variance $\sigma_{\text{p},k}^2$ depending on ranging and propagation.

5.1.5 Case Study

The operating environment is now described and the performance of monostatic and multistatic SRs is evaluated.

[6] $\hat{\boldsymbol{\tau}}_{\mathcal{P}_{\text{sel}}}(\mathbf{p}_{1:k}) \triangleq \{\hat{\tau}_{ij}(\mathbf{p}_h) \text{ s.t. } (i,j) \in \mathcal{P}_{\text{sel}}, h = 1, 2, ..., k\}$.

[7] Note that, in general, the observations follow a non-Gaussian distribution due to multipath and clutter residual.

[8] $\mathcal{N}(\boldsymbol{\mu}, \boldsymbol{\sigma}^2)$ denotes the d-dimensional Gaussian distribution with mean $\boldsymbol{\mu}$ and variance $\boldsymbol{\sigma}^2$.

Operating Environment

A SRs is considered, with UWB impulse radios deployed in the operating environment shown in Figure 5.1 with wall thickness of 15 cm. In the monostatic configuration, each sensor transmits and receives ($N_{\rm t} = N_{\rm s}$). In the multistatic configuration, one sensor per room transmits ($N_{\rm t} = 5$); specifically, the sensor closest to $\hat{\mathbf{p}}_{k-1}$ transmits at time $k > 1$ (random at $k = 1$). The target speed is $|\mathbf{v}| = 1\,\text{m/s}$ along 10 trajectories with $T_{\rm L} = 0.5\,\text{s}$. The performance for $N_{\rm s} = 5, 10, ..., 25$ sensors is evaluated (i.e., $n_{\rm s} = 1, 2, ..., 5$ sensors per room, respectively).[9]

Transmitters emit a sequence of RRC pulses with $T_{\rm g} = 200\,\text{ns}$ and transmitted PSD compliant with the European lower band. The transmitted PSDs for the monostatic and multistatic configurations are set to have the same total transmitted power. The minimum received power and the noise power spectral density are $P_{\rm R}^{\star} = -110\,\text{dBm}$ and $N_0 = -200\,\text{dBW/Hz}$, respectively. The channel impulse response is modeled with $L_{\rm p} = 20$ paths spaced by $\delta_{\rm p} = 4\,\text{ns}$, exponential power delay profile with decay constant $\epsilon = 20$ ns, and Nakagami-2 distributed path amplitudes. The target RCS is Swerling type III distributed with mean $1\,\text{m}^2$ (typical for the human body) [2]. The ED-based TOA estimates $\hat{\boldsymbol{\tau}}_{\mathcal{P}}(\mathbf{p})$ are obtained with $T_{\rm d} = 1, 2, 4\,\text{ns}$ and $N_{\rm p} = 32, 128$. A best-case analysis for ED-based ranging is provided by considering the threshold ξ_{ij} that minimizes the RMSE of TOA estimates for each received SNR value.

Static clutter is generated using 100 scatterers for each transmitter-receiver pair, with uniformly distributed TOAs and a Swerling type V distributed RCS with mean $1\,\text{m}^2$. The empty-room technique is employed for clutter mitigation [104]. Specifically, a reference waveform is subtracted from the received waveform for each transmitter-receiver pair. This reference waveform is obtained by averaging 100 received waveforms in the absence of target. The tracking algorithm is based on PF with $N_{\rm par} = 100$ and 1000, $\sigma_{{\rm p},k}^2 = 1$ for all k, and $N_{\rm w} = 2$. The value of $\sigma_{{\rm m},k}^2$ is chosen such that the nth estimated particle at time k is within a circle centered at $\hat{\boldsymbol{\mu}}_k^{(n)}$ of radius $|\hat{\mathbf{v}}_k|\,T_{\rm L}$ with probability 0.9. When the selection of observations is performed, the set $\hat{\boldsymbol{\tau}}_{\mathcal{P}_{\rm sel}}$ includes three observations $|\mathcal{P}_{\rm sel}| = 3$ corresponding to the signals received with the highest power; otherwise it includes all the available TOA estimates $|\mathcal{P}_{\rm sel}| = |\mathcal{P}|$.

[9] The $n_{\rm s}$ sensors are deployed on a circle inscribed in each room, equally spaced from each other, and with initial angle $\pi/6$.

Performance Evaluation

The tracking performance is quantified in the indoor environment shown in Figure 5.1 by simulating several configurations of the network and varying the setting of signal processing.[10] Specifically, we determine the effects of (i) network topology by employing monostatic and multistatic SR with $n_{\mathrm{s}} = 2, 3, 4$, and 5 sensors; (ii) TOA estimation by collecting $N_{\mathrm{pulse}} = 32$ and 128 pulses for energy detection with $T_{\mathrm{d}} = 1, 2$, and 4 ns; (iii) tracking algorithm by sampling with $N_{\mathrm{par}} = 100$ and 1000 particles; and (iv) selection of observations by considering all the available observations or a subset of them. Four processing settings are considered: (A) $N_{\mathrm{pulse}} = 32$, $N_{\mathrm{par}} = 100$, and $|\mathcal{P}_{\mathrm{sel}}| = |\mathcal{P}|$; (B) $N_{\mathrm{pulse}} = 32$, $N_{\mathrm{par}} = 100$, and $|\mathcal{P}_{\mathrm{sel}}| = 3$; (C) $N_{\mathrm{pulse}} = 32$, $N_{\mathrm{par}} = 1000$, and $|\mathcal{P}_{\mathrm{sel}}| = |\mathcal{P}|$; and (D) $N_{\mathrm{pulse}} = 128$, $N_{\mathrm{par}} = 100$, and $|\mathcal{P}_{\mathrm{sel}}| = |\mathcal{P}|$. Note that cases B, C, and D differ from A for the values of $|\mathcal{P}_{\mathrm{sel}}|$, N_{par}, and N_{pulse}, respectively. Tracking performance is evaluated in terms of tracking error, i.e., the Euclidean distance between the estimated and the true position, tracking RMSE, and tracking error outage (TEO), i.e., the probability that tracking error is above a given value e_{th}.[11]

Figure 5.2 shows the TEO for monostatic and multistatic configurations with $e_{\mathrm{th}} = 1\,\mathrm{m}$, $T_{\mathrm{d}} = 2\,\mathrm{ns}$, and different n_{s} values. It can be seen that, in each setting, the TEO tends to decrease as n_{s} increases, with negligible improvement for $n_{\mathrm{s}} > 3$. Moreover, the multistatic configuration is more sensitive to the number of sensors per room. For example in setting A, varying n_{s} from 1 to 5 reduces the TEO from 0.31 to 0.20 with the monostatic SR, whereas it reduces the TEO from 0.64 to 0.20 with the multistatic SR. In the setting D, the TEO reduces from 0.21 to 0.02 for the monostatic SR and from 0.52 to 0.03 for the multistatic SR. Figure 5.2 also shows that multistatic SR experiences a higher TEO than monostatic SR at low values of n_{s} because the number of LOS conditions is smaller for the former than the latter.

Figure 6.6 shows the TEO as a function of e_{th} for $T_{\mathrm{d}} = 2\,\mathrm{ns}$ with $N_{\mathrm{s}} = 20$. It can be seen that TEO benefits more from a larger number of pulses collected for ranging than from a larger number of particles used for tracking. For $e_{\mathrm{th}} = 0.5\,\mathrm{m}$, varying the processing from setting A to C or D changes the TEO from 0.57 to 0.51 or 0.14 with the monostatic SR and from 0.49 to 0.36 or 0.12 with the multistatic, respectively. Moreover, especially for monostatic SR, results obtained with $|\mathcal{P}_{\mathrm{sel}}| = 3$

[10] The main impairments affecting SR performance are taken into account, even though additional phenomena might occur in real scenarios.

[11] The TEO is evaluated over 10 trajectories each with 100 realizations of random processes.

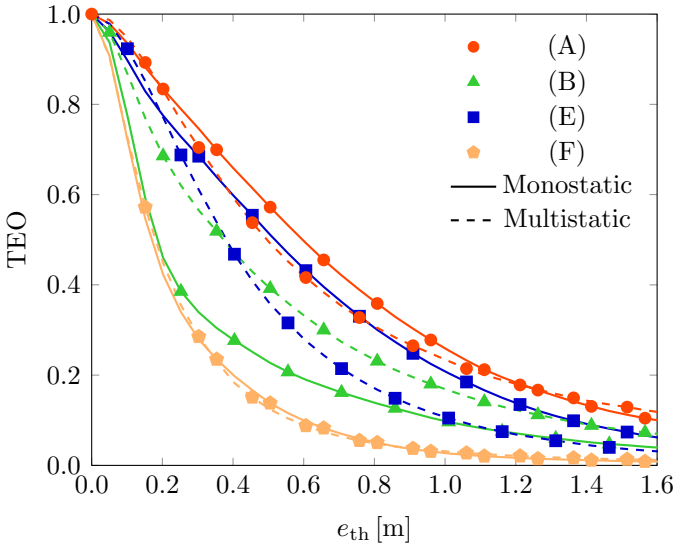

Figure 5.3: TEO as a function of e_{th} for the cases A, B, E, and F, with $N_{\text{s}} = 20$ (i.e., $n_{\text{s}} = 4$) sensors in monostatic or multistatic configuration.

	Monostatic			Multistatic		
n_{s}	$T_{\text{d}} = 4\,\text{ns}$	$T_{\text{d}} = 2\,\text{ns}$	$T_{\text{d}} = 1\,\text{ns}$	$T_{\text{d}} = 4\,\text{ns}$	$T_{\text{d}} = 2\,\text{ns}$	$T_{\text{d}} = 1\,\text{ns}$
1	1.12	1.31	0.97	14.41	14.41	14.41
2	0.63	0.55	0.57	0.88	0.73	0.78
3	0.30	0.21	0.39	0.48	0.40	0.35
4	0.28	0.24	0.20	0.35	0.30	0.26
5	0.30	0.22	0.20	0.40	0.29	0.32

Table 5.1: Tracking RMSE for $N_{\text{pulse}} = 128$, $N_{\text{par}} = 1000$, and $|\mathcal{P}_{\text{sel}}| = 3$ varying n_{s}, T_{d} [ns], and network configuration.

and $N_{\text{pulse}} = 32$ are comparable with those obtained with $|\mathcal{P}_{\text{sel}}| = 3$ and $N_{\text{pulse}} = 128$. Therefore, given N_{s} and e_{th}, the selection allows the collection of a lower number of pulses.

To investigate the effect of dwell time on the RMSE, Table I lists the tracking RMSE when $N_{\text{pulse}} = 128$, $N_{\text{par}} = 1000$, $|\mathcal{P}_{\text{sel}}| = 3$, $T_{\text{d}} = 1, 2$, and $4\,\text{ns}$, and with different numbers of sensors per room. Note that, for a given value of N_{pulse}, reducing T_{d} is less effective than increasing the number of n_{s}.

5.2 Tracking via Signals of Opportunity

Localization and tracking is important for a number of applications, especially in military, security, and safety sectors. Depending on the application, the processing of wireless signals at different receivers allows to infer the position of transmitters, receivers, or others (e.g., devices, objects, or persons). In particular, we refer to active or passive localization depending on whether the transmitting source is collaborative or non-collaborative, respectively. For example, the processing at different receivers of signals transmitted by non-collaborative sources, namely transmitters of opportunity, may be exploited to detect and localize the transmitter itself or a mobile receiver (e.g., passive network localization) or passive scatterers in the monitored environment (e.g., passive radar).

Passive radars exploit illuminators of opportunity for stealth and low-cost tracking [2]. In general, a network of receiving-only radars receives the signal of opportunity directly from the non-collaborative sources and backscattered by the target. Several signal processing techniques are proposed in literature to estimate the position of the target based on such received waveforms. For example, TDOA, FDOA and AOA metrics are often adopted in this context since no synchronization is guaranteed between receivers and transmitters [3, 4]. Since in a general case the transmitted signal is unknown and uncontrolled, a reference receiver is positioned so that it receives only the direct signal from the illuminator of opportunity (see, e.g., Figure 5.4). Then, the direct signal is decoded to provide to the network a reference signal, which is exploited by other receivers for signal processing.

Digital signals are excellent candidates for signals of opportunity, thanks to their wide availability and low error-rate decoding. Among digital signal, orthogonal frequency division multiplexing (OFDM) transmission recently gained interest for passive radar since it can be efficiently implemented as a fast Fourier transform and used to identify targets based on Fourier analysis across subsequent blocks [126, 127]. In particular, previous works on passive radar investigated radio/television stations, broadcasting in the VHF/UHF frequency bands, and WiFi base stations as illuminators of opportunity [128–130]. For active localization purposes, the LTE standard specifies a dedicated downlink signal for positioning, i.e. the positioning reference signal (PRS). Several works investigated active localization via LTE signals and evaluate the performance in different environments [131–133]. The LTE signals as illuminators of opportunity for tracking via passive radars are considered.

One of the main impairments affecting localization via passive radar are related

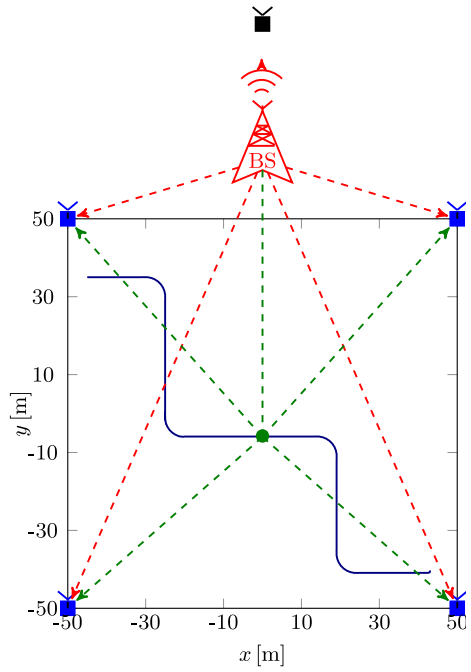

Figure 5.4: Passive radar scenario and monitored area. Base station, reference receiver and radars are illustrated in red, black, and blue, respectively. The blue line represents the target trajectory. Red and green dashed lines represents the direct and backscattered signal paths, respectively.

to the absence of control on illumination since they use broadcast signals, and a transmitted signal estimation has to be implemented. However, for many signals of opportunity this operation can be considered perfectly performed (e.g., perfect symbol recovering for LTE signals). Neverthless, the separation of the direct path and reflections within the received signal is challenging since the dynamic range between direct signal and reflections due to target is of the order of 100 dB and cannot be handled by analog-to-digital converters. Therefore, even when the source position is perfectly known, clutter pre-mitigation is required, which is performed via compensation techniques such as null-steering or directional antennas [134].

The main goals are to

- introduce a passive radar system using LTE signals of opportunity;
- propose a Bayesian framework for the passive tracking and velocity estimation of moving targets;
- evaluate the performance of a LTE-based passive radar in a case study with multipath fading channel.

Passive radar are explored by considering network configuration, wireless propagation, and signal processing.

5.2.1 System Model

A LTE base station is considered in known position $\mathbf{p}_{\mathrm{BS}}$ and transmits a broadcast signal

$$\tilde{s}(t) = \Re\{e^{j2\pi f_c t} s(t)\} \tag{5.5}$$

where the baseband signal is

$$s(t) = \sum_{i=-\infty}^{+\infty} s_i(t - i\,T')\,. \tag{5.6}$$

In particular, $s(t)$ is an OFDM signal using multicarrier modulation scheme given by

$$s_i(t) = \sum_{n=-N/2}^{N/2-1} a_i[n] e^{j2\pi\Delta_{\mathrm{f}} t}\, \mathbb{1}_{(-T_{\mathrm{cp}},T]}\{t\}, \tag{5.7}$$

where $a_{\mathrm{i}}[n]$ are the data symbols carried by each block, Δ_{f} is the frequency spacing between two subcarrier frequencies, $T' = T + T_{\mathrm{cp}}$, and the ciclic prefix time T_{cp} is used to maintain a cyclic convolution between the transmitted waveform and the channel.

A reference receiver in position $\mathbf{p}_{\mathrm{ref}}$ is such that it receives only the transmitted signal

$$r_{\mathrm{ref}}(t) = A_{\mathrm{ref}} s(t - \tau_{\mathrm{ref}}) + w_{\mathrm{ref}}(t)\,, \tag{5.8}$$

where $w_{\mathrm{ref}}(t)$ is the AWGN signal with one-sided spectral density N_0, A_{ref} is the amplitude attenuation, $\tau_{\mathrm{ref}} = \|\mathbf{p}_{\mathrm{ref}} - \mathbf{p}_{\mathrm{BS}}\|/c$ is the direct signal arrival time and c is the speed of light.

Based on the state of the art, we can assume that the LTE signal is decoded and perfectly reconstructed based on the direct signal and that the null steering attenuates the direct signal to the level of clutter, reducing the corresponding dynamic range [134]. Consider a network of radars indexed by $\mathcal{R}$ in position $\mathbf{r}_k$ with $k \in \mathcal{R}$

monitoring an area $\mathcal{A}$, which is illuminated by the LTE base station. Then, the signal received by the kth radar in the absence of target is $\tilde{r}_k(t) = \Re\{e^{j2\pi f_c t} r_k(t)\}$, where the baseband signal after down-conversion results in

$$r_k(t) = \sum_{l=1}^{L_\mathrm{k}} A_{k,l} x(t - \tau_{k,l}) + w(t) \tag{5.9}$$

where $w_k(t)$ is the AWGN signal with one-sided spectral density N_0, L_k is the number of multipath components; $A_{k,l}$ and $\tau_{k,l}$ are the amplitude and arrival time of the lth path.

When a target is present in the monitored environment in position $\mathbf{p}$, the received signal is composed of the direct signal, the signal backscattered by the target, and the multipath components of both direct and backscattered signals. Then (5.9) becomes

$$\begin{aligned} r_k(t) = &\sum_{l=1}^{L_\mathrm{k}} A_{k,l} x(t - \tau_{k,l}) \\ &+ \sum_{h=1}^{P_\mathrm{k}} B_{k,h} e^{jv\psi_{k,h}(\mathbf{p})} x(t - \theta_{k,h}(\mathbf{p})) + w(t) \end{aligned} \tag{5.10}$$

where the multipath components due to the direct signal, i.e., clutter, are indexed by l, while the reflections due to target backscattering are indexed by h. In particular, $\psi_{k,h}(\mathbf{p}) = 2\pi\alpha_{k,h}(\mathbf{p}) f_\mathrm{c} t$ where $\alpha_{k,h}(\mathbf{p}) = f_{k,h}(\mathbf{p})/(v f_\mathrm{c}) = \left(\cos\omega_\mathrm{t}(\mathbf{p}) + \cos\omega_{\mathrm{r},k}(\mathbf{p})\right)/c$ where $f_{k,h}(\mathbf{p})$ is the Doppler shift, which is assumed to be constant during the integration time, $\omega_\mathrm{t}(\mathbf{p})$ is the angle describing the relative direction between the transmitter and the target, and $\omega_{\mathrm{r},k}(\mathbf{p})$ is the angle describing the relative direction between the target and the kth receiver. The adoption of clutter mitigation techniques is considered, such that the

$$\begin{aligned} r_k(t) = \frac{1}{\xi} \Bigg(&\sum_{l=1}^{L_\mathrm{k}} A_{k,l} x(t - \tau_{k,l}) \\ &+ \sum_{h=1}^{P_\mathrm{k}} B_{k,h} e^{jv\psi_{k,h}(\mathbf{p})} x(t - \theta_{k,h}(\mathbf{p})) \Bigg) + w(t) \end{aligned} \tag{5.11}$$

In a general case, the transmitted signal is reconstructed by decoding the data symbol at the reference receiver. Based on such reconstruction, a reference signal, i.e. an estimation of the transmitted signal, is available for the entire network and it is given by

$$\hat{s}(t) = \sum_{i=-\infty}^{+\infty} \hat{s}_i(t - i\,T') \tag{5.12}$$

where

$$\hat{s}_i(t) = \sum_{n=-N/2}^{N/2-1} \hat{a}_i[n] e^{j2\pi\Delta_{\mathrm{f}} t} \, \mathbb{1}_{(-T_{\mathrm{cp}},T]}\{t\} \tag{5.13}$$

Without loss of generality, perfect signal recovery is considered so that $\hat{s}(t) = s(t)$ [134].

5.2.2 Bayesian Filtering

The signal received at each radar is processed to detect and track any object present in the monitored environment moving along a trajectory described by $\mathbf{p}(t)$ and absolute velocity $v(t)$. The localization update rate is $R_{\mathrm{L}} = 1/T_{\mathrm{L}}$, where T_{L} is the time between two position and absolute velocity estimations, e.g. $\hat{\mathbf{p}}_1 = \hat{\mathbf{p}}(T_{\mathrm{L}})$, $\hat{v}_1 = \hat{v}(T_{\mathrm{L}})$, $\hat{\mathbf{p}}_2 = \hat{\mathbf{p}}(2T_{\mathrm{L}})$, and $\hat{v}_2 = \hat{v}(2T_{\mathrm{L}})$. Tracking is based on a Bayesian approach for the estimation of the parameter $\boldsymbol{\theta}_q = [\mathbf{p}_q, v_q]$ [15]. In particular, at each time index q the estimated position and velocity are determined as

$$\hat{\boldsymbol{\theta}}_{\boldsymbol{q}} = [\hat{\mathbf{p}}_q, \hat{v}_q] = \underset{\boldsymbol{\theta}\in\boldsymbol{\Theta}}{\operatorname{argmax}} \, b_q(\boldsymbol{\theta}) \, . \tag{5.14}$$

where $b_q(\boldsymbol{\theta})$ is the belief function at time $t_q = q\,T_{\mathrm{L}}$ and $\boldsymbol{\Theta}$ depends on the monitored environment and the range of considered values for velocity. The belief function at time $t_q = q\,T_{\mathrm{L}}$ is determined as

$$b_q(\boldsymbol{\theta}) = \eta \prod_{k\in\mathcal{R}} f_k^{(q)}(\boldsymbol{\theta}|r_k^{(q)}(t)) \tag{5.15}$$

where $r_k^{(q)}(t)$ is the portion of received signal corresponding to an observation time T_{obs}, i.e., $r_k^{(q)}(t) = r_k(t)$ if $t \in [qT_{\mathrm{obs}}, (q+1)T_{\mathrm{obs}})$ and 0 otherwise, η is a normalization constant, and $f_k^{(q)}(\boldsymbol{\theta}|r_k^{(q)}(t))$ is the PDF for the kth radar, which is assumed statistically independent over the radars. In particular, the PDF for the kth radar is given by

$$f_k^{(q)}(\boldsymbol{\theta}|r_k^{(q)}(t)) = \Lambda_k(r_k^{(q)}(t)|\boldsymbol{\theta}) \int_{\boldsymbol{\Theta}} f_{\mathrm{m}}^{(q)}(\boldsymbol{\theta}|\tilde{\boldsymbol{\theta}}) \, b_{q-1}(\tilde{\boldsymbol{\theta}}) d\tilde{\boldsymbol{\theta}} \tag{5.16}$$

where $\Lambda_k(r_k^{(q)}(t)|\mathbf{p})$ is the likelihood function for the observed waveform $r_k^{(q)}(t)$, $f_{\mathrm{m}}^{(q)}(\boldsymbol{\theta}|\tilde{\boldsymbol{\theta}})$ is the mobility model and $b_{q-1}(\tilde{\boldsymbol{\theta}})$ is the belief at the previous time index $q-1$. The likelihood function for the jth reader becomes

$$\Lambda_k(r_k^{(q)}(t)|\boldsymbol{\theta}) \propto \exp\left\{-\frac{1}{N_0}\int_{t_q}^{t_q+T_{\mathrm{obs}}} \left(\hat{r}_k^{(q)}(t,\boldsymbol{\theta}) - r_k^{(q)}(t)\right)^{\star} \times \left(\hat{r}_k^{(q)}(t,\boldsymbol{\theta}) - r_k^{(q)}(t)\right) dt\right\} \tag{5.17}$$

$\hat{r}_k^{(q)}(t,\boldsymbol{\theta})$ is a reference signal, which depends on the prior knowledge of the channel. In the absence of such prior information, we can assume $\hat{r}_k^{(q)}(t,\boldsymbol{\theta}) = e^{jv\psi_{k,h}(\mathbf{p})t}\hat{s}(t - \|\mathbf{p}-\mathbf{r}_k\|\,c)$. In this case, the likelihood reduces to

$$\Lambda_k(r_k^{(q)}(t)|\boldsymbol{\theta}) \propto z_k^{(q)}(\|\mathbf{p}-\mathbf{r}_k\|\,c, v\psi(\mathbf{p})) \tag{5.18}$$

where $z_k^{(q)}(\tau,\zeta)$ is the correlation function including the Doppler effect in ζ, as given by

$$z_k^{(q)}(\tau,\zeta) = \int_{qT_{\mathrm{obs}}}^{(q+1)T_{\mathrm{obs}}} e^{-j\zeta t}\,\hat{s}^{\star}(t-\tau) r_k^{(q)}(t)dt \tag{5.19}$$

The mobility model $f_{\mathrm{m}}^{(q)}(\mathbf{p}|\tilde{\boldsymbol{\theta}})$ is based on the previous position estimates. In particular, a Gaussian mobility model is given by

$$f_{\mathrm{m}}(\boldsymbol{\theta}|\tilde{\boldsymbol{\theta}}) = \frac{1}{\sqrt{2\pi}\sigma_{\mathrm{m},k}} e^{-\frac{\left\|\boldsymbol{\theta}-(\tilde{\boldsymbol{\theta}}+\dot{\boldsymbol{\theta}}T_{\mathrm{L}})\right\|^2}{2\sigma_{\mathrm{m},k}^2}} \tag{5.20}$$

where $\sigma_{\mathrm{m},k}^2$ depends on the target mobility. The parameter $\dot{\boldsymbol{\theta}}$ is determined based on previous position estimates as the average speed and acceleration calculated over N_{w} previous position and speed estimations.

5.2.3 Case Study

The case study is now presented by describing the performance metrics, system parameters, and numerical results.

Performance Metrics

As performance metrics for positioning we consider the localization error and the TEO. The TEO is defined as the probability that the localization error is below a

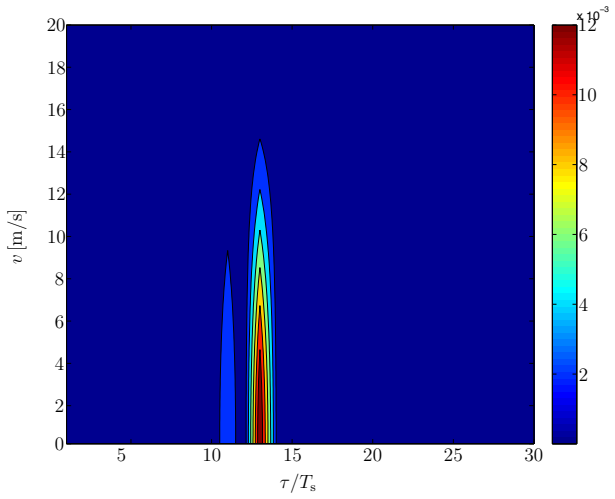

(a) $\xi_{\mathrm{dB}} = 0\,\mathrm{dB}$

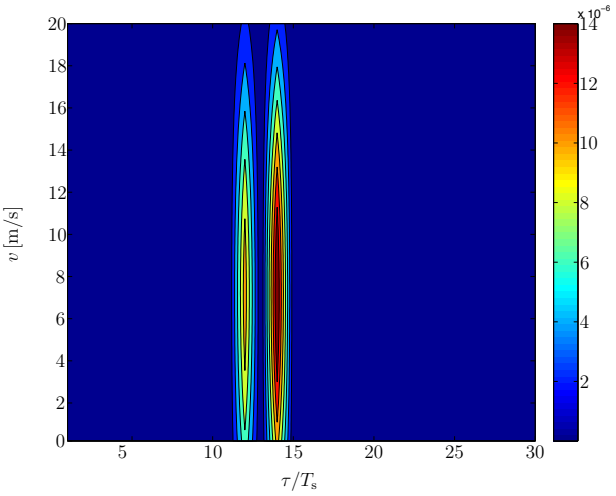

(b) $\xi_{\mathrm{dB}} = 50\,\mathrm{dB}$

Figure 5.5: Example of $z_k^{(q)}(\tau(\mathbf{p}), v\psi(\mathbf{p}))$ when the true value of $\tau/T_{\mathrm{s}} = 12$ and $\tau/T_{\mathrm{s}} = 11$ for the direct path, and the clutter mitigation factor is $\xi_{\mathrm{dB}} = 0, 50, 100\,\mathrm{dB}$

.

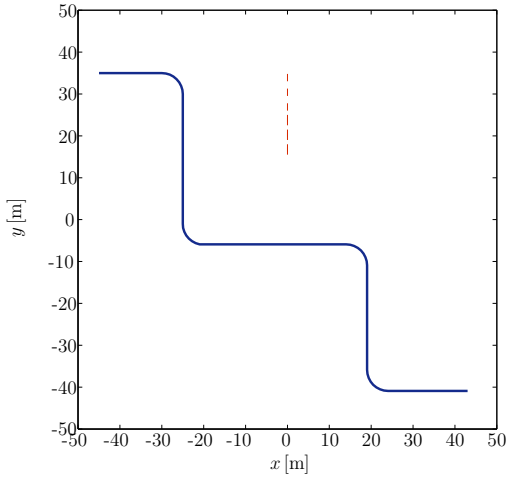

(a) $\xi_{\mathrm{dB}} = 0\,\mathrm{dB}$

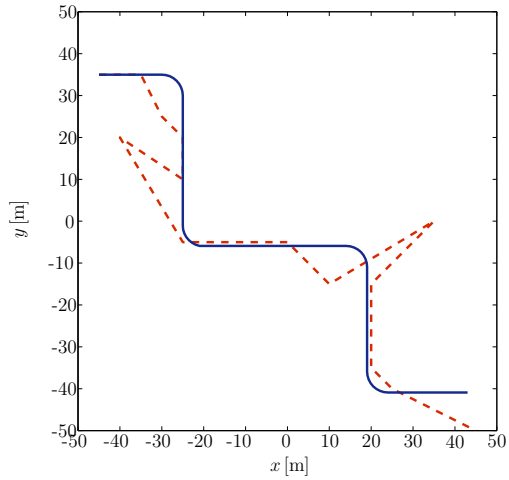

(b) $\xi_{\mathrm{dB}} = 50\,\mathrm{dB}$

Figure 5.6: Example of true and estimated trajectory for $\xi_{\mathrm{dB}} = 0$ and $50\,\mathrm{dB}$.

given target value e_{th} over the trajectory length. In particular, such probability is defined as

$$\begin{aligned} P_{\text{TEO}} &= \mathbb{P}\{e_{\text{p}}(\mathbf{p}_q) > e_{\text{th}}\} \\ &= \frac{1}{Q}\sum_{q=1}^{Q}\mathbb{E}\{\mathbb{1}_{(e_{\text{th}},+\infty)}\{\|\hat{\mathbf{p}}_q - \mathbf{p}_q\|\}\} \end{aligned} \tag{5.21}$$

where $\{\cdot\}$ is the indicator function, which is zero when the proposition is false and one otherwise, and $\mathbb{E}\{\cdot\}$ represents the spatial-temporal statistical expectation. Analogously we define $e(v) = |v - \hat{v}|$ as the velocity error, i.e. the error on absolute velocity estimation, and the speed error outage (SEO) as the probability that the velocity error is below a given target value e_{th} over the trajectory length. In particular, such probability' is defined as

$$\begin{aligned} P_{\text{SEO}} &= \mathbb{P}\{e_{\text{v}}(v) > e_{\text{th}}\} \\ &= \frac{1}{Q}\sum_{q=1}^{Q}\mathbb{E}\{\mathbb{1}_{(e_{\text{th}},+\infty)}\{|\hat{v}_q - v_q|\}\}\,. \end{aligned} \tag{5.22}$$

System Parameters

A squared monitored environment of length $L = 50\,\text{m}$ is considered as that shown in Figure 5.4, with four radars at the corners. The LTE base station is positioned on the border of the monitored environment at $\mathbf{p}_{\text{BS}} = (0\,\text{m}, 50\,\text{m})$ with respect to the origin assumed in the center of the monitored area. The transmitted signal is compliant with the LTE standard in the 20 MHz band, with 16-QAM modulation. The noise spectral density is $N_0 = -200\,\text{dBm}$. The channel is compliant to the Extended Pedestrian A model with Rayleigh fading. The target trajectory is a Gaussian random walking inside the monitored area with constant target velocity such that $v/R_{\text{L}} = 10\,\text{m}$. Results are obtained by considering the target moving along a trajectory of 100 m. The tracking algorithm is set with $\sigma_{\text{m}} = 10$.

Results

Figure 5.5 shows the correlation $z(\tau, v)$ when the true value of $\tau/T_{\text{s}} = 12$ and $\tau/T_{\text{s}} = 11$ for the direct path, and the clutter mitigation is $\xi_{\text{dB}} = 0, 50, 100\,\text{dB}$. In particular, it can be noticed that when no clutter mitigation is performed, i.e. for $\xi = 0\,\text{dB}$, the direct path is those providing the maximum value of correlation, while the useful contribution due to target is similar to the noise floor. Differently, for $\xi_{\text{dB}} = 50\,\text{dB}$

the backscattered signal is much more evident even though the multipath and static clutter are so that the useful contribution does not provide the maximum correlation. Finally, for quasi-ideal clutter mitigation, i.e. $\xi_{\mathrm{dB}} = 100\,\mathrm{dB}$, the first path due to target is those providing maximum correlation.

Figure 5.6 shows an example of true and estimated trajectory for $\xi_{\mathrm{dB}} = 0\,\mathrm{dB}$ and $\xi_{\mathrm{dB}} = 50\,\mathrm{dB}$. It is evident that in the case without clutter mitigation, in which the correlation and therefore the predicted belief is due only to the direct path, the trajectory is estimated to be closer to the transmitter position. Differently, with clutter mitigation good results with respect to the available time resolution are obtained.

Figure 6.6 shows the TEO and SEO as a function of e_{th} for different values of ξ_{dB}. Results show that a clutter mitigation factor of 20 dB it is sufficient to obtain a tracking error below 10 m in the 70% of cases, while it is below 10 m in only the 1% of cases without clutter mitigation. By comparing this result with Figure 5.5 we can see that the improvement is due also to the tracking algorithm with mobility model, since the correlation alone is not enough even for $\xi_{\mathrm{dB}} = 50\,\mathrm{dB}$ as shown in Figure 5.5(b).

Chapter 6

RFID for Identification and Tracking

An RFID system is composed of a network of readers aiming to identify tags attached to objects and persons through wireless communications. In particular, the reader interrogates via a radio link the tags that answer by communicating both their identification and stored data [135]. Among all possible solutions, semi-passive tags are very promising for applications requiring extremely low power consumption as the energy, available from batteries or harvesters, is used only for control logic operations. In fact, the tag-reader communication is based on backscatter modulation, which consists in changing the tag's antenna load according to the data to be transmitted, therefore modifying how the antenna reflects back the interrogation signal [135]. Note that the backscatter modulation does not require the emission of new radiofrequency (RF) energy and hence it is usually classified as a passive communication scheme.

Considering the convergence of RFID and high-definition real time locating systems (RTLS) toward the radio detection, identification, and localization (RaDIAL) concept for enhancing the functionalities offered to the end user and enabling new potential wide market applications [136], the adoption of the UWB technology [93, 108] is particularly appealing for its capability of communication robustness and localization accuracy even in harsh propagation environments [5, 22, 24, 29, 94, 137].

Figure 6.1 shows an example scenario with a reader that interrogates semi-passive UWB tags located in the same area. To save energy, tags are normally in sleep mode and are woken-up through the transmission of a wake-up signal (e.g., an unmodulated ultra-high frequency (UHF) carrier) [138, 139]. Each tag reflects the incoming UWB interrogation signal by means of backscatter modulation according to its internal

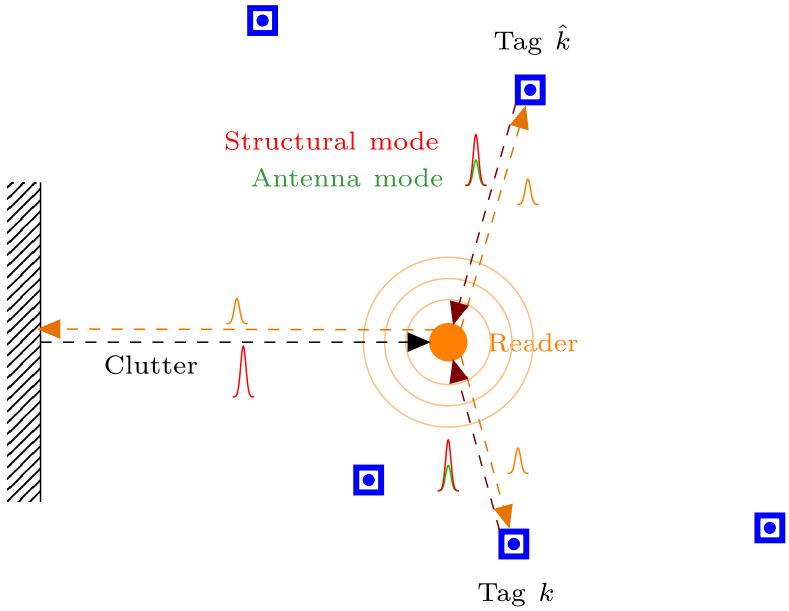

Figure 6.1: Scenario with a reader interrogating several tags.

information and identification code. Signals backscattered by different tags can be distinguished through the adoption of different spreading codes [140], therefore an anti-collision protocol (used, e.g., in Gen. 2 RFID [141–143]) is not required.

The reader-tag communication suffers from the presence of clutter (the signal backscattered by the environment), multi-tag interference, tag clock drift (due to the low-cost local oscillators), and poor link budget of the backscatter two-way link [124, 144]. The near-far interference effect [145, 146], which is typical of code division multiple access (CDMA) systems in the presence of multiple users, is detrimental for reader-tag communication, as classic power control approaches cannot be adopted in this scenario due to the passive nature of the tags. These issues have been only separately investigated in the literature [147–151], and classically focus on narrowband rather than UWB systems [152–156].

In [157] an UWB-RFID reader architecture capable of robust tag detection, even in the presence of multi-tag interference and clock drift effects, is presented. A low-complexity partially-non-coherent detection scheme is proposed and analyzed, and tag code design criteria are given. Specifically, the proposed technique enables robust tag detection in multi-tag scenario even in the presence of strong near-far interference effect, which stems from the two-hop communication nature of the system. Simulation results show the performance in terms of tags detection capability.

The key contributions can be summarized as follows:

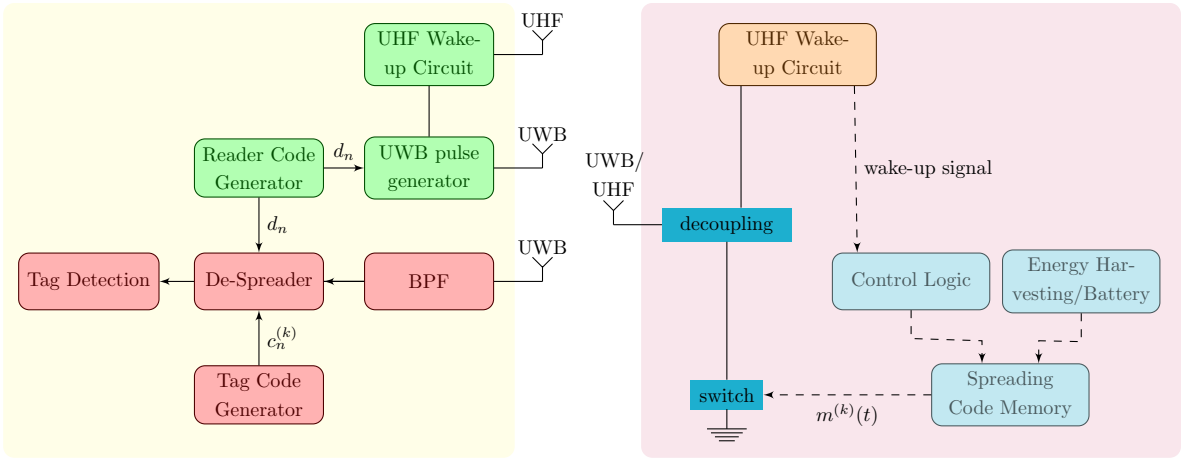

Figure 6.2: Reader (left) and tag (right) block schemes.

- proposal of a low-complexity tag detection scheme robust to near-far interference effects for UWB-RFID system based on backscatter modulation;
- design of spreading codes for backscatter modulation and multi-tag coexistence;
- analysis of the proposed UWB-RFID system in the presence of multi-tag interference and non-idealities such as clock drift and near-far interference effects;
- quantification of system performance for various settings and conditions.

6.1 Multi-tag RFID Systems

6.1.1 Backscatter Communication

The backscatter communication for the considered system is now described.

Transmitted Signal Format

In semi-passive UWB-RFID systems based on backscatter modulation, the reader is the only active device, thus with capability of transmitting, receiving, and processing signals. Tags act as passive reflectors only. Consider a reader scheme as shown in Figure 6.2 composed of a transmitter and receiver sections. The transmitter section emits periodic interrogation signals while the receiver section analyzes the received backscattered response to detect tags located in the area of interest. Figure 6.3

shows the structure of the reader's interrogation signal. Initially, tags are in sleeping mode to save energy and a wake-up signal is used for waking up all the tags present in the environment monitored by the reader. For example, a wake-up signal in the UHF band can be used [138], which requires a dedicated transmitter and antenna as shown in Figure 6.2. The same wake-up signal can be also exploited to provide energy to the tag. The presence of N_{tag} tags is considered in the monitored environment. After the transmission of the wake-up signal, the reader starts emitting the UWB interrogation signal, which contains a sequence of N_{S} symbols each composed of N_{c} chips carrying N_{pc} pulses per chip.

The chips are modulated in amplitude by an antipodal binary spreading sequence $\{d_n\}$ of length N_{c}, which is specific of the reader (namely reader's code). In particular, the interrogation signal transmitted by the reader is

$$s_{\text{reader}}(t) = \sum_{m=0}^{N_{\text{S}}-1} s(t - mN_{\text{c}}T_{\text{c}}) \tag{6.1}$$

with symbol duration $T_{\text{s}} = N_{\text{c}}T_{\text{c}}$, chip duration T_{c}, and

$$s(t) = \sum_{n=0}^{N_{\text{c}}-1} d_n \, g(t - nT_{\text{c}}) \tag{6.2}$$

where

$$g(t) = \sum_{i=0}^{N_{\text{pc}}-1} p(t - iT_{\text{p}}) \, . \tag{6.3}$$

The signal $g(t)$ is composed of N_{pc} UWB pulses $p(t)$, centered at frequency f_{c} with bandwidth W and energy E_{p}. The PRP T_{p} is chosen so that all backscattered signals are received by the reader before the transmission of the following pulses, thus avoiding inter-frame interference. The pulse energy E_{p} and the PRP T_{p} are chosen to guarantee a spectrum emission compliant with the regulation mask in terms of Equivalent Isotropic Radiated Power (EIRP).[1]

After the transmission of each pulse, the reader's receiver section (see Figure 6.2) collects the response backscattered from all tags located in the monitored environment, as well as the clutter. Then, the collected signal responses are processed to detect the presence of an intended tag, as detailed in the next sections.

[1] While the considered scheme is general, in the numerical results the European lower-band mask will be fulfilled.

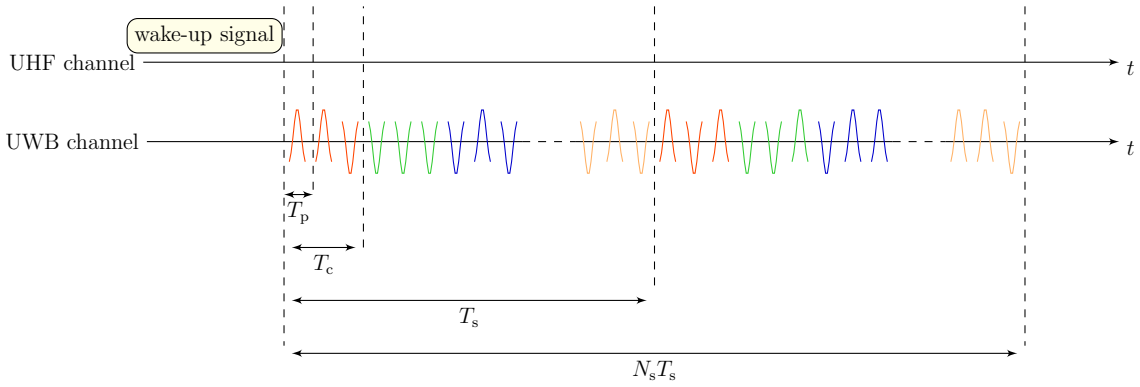

Figure 6.3: The interrogation signal structure.

Backscatter Modulation

When a reader transmits the interrogation signal, each tag sends its information back to the reader by modulating the backscatter signal through a proper variation of the load connected to its antenna (backscatter modulation) [108]. The response of each tag is composed of two contributions: the structural mode scattering and the antenna mode scattering. The former stems from all the reflections given by the antenna and its support, while the latter depends on how the antenna is loaded thus on the tag ID [158]. Figure 6.2 shows also the tag scheme in which the antenna backscattering properties are changed by varying the antenna load through a UWB switch. Specifically, the switch connects the antenna to two different loads according to the modulating signal $m^{(k)}(t)$, which is specific of the kth tag. When open and short circuit loads are adopted, the resulting modulation corresponds ideally to a phase inversion of 180° of the antenna mode pulse polarity.[2] To mitigate clutter and interference, each tag is designed to change its status (short or open circuit) at each chip time $T_c = N_{pc}\, T_p$ according to an antipodal tag's code $c_n^{(k)} \in \{-1, 1\}$, for $n = 0, 1, \ldots, N_c - 1$. In case the code is unique for each tag in the area, it represents the tag ID, hence tag detection and identification reduce to code detection. Provided that the total number of pulses per symbol $N_p = N_c N_{pc}$ is identical for readers and tags, the same values N_{pc} and N_c at both reader and tag sides is considered. Note that the same symbol structure can also be adopted to allow tag-to-reader data transmission, as discussed in [140, 151].

[2]Note that non-idealities related to the adopted switch or to the presence of objects may affect the pulse shape for the two different loads thus degrading the performance [159].

Tag-to-Reader Communication

After the reception of the wake-up signal, tags activate their backscatter modulator that starts switching the antenna load according to the modulating signals $m^{(k)}(t)$ (i.e., according to tags' codes $\{c_n^{(k)}\}$). Besides reader and tags are asynchronous as they have independent clock sources, the wake-up signal can also be exploited to reset the tag spreading code generator (see Figure 6.2), thus providing a coarse synchronization. Therefore, the system can be considered as quasi-synchronous, as discussed afterward in Section 6.1.2.

The presence of a low cost oscillator in the tag and the long symbol duration make clock drift effects not negligible after the reception of a few symbols.[3] Consider a model for the clock difference between the clock at the kth tag and that at the reader as $S^{(k)}(t) = T_{\mathrm{o}}^{(k)} + D^{(k)}t$, where $T_{\mathrm{o}}^{(k)}$ is the residual time-offset after the wake-up, and $D^{(k)}$ is the clock drift.[4] This model leads to the modulating signal commanding the switch of the kth tag given by

$$m^{(k)}(t) = \sum_{j=0}^{N_{\mathrm{S}}-1} \sum_{n=0}^{N_{\mathrm{c}}-1} c_n^{(k)} \; \Pi\left(\frac{t - jN_{\mathrm{c}}\widetilde{T}_{\mathrm{c}}^{(k)} - n\widetilde{T}_{\mathrm{c}}^{(k)} - T_{\mathrm{o}}^{(k)}}{\widetilde{T}_{\mathrm{c}}^{(k)}}\right) \tag{6.4}$$

with $\widetilde{T}_{\mathrm{c}}^{(k)} = T_{\mathrm{c}}\left(1 + D^{(k)}\right)$, $\Pi(t) \triangleq 1$ for $t \in [0, 1]$ and 0 elsewhere. Thus, the polarity of the reflected signal changes at each chip time (i.e., every N_{pc} pulses) according to the kth tag's code $\{c_n^{(k)}\}$.

The signal backscattered by the tag propagates back to the reader's antenna through the reader-tag link [124]. Over the symbol time T_{s}, the one-way channel impulse responses (CIRs) $h^{(k)}(t)$, related to the reader-kth tag link, and $h^{(\mathrm{c})}(t)$, related to the environment forming the clutter are static. By channel reciprocity, the received signal at the reader is[5]

$$r_{\mathrm{reader}}(t) = w(t) + n(t) \tag{6.5}$$

[3] Note that the symbol duration is longer than that used in conventional active UWB transmission [160] due to the need of collecting a high number of UWB pulses per symbol to counteract the poor link budget of backscatter links [124].

[4] This is equivalent to consider, as a first approximation, the effects of the phase noise constant over a symbol time T_{s}.

[5] Operator $\otimes$ denotes the convolution.

where

$$w(t) = \sum_{k=1}^{N_{\text{tag}}} \left[\left(s_{\text{reader}}(t) \otimes h^{(k)}(t) \right) m^{(k)}(t) \right] \otimes h^{(k)}(t) + s_{\text{reader}}(t) \otimes h^{(\text{c})}(t) \tag{6.6}$$

and $n(t)$ is the AWGN with one-sided power spectral density N_0. The tag structural mode is treated as part of clutter since it is not affected by backscatter modulation. Note that the received signal is obtained through the double convolution of the interrogation signal with the one-way CIR $h^{(k)}(t)$ [124, 161].

In conventional active UWB communication systems, the clock drift affects the timing of UWB pulse transmission in tags. Thus, the TOA and the PRP seen by the receiver result different from those expected and a proper fine synchronization scheme is required if large T_{s} is adopted. On the contrary, in backscattering communication, the TOA and the PRP of the backscattered pulses, generated by the reader itself, are not affected by the tag clock drift, which modifies only how they are modulated, that is, the code phase of the backscattered signal. Tag code acquisition will be investigated in the next section.

6.1.2 System Design

Receiver Design

A partially-non-coherent architecture is considered, where the received signals are first de-spread using the intended reader and tag codes and then coherently accumulated to enhance the SNR. Subsequently, a low-complexity energy detector is used to detect the presence of a tag. This receiver does not require CIR estimation and it results to be a good compromise between performance and complexity. An example of implementation of such a receiver is presented in [162]. The de-spreading procedure and the tag detection scheme are described in the following.

Signal De-Spreading

After the spreading process at the transmitter and the backscatter modulation at a tag indexed by k, the received signal results to be spread by the composed code $\{d_n\, c_n^{(k)}\}$, whereas the clutter only by the reader code $\{d_n\}$. This property can

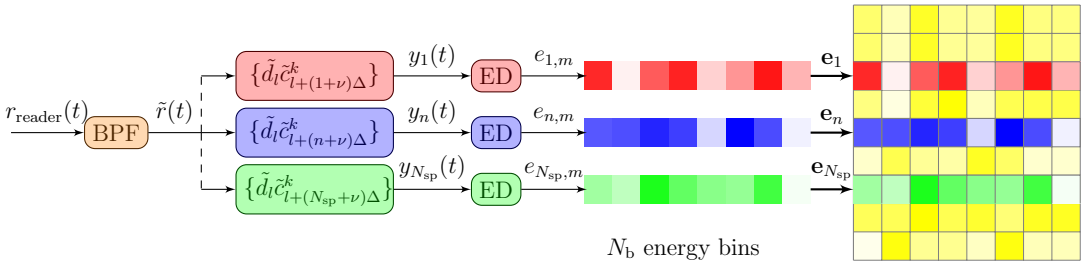

Figure 6.4: Partially-non-coherent tag detection scheme.

be exploited to discriminate the intended signal from interfering signals associated to other tags and from the clutter. Specifically, signal de-spreading is operated coherently through the accumulation of the received signals corresponding to the N_{p} transmitted pulses $p(t)$ within a symbol. Such an accumulation enhances the SNR, allowing a better discrimination of the backscatter signal associated to a specific reader-tag pair. The periodically repeated sequences of length N_{c} and period $N_{\text{p}} = N_{\text{c}}N_{\text{pc}}$ is defined as $\tilde{c}_l^{(k)} \triangleq c^{(k)}_{\lfloor l/N_{\text{pc}} \rfloor}$ and $\tilde{d}_l \triangleq d_{\lfloor l/N_{\text{pc}} \rfloor}$ for $l = 0, 1, \ldots, N_{\text{p}} - 1$, with $\tilde{c}^{(k)}_{l+N_{\text{p}}} = \tilde{c}^{(k)}_l$, $\tilde{d}_{l+N_{\text{p}}} = \tilde{d}_l$, and $\lfloor \cdot \rfloor$ denoting the floor operation.

The wake-up offset $T_{\text{o}}^{(k)}$ and the clock drift $D^{(k)}$ associated with the kth tag cause an uncertainty on the offset (phase) of the tag's spreading code with respect to the local clock of the reader. The typical long symbol time discourages the adoption of serial code acquisition schemes, as they would imply intolerable acquisition time. Tag detection can be performed jointly with code acquisition by employing parallel de-spreaders, each tuned to a differently shifted version of sequence $\{\tilde{c}_l^{(\hat{k})}\}$ and to in-phase version of sequence $\{\tilde{d}_l\}$ according to the scheme in Figure 6.4. In particular, we consider code acquisition with N_{sp} shifts (i.e., N_{sp} parallel de-spreaders) and step Δ, which determines an overall code acquisition window of $\Delta(N_{\text{sp}} - 1)$ chips. The values of N_{sp} and Δ are chosen based on the robustness of the spreading codes to clock drift and the wake-up offset. Note that N_{sp} is upper limited by the sustainable receiver complexity.

Without loss of generality, consider the detection of the tag indexed by $\hat{k}$ (useful tag) observing the first symbol (i.e., acquiring N_{p} pulses).[6] According to the receiver architecture shown in Figure 6.4, first, the received signal $r_{\text{reader}}(t)$ is filtered[7] to eliminate the out-of-band noise (this operation is necessary for energy-based detec-

[6]Note that the decision can be taken after the observation of many symbols to guarantee a more robust tag detection.

[7]An ideal band-pass filter of bandwidth W with center frequency f_{c} is considered.

tors [44]). The filtered signal is denoted by

$$\tilde{r}(t) = \tilde{w}(t) + \tilde{n}(t) \tag{6.7}$$

where $\tilde{w}(t) = w(t) \otimes h_{\mathrm{F}}(t)$, with $h_{\mathrm{F}}(t)$ being the filter impulse response, and $\tilde{n}(t) = n(t) \otimes h_{\mathrm{F}}(t)$ a zero-mean Gaussian random process. Subsequently, the filtered signal is de-spread giving N_{sp} outputs corresponding to N_{sp} different code shifts

$$y_n(t) = \sum_{l=0}^{N_{\mathrm{p}}-1} \tilde{d}_l \, \tilde{c}^{(\hat{k})}_{l+(n+\nu)\Delta} \, \tilde{r}(t+lT_{\mathrm{p}}) \tag{6.8}$$

with $t \in [0, T_{\mathrm{p}}]$, $\nu = -\lfloor (N_{\mathrm{sp}}+1)/2 \rfloor$ and $n = 1, 2, \ldots, N_{\mathrm{sp}}$. In the absence of code acquisition (only 1 de-spreader) it is $N_{\mathrm{sp}} = 1$ and $(n+\nu)\Delta = 0$.

It is possible to decompose (6.8) as $y_n(t) = x_n(t) + z_n(t)$, with the noise term $z_n(t)$ given by

$$z_n(t) = \sum_{l=0}^{N_{\mathrm{p}}-1} \tilde{d}_l \, \tilde{c}^{(\hat{k})}_{l+(n+\nu)\Delta} \, \tilde{n}(t+lT_{\mathrm{p}}) \tag{6.9}$$

and the term $x_n(t)$ expressed as

$$\begin{aligned} x_n(t) = &\sum_{l=0}^{N_{\mathrm{p}}-1} \tilde{d}_l \, \tilde{c}^{(\hat{k})}_{l+(n+\nu)\Delta} \, \tilde{r}_{\mathrm{t}}(t+lT_{\mathrm{p}}) \\ &+ \sum_{l=0}^{N_{\mathrm{p}}-1} \tilde{d}_l \, \tilde{c}^{(\hat{k})}_{l+(n+\nu)\Delta} \, \tilde{r}_{\mathrm{c}}(t+lT_{\mathrm{p}}) \end{aligned} \tag{6.10}$$

where $\tilde{r}_{\mathrm{t}}(t+lT_{\mathrm{p}})$ is the signal component related to tags, and $\tilde{r}_{\mathrm{c}}(t+lT_{\mathrm{p}})$ is the clutter component. In (6.10), $\tilde{r}_{\mathrm{c}}(t) = s_{\mathrm{reader}}(t) \otimes h^{(\mathrm{c})}(t) \otimes h_{\mathrm{F}}(t)$ denotes the clutter component. The received signal component $\tilde{r}_{\mathrm{t}}(t)$ is given by

$$\begin{aligned} \tilde{r}_{\mathrm{t}}(t) = &\sum_{k=1}^{N_{\mathrm{tag}}} \left[\left(s_{\mathrm{reader}}(t) \otimes h^{(k)}(t) \right) \, m^{(k)}(t) \right] \\ &\otimes h^{(k)}(t) \otimes h_{\mathrm{F}}(t) \end{aligned} \tag{6.11}$$

and comprises signals backscattered by both the useful and the interfering tags. By considering the clutter CIR $h^{(\mathrm{c})}(t)$ stationary over a symbol time T_{s}, we have $\tilde{r}_{\mathrm{c}}(t+lT_{\mathrm{p}}) = \tilde{d}_l \, \zeta(t)$, for $t \in [0, T_{\mathrm{p}}]$ with $l = 0, 1, \ldots, N_{\mathrm{p}}-1$, and $\zeta(t) \triangleq p(t) \otimes h^{(\mathrm{c})}(t) \otimes h_{\mathrm{F}}(t)$. Therefore, the clutter component at the output of the de-spreader results in

$$\sum_{l=0}^{N_{\mathrm{p}}-1} \tilde{d}_l \, \tilde{c}^{(\hat{k})}_{l+(n+\nu)\Delta} \, \tilde{r}_{\mathrm{c}}(t+lT_{\mathrm{p}}) = \zeta(t) \sum_{l=0}^{N_{\mathrm{p}}-1} \tilde{c}^{(\hat{k})}_{l+(n+\nu)\Delta} \, . \tag{6.12}$$

From (6.12), it can be noticed that the clutter component at the output of the despreader is canceled when the tag code $\{\tilde{c}_l^{(\hat{k})}\}$ is exactly balanced (i.e., with the same number of ± 1). This is an important property tags' codes have to satisfy in addition to those presented in Section 6.1.2.

The superposition of the large signal due to clutter and of the small backscattered signals from tags requires a radiofrequency front-end of the UWB-RFID reader with high-dynamic range. This affects the design of the sampling rate and of the number of quantization levels for digital conversion depending on the receiver architecture chosen. In a fully digital architecture it is necessary to ensure a proper digital conversion of the small backscattered signals while preventing saturation due to clutter. This requires sampling at Nyquist rate and a high number of quantization levels. In a hybrid analog-digital architecture, the analog mitigation of clutter reduces the dynamic range which now depends on the reader-tag distances and near-far effects discussed in the following sections. This can result in a reduced sampling rate and number of quantization levels.[8]

Tag Detection

The detection in parallel of N_{tag} tags requires replicating for each tag the same receiver structure which is here described.[9] According to the consideration made in Section 6.1.2, balanced codes are adopted, for which (6.10) reduces to

$$x_n(t) = \sum_{l=0}^{N_{\text{p}}-1} \tilde{d}_l \, \tilde{c}_{l+(n+\nu)\Delta}^{(\hat{k})} \, \tilde{r}_{\text{t}}(t+lT_{\text{p}}) \, . \tag{6.13}$$

The term $x_n(t)$ can be further decomposed by noticing that $\tilde{r}_{\text{t}}(t)$ is the combination of N_{tag} tags channel responses to the interrogation signal as given by

$$x_n(t) = \sum_{l=0}^{N_{\text{p}}-1} \tilde{d}_l \, \tilde{c}_{l+(n+\nu)\Delta}^{(\hat{k})} \sum_{k=1}^{N_{\text{tag}}} \omega^{(k)}(t + lT_{\text{p}}) \quad t \in [0, T_{\text{p}}] \tag{6.14}$$

where the single-tag channel response to the interrogation signal is

$$\omega^{(k)}(t) = \left[\left(s_{\text{reader}}(t) \otimes h^{(k)}(t) \right) m^{(k)}(t) \right] \otimes h^{(k)}(t) \otimes h_{\text{F}}(t) \, . \tag{6.15}$$

[8] An example of front-end architecture for UWB-RFID adopting 12 bits and sub-Nyquist sampling is presented in [150].

[9] Note that the partially-non-coherent detector reported in Figure 6.4, helps to keep the system complexity affordable.

The de-spreading process is followed by the evaluation, for each de-spreader output $y_n(t)$, of energy bins performed over a PRP T_p as follows

$$e_{n,m} = \int_{(m-1)\,T_\mathrm{ED}}^{m\,T_\mathrm{ED}} [y_n(t)]^2 \, dt \tag{6.16}$$

with $n = 1, 2, \ldots, N_\mathrm{sp},\ m = 1, 2, \ldots, N_\mathrm{b}$ and where $N_\mathrm{b} = \lfloor T_\mathrm{p}/T_\mathrm{ED} \rfloor$ represents the number of integration bins in which each PRP is divided in for an energy detector integration time T_ED. Such energy bins can be arranged, for convenience, into a $N_\mathrm{sp} \times N_\mathrm{b}$ energy matrix $\mathbf{E} = \{e_{n,m}\}$. Each element $e_{n,m}$ of the energy matrix is then compared with a threshold $\xi_{n,m}$: if at least one element is above the threshold, then the tag is considered detected. The design of the threshold $\xi_{n,m}$ is challenging and is addressed in the following section.

Tag Code Design

Backscatter communication carries several challenges that can be partially mitigated by carefully designing the spreading codes used by tags. The requirements for tags code design are: availability of a sufficient number of sequences given a specific code length N_c; mitigation of clutter and clock drift effects; and suppression of multi-tag interference. Hereafter, these aspects and their impact on tag code design are discussed.

6.1.3 Threshold Design

We now derive a strategy to determine the thresholds $\xi_{n,m}$ associated to each energy bin with the purpose to obtain a robust detection performance even in the presence of several tags. In particular, such strategy aims to improve the overall probability of detection (PD), that is, the probability of taking the correct decision when the tag is present, for a given target overall probability of false alarm (PFA), that is, the probability that a tag is erroneously detected as present when absent. Overall PFA and overall PD are indicated by P_FA and P_D, respectively. By defining $\mathcal{H}_1$ and $\mathcal{H}_0$ the hypotheses related to the presence and absence of the tag, respectively, and the set $\mathcal{D} = \{(n, m) : e_{n,m} > \xi_{n,m}\}$ with cardinality $|\mathcal{D}|$, the decision rule is given by

$$\text{Decide:} \begin{cases} \widehat{\mathcal{H}}_0 \ ; & |\mathcal{D}| = 0 \\ \widehat{\mathcal{H}}_1 \ ; & |\mathcal{D}| > 0 \, . \end{cases} \tag{6.17}$$

The threshold values affect the performance of the detection scheme in terms of both PD and PFA. In fact, low values for the thresholds $\xi_{n,m}$ lead to high PFA and high PD, while high values lead to low PFA and low PD. We define the single-bin PFA $p_{\mathrm{FA}}^{(n,m)}$ as the probability that the single energy bin $e_{n,m}$ exceeds the threshold $\xi_{n,m}$ in the absence of tag, and the single-bin PD $p_{\mathrm{D}}^{(n,m)}$ as the probability that the single energy bin exceeds the threshold in presence of the tag.

The coordinates

$$(\widehat{n}, \widehat{m}) = \underset{(n,m)\in\mathcal{D}}{\operatorname{argmax}} \{e_{n,m}\} \tag{6.18}$$

associated to the maximum energy bin exceeding the threshold, provide an estimate of the tag clock offset in terms of number of PRPs and a coarse estimate of the signal TOA $\hat{\tau} = \hat{m}\, T_{\mathrm{ED}}$, respectively. Note that the maximum resolution in TOA estimation, which is essential for time-based ranging, depends on T_{ED} [29]. TOA estimates can be further improved by adopting ranging strategies described in [29].

The typical bin-independent approach, employing a constant threshold $\xi_{n,m} = \xi$ for all (n, m), is not suitable for UWB-RFID systems based on backscatter modulation in the presence of multi-tag interference. In fact, the useful tag can be hidden by residual interference peaks coming from tags that are closer to the reader than the useful one (i.e., near-far interference effect). Therefore, a bin-independent threshold would increase the PFA significantly, which is detrimental especially in the two-hop propagation channel. In such a channel, the received power in free-space propagation is proportional to d^{-4} where d is the reader-tag distance [124]. For instance, for a useful and an interferer tag at distance d_{U} and d_{I} from the reader, respectively, the difference (in dB) in the receiving power at reader side from the two tags is $40[\log_{10}(d_{\mathrm{U}}) - \log_{10}(d_{\mathrm{I}})]$ dB. If this difference is not properly mitigated by the de-spreading with the useful tag code, a high PFA is expected due to near-far interference effects.[10]

To comply with this phenomenon, a bin-dependent threshold is proposed. In particular, we derive the threshold providing a target overall PFA $P_{\mathrm{FA}}^{\star}$, in the presence of multi-tag interference. To this purpose, consider the normalized energy detector test

$$\Lambda^{(n,m)} = \frac{2}{N_{\mathrm{p}} N_0} e_{n,m} \underset{\widehat{\mathcal{H}}_0}{\overset{\widehat{\mathcal{H}}_1}{\gtrless}} \tilde{\xi}_{n,m} \tag{6.19}$$

[10] Such effects are obviously even more evident in the presence of multiple interfering tags and multipath propagation. Note that power control techniques (see, e.g., [163]) cannot be used due to the passive nature of the communication here considered.

where $\tilde{\xi}_{n,m} \triangleq \frac{2\,\xi_{n,m}}{N_{\rm p} N_0}$. By following the approach proposed in [44], we obtain

$$\Lambda^{(n,m)} = \frac{2}{N_{\rm p} N_0} \int_{(m-1)\,T_{\rm ED}}^{m\,T_{\rm ED}} [y_n(t)]^2\, dt \simeq \frac{1}{\sigma^2} \sum_{i=(m-1)N}^{mN} \hat{y}_{n,i}^2 \tag{6.20}$$

for $n = 1, 2, \ldots, N_{\rm sp}$ and $m = 1, 2, \ldots, N_{\rm b}$, with $\hat{y}_{n,i} = \hat{x}_{n,i} + \hat{z}_{n,i}$, $N \triangleq 2WT_{\rm ED}$, and noise variance $\sigma^2 = N_{\rm p} N_0 W$.[11] The terms $\hat{y}_{n,i}$, $\hat{x}_{n,i}$, and $\hat{z}_{n,i}$ represent for odd i (even i) the samples of the real (imaginary) part of the equivalent low-pass $\hat{y}_n(t)$, $\hat{x}_n(t)$, and $\hat{z}_n(t)$ of signals $y_n(t)$, $x_n(t)$ and $z_n(t)$, respectively, with sampling at Nyquist rate W in each interval. Noise samples $z_{n,i}$ are statistically independent Gaussian RVs with zero mean and unitary variance.

Consider the $\hat{k}$th useful tag to be detected, while other tags indexed by $k \neq \hat{k}$ cause interference. For further convenience, the case whether the desired tag is present or absent are distinct, by defining

$$x_n^{(\mathcal{H})}(t) = \begin{cases} \sum_{l=0}^{N_{\rm p}-1} \tilde{d}_l\, \tilde{c}_{l+(n+\nu)\Delta}^{(\hat{k})} \sum_{k=1,\, k\neq\hat{k}}^{N_{\rm tag}} \omega_k(t)\ ; & \mathcal{H} = \mathcal{H}_0 \\ \sum_{l=0}^{N_{\rm p}-1} \tilde{d}_l\, \tilde{c}_{l+(n+\nu)\Delta}^{(\hat{k})} \sum_{k=1}^{N_{\rm tag}} \omega_k(t)\ ; & \mathcal{H} = \mathcal{H}_1\,. \end{cases} \tag{6.21}$$

Note that in the absence of the useful tag, $x_n(t)$ could be different from 0 due to the presence of a residual interference term after the de-spreading responsible for the near-far effect.

Under the hypothesis $\mathcal{H}_0$ (absence of useful tag), the normalized decision variable results in

$$\begin{aligned} \Lambda^{(n,m)}|_{\mathcal{H}_0} &= \frac{2}{N_{\rm p} N_0} \int_{(m-1)\,T_{\rm ED}}^{m\,T_{\rm ED}} \left[x_n^{(\mathcal{H}_0)}(t) + z_n(t)\right]^2\, dt \\ &\simeq \frac{1}{\sigma^2} \sum_{i=(m-1)N}^{mN} \left(\hat{x}_{n,i}^{(\mathcal{H}_0)} + \hat{z}_{n,i}\right)^2 \end{aligned} \tag{6.22}$$

where $x_{n,i}^{(\mathcal{H}_0)}$ are the sampling expansion coefficients of the equivalent low-pass $\hat{x}_n^{(\mathcal{H}_0)}(t)$ of $x_n^{(\mathcal{H}_0)}(t)$. Under both hypotheses $\mathcal{H}_0$ and $\mathcal{H}_1$, the RV $\Lambda^{(n,m)}$ describing the energy detector output is non-central Chi-square distributed with N degrees of freedom, and with PDF $f_{\rm NC}(y, \lambda, N)$ given by

$$f_{\rm NC}(y, \lambda, N) = \frac{1}{2} e^{-\frac{y+\lambda}{2}} \left(\frac{y}{\lambda}\right)^{\frac{N-2}{4}} I_{\frac{N}{2}-1}(\sqrt{y\lambda}) \tag{6.23}$$

[11] The approximation is valid for large values of N [44, 164], and $WT_{\rm ED}$ is considered integer.

for $y \geq 0$, where the non-centrality parameter λ depends on $\mathcal{H}_0$ and $\mathcal{H}_1$ and $I_\kappa(\cdot)$ denotes the κth order modified Bessel function of the first kind. In particular, under the hypotheses $\mathcal{H}_0$, the presence of $\hat{x}_{n,i}^{(\mathcal{H}_0)}$ leads to the non-centrality parameter $\lambda_{n,m}^{(\mathcal{H}_0)} = 2\gamma_{n,m}^{(\mathcal{H}_0)}$ [44] , where $\gamma_{n,m}^{(\mathcal{H}_0)}$ is the interference-to-noise ratio (INR) per bin given by

$$\begin{aligned}\gamma_{n,m}^{(\mathcal{H}_0)} &= \frac{1}{N_\mathrm{p} N_0} \int_{(m-1)\,T_\mathrm{ED}}^{m\,T_\mathrm{ED}} \left[x_n^{(\mathcal{H}_0)}(t)\right]^2 dt \\ &\simeq \frac{1}{2\sigma^2} \sum_{i=(m-1)N}^{mN} \left(\hat{x}_{n,i}^{(\mathcal{H}_0)}\right)^2 . \end{aligned} \tag{6.24}$$

A threshold-crossing event under hypothesis $\mathcal{H}_0$, that is, $\Lambda^{(n,m)}|_{\mathcal{H}_0} > \tilde{\xi}_{n,m}$, causes a false alarm event. This results in a single-bin PFA $p_\mathrm{FA}^{(n,m)}$ given by [48]

$$\begin{aligned} p_\mathrm{FA}^{(n,m)} &= \int_{\tilde{\xi}_{n,m}}^{\infty} f_\mathrm{NC}(y, \lambda_{n,m}^{(\mathcal{H}_0)}, N)\, dy \\ &= Q_h\left(\sqrt{\lambda_{n,m}^{(\mathcal{H}_0)}}, \sqrt{\tilde{\xi}_{n,m}}\right) \end{aligned} \tag{6.25}$$

with $Q_h(\alpha,\beta) = \int_\beta^\infty x\,(\frac{x}{\alpha})^{k-1} \exp\left(-\frac{x^2+\alpha^2}{2}\right) I_{k-1}(\alpha x)\, dx$ denoting the generalized Marcum's Q function of order $h = N/2$ [165]. The non-centrality parameters are strictly related to the interference level at each bin $e_{n,m}$. In case of bin-dependent threshold $\xi_{n,m}$ the same PFA for all bins is imposed, (i.e., $p_\mathrm{FA}^{(n,m)} = p_\mathrm{FA}\ \forall\,(n,m)$). Considering independence among energy bins, the overall PFA results in[12]

$$P_\mathrm{FA} = 1 - (1 - p_\mathrm{FA})^M \simeq M p_\mathrm{FA} \tag{6.26}$$

where $M = N_\mathrm{b}\, N_\mathrm{sp}$. The threshold $\xi_{n,m}$, corresponding to a target overall PFA $P_\mathrm{FA}^\star$ can be determined from (6.25) and (6.26) as given by

$$\xi_{n,m} = \frac{N_\mathrm{p} N_0}{2}\left[Q_h^{-1}\left(\sqrt{\lambda_{n,m}^{(\mathcal{H}_0)}}\,, \frac{P_\mathrm{FA}^\star}{M}\right)\right]^2 \tag{6.27}$$

with $Q_h^{-1}(\cdot,\cdot)$ denoting the inverse generalized Marcum Q function [165].

Once the bin-dependent threshold is set to guarantee a certain overall PFA, it is possible to determine the correspondent single-bin PD as follows. Consider now the

[12] This approximation is exact in case of $N_\mathrm{sp} = 1$, because the noise components are independent in different bins. Differently, when $N_\mathrm{sp} > 1$ the energy matrix elements corresponding to shifted local replicas of the useful tag code, but to the same bin index, are correlated and thus are not independent. Consequently a threshold more conservative than the necessary is expected.

hypothesis $\mathcal{H}_1$ and the corresponding normalized decision variable, which is described by

$$\begin{aligned}\Lambda^{(n,m)}|_{\mathcal{H}_1} &= \frac{2}{N_\mathrm{p}N_0}\int_{(m-1)\,T_\mathrm{ED}}^{m\,T_\mathrm{ED}} \left[x_n^{(\mathcal{H}_1)}(t)+z_n(t)\right]^2\,dt \\ &\simeq \frac{1}{\sigma^2}\sum_{i=(m-1)N}^{mN}\left(x_{n,i}^{(\mathcal{H}_1)}+z_{n,i}\right)^2 \end{aligned} \tag{6.28}$$

where $x_{n,i}^{(\mathcal{H}_1)}$ are the sampling expansion coefficients of the equivalent low-pass $\hat{x}_n^{(\mathcal{H}_1)}(t)$ of $x_n^{(\mathcal{H}_1)}(t)$, leading to a non-centrality parameter $\lambda_{n,m}^{(\mathcal{H}_1)} = 2\gamma_{n,m}^{(\mathcal{H}_1)}$, where the interference-plus-signal-to-noise-ratio (ISNR) $\gamma_{n,m}^{(\mathcal{H}_1)}$ per bin is defined as

$$\begin{aligned}\gamma_{n,m}^{(\mathcal{H}_1)} &= \frac{1}{N_\mathrm{p}N_0}\int_{(m-1)\,T_\mathrm{ED}}^{m\,T_\mathrm{ED}} \left[x_n^{(\mathcal{H}_1)}(t)\right]^2\,dt \\ &\simeq \frac{1}{2\sigma^2}\sum_{i=(m-1)N}^{mN}\left(\hat{x}_{n,i}^{(\mathcal{H}_1)}\right)^2 . \end{aligned} \tag{6.29}$$

The single-bin PD $p_\mathrm{D}^{(n,m)}$ is given by [48]

$$p_\mathrm{D}^{(n,m)} = Q_h\left(\sqrt{\lambda_{n,m}^{(\mathcal{H}_1)}}, \sqrt{\tilde{\xi}_{n,m}}\right) \tag{6.30}$$

and the overall PD P_D can be finally computed as

$$P_\mathrm{D} = 1 - \prod_{n=1}^{N_\mathrm{sp}}\prod_{m=1}^{N_\mathrm{b}}\left(1-p_\mathrm{D}^{(n,m)}\right) \tag{6.31}$$

for independent energy bins.

Note that the multi-tag detection approach in the presence of interference requires the knowledge of the INR per bin $\gamma_{n,m}^{(\mathcal{H}_0)}$ to define a proper bin-dependent threshold $\xi_{n,m}$ according to (6.27). In [157] a practical approach is presented for determining the threshold without an exact prior knowledge of the interference level (i.e., of the non-centrality parameters).

6.1.4 Tracking Results

Localization and tracking algorithms rely on TOA estimations based on backscattered received signal at each reader in the network [5, 22, 29, 166]. Specifically, we consider here tracking algorithms based on extended Kalman filters (EKFs) and

particle filters (PFs) for dynamic tags, reducing to least square (LS) for static tags. Localization and tracking performance are given in terms of root mean square error (RMSE), localization error outage (LEO), and tracking error outage (TEO) [13]. The dependence of performance on the operating scenario and the time interval between two consecutive TOA estimations T_{r} is investigated.

A 10m x 10m square room with four readers located at the corners is chosen as bi-dimensional reference scenario. Preliminary results are obtained by considering a channel model simulated as the combination of a two-way IEEE 802.15.4a channel model with backscattering antenna response. For this case, details of signal processing and TOA estimation can be found in [167].

Measurement campaigns have been carried out within SELECT to investigate channel propagation and antenna response in different environments (warehouse-like, room-like, and laboratory-like) presenting different multipath and LOS conditions [168]. Results enabled the derivation of a channel model and antenna response based on measurements. Furthermore, the effects of the presence of interfering tags on TOA estimation accuracy is investigated by simulations.

Preliminary tracking results are obtained with EKF-based algorithm by considering the simulated channel model in the absence of interferers, for a tag moving with a maximum speed of 1m/s. Specifically, the RMSE over 100 random trajectories is 0.17m and 0.39m for $T_{\mathrm{r}} = 0.5$s and $T_{\mathrm{r}} = 1$s, respectively.

Localization and tracking are then evaluated for PF-based algorithm by considering measured channel models and antenna responses, and the presence of 21 interferers located between 2 and 8m from each reader.

For tracking with PFs, a Gaussian model is assumed for mobility, where at each instant the standard deviation depends on the uncertainty of the target movement, and the mean depends on the previous position estimate. The tracking algorithm estimates the tag position every T_{r} seconds and is based on the speed and direction learning model (SDL), in which at each time $t_k = t_0 + kT_{\mathrm{r}}$ (with $k = 1, ..., N$ and t_0 being the time of the first estimate) the speed vector $\mathbf{v}_{k-1}$ is determined from previously estimated positions. We assume a perception model with Gaussian distribution, whose standard deviation depends on both the TOA estimation technique and propagation conditions. Details on the mobility and perception models chosen can be found in [169].

Figure 6.5 shows LEO for the LS algorithm obtained over 1000 position estimations for a static tag within the monitored area. The localization error is below

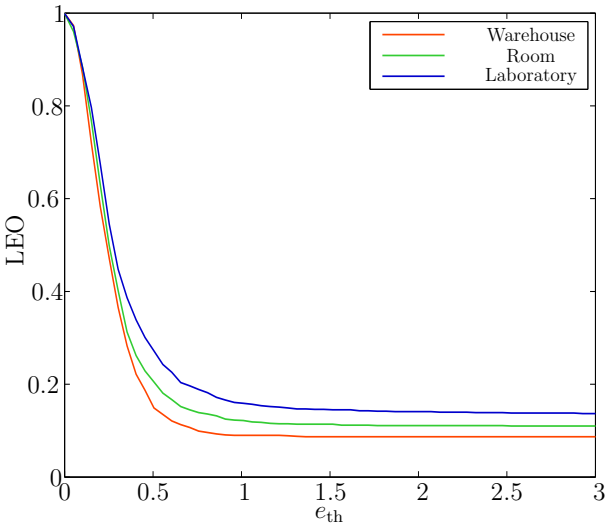

Figure 6.5: LEO over 1000 tag positions for three different channel models.

0.37m, 0.4m, and 0.56m in the 75% of cases for the warehouse, room, and laboratory scenario, respectively. The TEO shown in Figure 6.6 is evaluated over 10 different

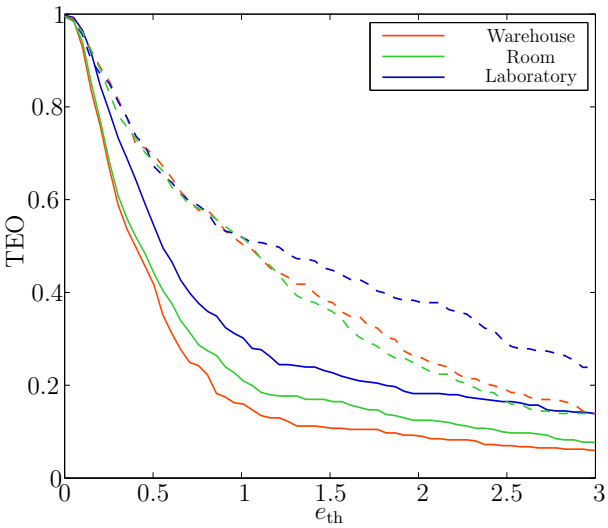

Figure 6.6: TEO over 10 random trajectories each of length 20m for $T_{\text{r}} = 1s$ (solid) and $T_{\text{r}} = 0.5s$ (dashed), and three different channel models.

random trajectories for $T_{\text{r}} = 1s$ and $T_{\text{r}} = 0.5s$, for a tag moving at 1m/s. Specifically, for the warehouse scenario, the tracking error is below 0.7m and 2.07m in the 75% of cases for $T_{\text{r}} = 0.5s$ and $T_{\text{r}} = 1s$, respectively.

6.2 RFID for OOA estimation

Network localization is of great interest for numerous new wireless applications [5]. In passive wireless systems, such as those based on RFID [170, 171], high-accuracy localization enables context-aware applications that could spread the adoption of such a technology [172–174]. Among all, the estimation of the tags OOA for sorting and tracking of goods moving on a conveyor belt is finding great interest for industrial and logistics applications [175–180]. Examples of applications are the management of goods in warehouses, the automatic processing of items in supply chains and the routing of luggage in airports.

Current localization techniques adopted for sorting with standard Gen. 2 UHF-RFID are based on received signal strength indicator (RSSI) measurements [173], phase measurements (also at different operating frequencies) [179–182], and AOA [176,183,184]. These solutions are affected by several drawbacks in real environments where non-idealities such as NLOS channel conditions and multipath propagation cause localization/sorting errors. On the other hand, barcode-based optical sorting can guarantee tags discrimination down to an inter-tag distance of about 30 cm, which is challenging to be achieved by actual UHF-RFID systems. Differently, optical systems are not appealing for the small amount of data which can be included in the barcode.

The UWB technology is able to guarantee high localization and sorting performance even in harsh propagation environments [13, 22, 29]. Recently, UWB has been proposed also for RFID systems [108, 140, 146, 149]. Another interesting feature enabled by the adoption of UWB signals is the possibility of integrating localization of RFID tags with radar signal processing for detection and tracking of untagged objects and persons (e.g., for detecting untagged items on the conveyor) [137, 185].

A hybrid UHF-UWB RFID system based on backscatter modulation for identifying and sorting tags moving on a conveyor belt is proposed. The main contributions are: the introduction of performance metrics for OOA estimation performance characterization; the proposal of a novel UHF-UWB RFID system with Bayesian tracking for OOA estimation; the quantification of OOA estimation performance for a case study of practical interest.

6.2.1 System Model for OOA Estimation

We now describe the network model and system architecture for OOA estimation.

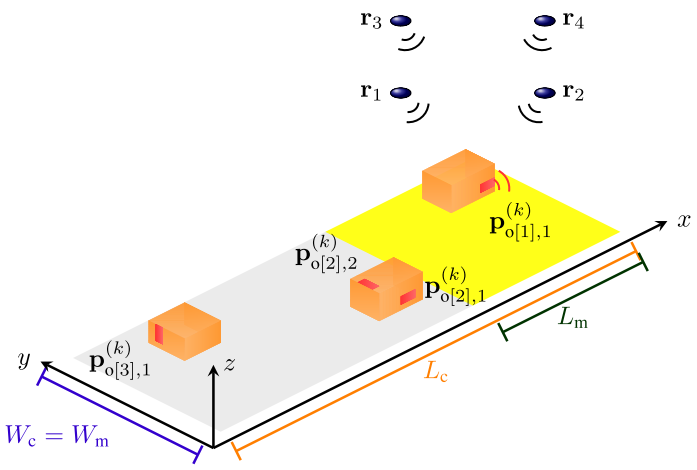

Figure 6.7: Conveyor belt scenario, the OOA of the objects with respect to the monitored area is indicated by the vector $\mathbf{o}$.

Network Model

We consider a stream of N_{o} objects with index set $\mathcal{O}$ laying on a conveyor belt with length L_{c}, width W_{c}, and moving with a known speed vector $\mathbf{v}= [v_{\mathrm{x}}, v_{\mathrm{y}}, v_{\mathrm{z}}] \in \mathbb{R}^3$ and magnitude v_{c} according to a Cartesian coordinate system (see, e.g., Figure 6.7). We are interested in detecting, identifying, and estimating the OOA of the objects within a monitored area $\mathcal{A}_{\mathrm{m}}$ of length L_{m} and width W_{m} of the conveyor belt (i.e., a sorting process). The OOA estimation is determined by the order with which objects leave the monitored area. Specifically, the system tracks each object along the conveyor belt and estimates the OOA of the stream, based on the position estimates corresponding to the last detection of each object within the monitored area. In particular, $\mathbf{o}$ is the vector representing the true OOA, therefore $\mathbf{o}[k] = l$ indicates that the lth object is the kth to cross the monitored area.

Each object is equipped with N_{to} tags. In particular, the jth tag on the ith object at time index k is in position $\mathbf{p}^{(k)}_{ij} = [x^{(k)}_{ij}, y^{(k)}_{ij}, z^{(k)}_{ij}] \in \mathbb{R}^3$ with respect to the reference system in Figure 6.7, $i = 1, ..., N_{\mathrm{o}}$ and $j = 1, ..., N_{\mathrm{to}}$.[13] Time indexes correspond to the instants in which measurements are taken by the readers. We consider N_{r} readers, with index set $\mathcal{R}$. The rth reader is in known position $\mathbf{r}_r$ and transmits signals to detect, identify, and localize the tags in the monitored area. Specifically, in the example shown in Figure 6.7, $N_{\mathrm{r}} = 4$, $\mathbf{v} = [v_{\mathrm{c}}, 0, 0]$, $x^{(k)}_{ij} = x^{(1)}_{ij} + (k-1)\, v_{\mathrm{c}} T_{\mathrm{u}}$,

[13] Note that the position of each tag at time index k depends on the first position $\mathbf{p}^{(1)}_{ij}$ and varies according to the conveyor belt speed.

$y_{ij}^{(k)} = y_{ij}^{(1)}$ and $z_{ij}^{(k)} = z_{ij}^{(1)}$, where v_{c} is the constant speed of the conveyor belt along the $\vec{x}$ direction and T_{u} is the interrogation repetition time (i.e., the difference between adjacent tag position estimations).

A position estimate $\widehat{\mathbf{p}}_{ij}^{(k)}$ is determined for each time index $k \in \mathcal{K}_{ij}$, where $\mathcal{K}_{ij}$ is the set of time indices in which the jth tag of the ith object is detected and identified after that a measurement is taken. The maximum localization update rate is $R_{\mathrm{u}} = 1/T_{\mathrm{u}}$. Let $\mathcal{D} \subseteq \mathcal{O}$ be the set of objects that have been detected at the end of the process. An object is considered detected if at least one of its tags is detected by one reader during the time it is within the monitored area. We define $\mathbf{o}_{\mathrm{d}}$ as the OOA vector conditional on detection, which represents the relative OOA among the objects in $\mathcal{D}$. Starting from the tag position estimates, the OOA vector $\widehat{\mathbf{o}}$ is estimated by considering as object position the tag's position which is the greatest with respect to the conveyor direction. Note that the dimension of the vector $\mathbf{o}$ is unknown, then $\widehat{\mathbf{o}}$ and $\mathbf{o}$ have different length in case of misdetections since $|\mathcal{D}| \leq N_{\mathrm{o}}$.[14]

Let $\widehat{\mathbf{k}}_{\mathrm{o}}$ be the vector of the greatest time indices at which each object has been detected and localized within the monitored area, with elements $\widehat{k}_{\mathrm{o}}[i]$ and $i \in \mathcal{D}$, (i.e., $\widehat{\mathbf{k}}_{\mathrm{o}}[1] = n$ if n is the last time index at which the object indexed by 1 has been detected). This vector is determined based on the tag position estimates

$$\widehat{\mathbf{k}}_{\mathrm{o}}[i] = \max\{k \in \mathcal{K}_{ij} : \widehat{\mathbf{p}}_{ij}^{(k)} \cdot \mathbf{v} \in \mathcal{A}_{\mathrm{m}}\,,\ j = 1, 2, \ldots, N_{\mathrm{to}}\} \tag{6.32}$$

where $\mathbf{a} \cdot \mathbf{b}$ is the scalar product between vectors $\mathbf{a}$ and $\mathbf{b}$. The OOA estimate $\widehat{\mathbf{o}}$ is determined in $|\mathcal{D}|$ steps. At each step h, with $h = 1, 2, \ldots, |\mathcal{D}|$, the hth element $\widehat{\mathbf{o}}[h]$ is determined by considering only the set of objects which have not been ordered until the previous step, i.e. having index $i \notin \{\widehat{\mathbf{o}}[1], ..., \widehat{\mathbf{o}}[h-1]\}$. Based on such a set of indices, we choose the minimum time index k_h at which at least one object has been detected for the last time, i.e. $k_h = \min\left\{\widehat{\mathbf{k}}_{\mathrm{o}}[i] : i \notin \{\widehat{\mathbf{o}}[1], ..., \widehat{\mathbf{o}}[h-1]\}\right\}$. We focus on the objects having index i such that $\widehat{\mathbf{k}}_{\mathrm{o}}[i] = k_h$, i.e. those detected for the last time at k_h, and we sort their position with respect to the conveyor belt speed direction.[15] Then, the hth element of $\widehat{\mathbf{o}}$ is determined as

$$\widehat{\mathbf{o}}[h] = \underset{i \text{ s.t. } \widehat{\mathbf{k}}_{\mathrm{o}}[i] = k_h}{\operatorname{argmax}} \left\{\widehat{\mathbf{p}}_{ij}^{(k_h)} \cdot \mathbf{v} \ :\ j = 1, 2, \ldots, N_{\mathrm{to}}\right\}. \tag{6.33}$$

[14] Notation $|\mathcal{A}|$ indicates the cardinality of the set $\mathcal{A}$.

[15] Note that if $\mathbf{v}$ varies with time, we refer to the conveyor speed at the time indexed by k_h.

System Architecture

We consider an UHF-UWB RFID system based on the modulation of the backscatter signal to have a low-cost, low-complexity and low-energy consuming tag. The UHF link serves for both network synchronization and reader-tag data communication (e.g., using a standard Gen. 2 protocol), while the UWB link serves for reader-tag ranging and tag-to-reader data transmission [140]. Each reader consists of a joint UHF-UWB transmitting/receiving unit designed to enable network synchronization, tag detection and identification, tag TOA estimation for localization and sorting, even in the presence of non-idealities such as multi-tag interference and tag clock drift [146].[16]

To save energy, tags are most of the time on a power-saving mode and they need a wake-up procedure to start the UWB backscatter modulation necessary for ranging [138]. Readers modulate the UWB transmitted pulses using an antipodal binary code which allows to uniquely identify the reader (reader's code). Each transmitted pulse is backscattered by a tag which modulates its antenna load according to a specific code (tag's code). The adoption of readers' and tags' codes allows to discriminate the useful signal from environmental clutter and it permits to suppress the inter-tags interference [108]. Thus, a unique UWB tag-to-reader communication channel is established. Note that, differently from standard Gen. 2 UHF-RFID and thanks to the adoption of different tag's codes, a medium access control is not necessary for UWB multi-tag communication and ranging.

6.2.2 Bayesian OOA Estimation

The performance metrics and the Bayesian tracking for OOA estimation are now described.

Performance Metrics

To evaluate the system's ability to estimate the OOA of a stream of objects $\mathbf{o}$, we consider the absolute position of each object (the true position in the stream) and the relative position with respect to the other objects (following or preceding). We define the absolute OOA success rate R_{a}, the relative OOA success rate R_{r}, the object detection rate R_{d}, and the object misdetection rate R_{m}, all over N trials,

[16] A survey on TOA estimation techniques suitable for UWB signals and exploitable in this context can be found in [29].

respectively as

$$R_{\mathrm{a}} = \frac{1}{N\,N_{\mathrm{o}}} \sum_{n=1}^{N} \sum_{i=1}^{|\mathcal{D}^{(n)}|} \delta(\mathbf{o}^{(n)}[i], \widehat{\mathbf{o}}^{(n)}[i]) \tag{6.34}$$

$$R_{\mathrm{r}} = \frac{1}{N\,|\mathcal{D}^{(n)}|} \sum_{n=1}^{N} \sum_{i=1}^{|\mathcal{D}^{(n)}|} \delta(\mathbf{o}_{\mathrm{d}}^{(n)}[i], \widehat{\mathbf{o}}^{(n)}[i]) \tag{6.35}$$

$$R_{\mathrm{d}} = \frac{1}{N} \sum_{n=1}^{N} \frac{\left|\mathcal{D}^{(n)}\right|}{|\mathcal{O}^{(n)}|} \tag{6.36}$$

$$R_{\mathrm{m}} = 1 - R_{\mathrm{d}} \tag{6.37}$$

where, for the nth trial: $\delta(m,n)$ is the Kronecker delta function; $\mathbf{o}^{(n)}[i]$ is the ith element of the true OOA vector; $\widehat{\mathbf{o}}^{(n)}[i]$ is the estimated vector; $\mathbf{o}_{\mathrm{d}}^{(n)}[i]$ is the true OOA vector conditional on detection; $\mathcal{D}^{(n)}$ is the set of detected objects; and $\mathcal{O}^{(n)}$ is the set of objects. Consider, for example, $N_{\mathrm{o}} = 3$, $N = 1$, $\mathbf{o}^{(1)} = [2,1,3]$, $\widehat{\mathbf{o}} = [1,3]$ that gives $R_{\mathrm{d}} = 2/3$, and $R_{\mathrm{m}} = 1/3$. Then, $R_{\mathrm{a}} = 0$ because the absolute position of all the objects in the stream is wrong due to the misdetection of the object with index $i = 2$. Differently, $R_{\mathrm{r}} = 1$ because the relative position among the detected objects is preserved.

TOA Estimation

Once the reader receives the UWB backscattered signal, it performs TOA estimation to determine the distance from the tag. To discriminate the signal of a specific tag from clutter and inter-tags interference, a de-spreading operation is conducted at reader side on the received signal, exploiting the knowledge of the tag code of interest [108, 140]. This allows to extract the signal component due to the backscattering of a specific tag from the received waveform [146]. At the rth reader, the round-trip time (RTT) estimation $\widehat{\tau}_{ij,r}^{(k)}(\mathbf{p}_{ij}^{(k)})$ with respect to the jth tag attached on the ith object is obtained. From the RTT estimation, the reader-tag distance $\widehat{d}_{ij,r}^{(k)}$ is determined as $\widehat{d}_{ij,r}^{(k)} = c\,\widehat{\tau}_{ij,r}^{(k)}(\mathbf{p}_{ij}^{(k)})/2$ where c is the speed of light. Note that, we consider each reader estimating the TOA of the signal backscattered by the tag related to the interrogation signal emitted by the reader itself; due the passive nature of the system, other multi-static ranging and localization techniques typical of SR can be adopted to improve the performance [137].

De-spreading and ranging based on the received signal can be implemented in severely ways depending on the required performance and on complexity limitation at

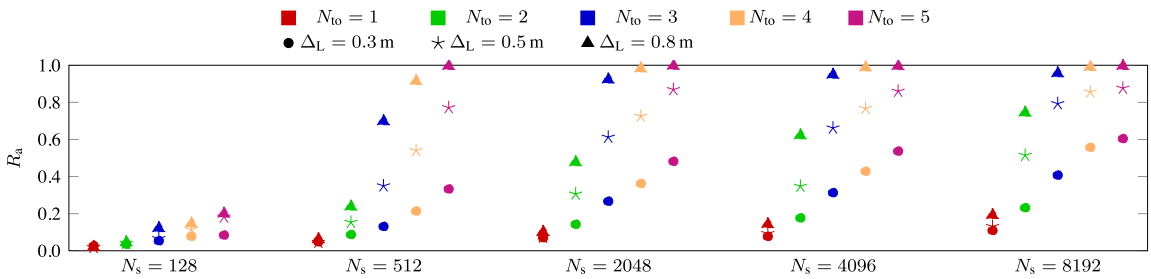

Figure 6.8: Absolute OOA success rate for $R_u = 10\,\text{Hz}$ and different values of N_s, Δ_L, and N_{to}.

reader side. Here, a low-complexity energy-based receiver architecture, as described in [146, 186] is considered, in which the TOA estimate resolution is bounded by the energy detector integration window T_{ED}. Detection and ranging performance depend on the SNR, which is function of the reader-tag distance. The mean received power averaged over the multipath fading at the rth reader side is given by

$$P_{ij,r}^{(k)} = \int_{f_c-\frac{W}{2}}^{f_c+\frac{W}{2}} \frac{P_t(f)G_t^2(f,\boldsymbol{\Theta}_t)G_r^2(f,\boldsymbol{\Theta}_r)}{\left(d_{ij,r}^{(k)}\right)^4 L_{tag}} \left(\frac{c}{4\pi f}\right)^4 df \tag{6.38}$$

where f_c is the central frequency, W is the transmitted signal bandwidth, $P_t(f)$ is the transmitted one-sided PSD, $G_t(f,\boldsymbol{\Theta})$ and $G_r(f,\boldsymbol{\Theta})$ are the tag and reader antenna gains that vary with the frequency and they are function of $\boldsymbol{\Theta} = (\theta,\phi)$ representing the couple of elevation and azimuthal angles specific of the reader-tag link under consideration. L_{tag} accounts for tag losses and $d_{ij,r}^{(k)}$ is the reader-tag distance. Angles $\boldsymbol{\Theta}_t$ and $\boldsymbol{\Theta}_r$ are related to reciprocal tag and reader orientations, respectively. The received SNR, at reader side, is $\mathsf{SNR}_{ij,r}^{(k)} = N_s P_{ij,r}^{(k)} T_f / N_0$, where N_s is the number of accumulated UWB pulses [146] and T_f is the PRP. The one-sided noise PSD N_0 is given by $N_0 = \kappa F T_0$ where F is the noise figure, T_0 the reference temperature, and κ the Boltzmann constant. In the following, a tag is considered detected if the received SNR is above a threshold SNR_{th} dependent on the system parameters.

Bayesian Tracking

In relation to the signal processing techniques in 2.3, the tracking algorithm infers the tag position $\mathbf{p}_{ij}^{(k)}$ (i.e., the state vector) at each time index k from a set of ranging estimates (i.e., observations), a mobility model (i.e., relation between the current and the prior state vectors), and the perception model (i.e., relation between the

observations and the current state vector) [15]. Following a Bayesian approach, the position estimate $\widehat{\mathbf{p}}_{ij}^{(k)}$ is determined as the value that maximizes the position belief $b(\mathbf{p}) = p(\mathbf{p}|\widehat{\boldsymbol{\tau}}_{ij}^{(1:k)})$, which is the posterior distribution of the state vector given the set of observations $\widehat{\boldsymbol{\tau}}_{ij}^{(1:k)} \triangleq \{\widehat{\tau}_{ij,r}^{(h)} \text{ s.t. } r \in \mathcal{R}, h = 1, 2, \ldots, k\}$. In particular, at each time k, $\widehat{\boldsymbol{\tau}}_{ij}^{(1:k)}$ is the vector of RTT estimates and $\widehat{\tau}_{ij,r}^{(1:k)}$ is provided by the energy detector at time k if the rth receiver detected and identified the target. Among the possible implementations of Bayesian algorithms, we consider the PF algorithm, which can outperform the EKF in non-Gaussian noisy observations [15].[17] In particular, the position belief at time k is represented by a set of N_{par} random samples (particles) at $\{\mathbf{s}_s^{(k)}\}$, with $s = 1, 2, ..., N_{\text{par}}$. Mobility and perception models are used to predict, update, and resample the position belief at each k. In particular, a Gaussian mobility model is given by

$$p(\mathbf{s}_s^{(k)}|\mathbf{s}_s^{(k-1)}) = \frac{1}{\sqrt{2\pi}\sigma_{\text{m},k}} e^{-\frac{\left\|\mathbf{s}_s^{(k)} - \widehat{\boldsymbol{\mu}}_k^{(n)}\right\|^2}{2\sigma_{\text{m},k}^2}} \tag{6.39}$$

where $\sigma_{\text{m},k}^2$ depends on the mobility of the target and $\widehat{\boldsymbol{\mu}}_n^{(k)} = \mathbf{s}_s^{(k-1)} + \mathbf{v}\, T_{\text{u}}$, where $\mathbf{v}$ is the conveyor speed vector that is assumed known. A perception model for particles with independent observations, is given by

$$p(\widehat{\boldsymbol{\tau}}_{ij}^{(k)}|\mathbf{s}_s^{(k)}) = \prod_{r \in \mathcal{R}} \frac{1}{\sqrt{2\pi}\sigma_{\text{p},k}} e^{-\frac{\left[\widehat{\tau}_{ij,r}^{(k)}\, c/2 - \|\mathbf{r}_r - \mathbf{s}_s^{(k)}\|\right]^2}{2\sigma_{\text{p},k}^2}} \tag{6.40}$$

where $\sigma_{\text{p},k}^2$ depends on the ranging techniques and the propagation conditions.

6.2.3 Results

We first describe the operating scenario and the main system parameters. Then, we evaluate the performance of the considered system in terms of relative and absolute OOA success rate, as well as of object misdetection rate.

Scenario and System Parameters

We consider an UHF-UWB RFID system composed of 4 readers located on the edge of a monitored area of length $L_{\text{m}} = 2\,\text{m}$ and width $W_{\text{m}} = 1.5\,\text{m}$, with height

[17] Note that, in general, the set of observations have a non-Gaussian distribution due to multipath and clutter residual.

1.5 m with respect to the z axes, as shown in Figure 6.7. We consider streams of $|\mathcal{O}^{(n)}| = N_{\mathrm{o}} = 20$ with $n = 1, 2, \ldots, N$ objects, where n indicates the nth Monte-Carlo trial and $N = 100$. Objects have parallelepiped shape with two possible dimensions described by the following edge lengths: a) 0.45 m, 0.22 m, and 0.41 m or b) 0.58 m, 0.36 m, and 0.86 m. Each object is equipped with a number of tags $N_{\mathrm{to}} = 1, 2, \ldots, 5$; at most one tag per face and no tags on the bottom face. At time index $k = 0$, each object is at a random position within the conveyor belt and the bottom face laying on the conveyor is chosen randomly. Tags are at a uniformly distributed random positions on object faces. To preserve the time resolvability of signals correspondent to different objects, a minimum Euclidean distance Δ_{L} is required between two tags attached to two different objects. Results are obtained with $\Delta_{\mathrm{L}} = 0.3, 0.5$, and 0.8 m. The conveyor belt has length $L_{\mathrm{c}} = 50\Delta_{\mathrm{L}}$ m to preserve a certain density of objects, and $W_{\mathrm{c}} = W_{\mathrm{m}}$. The conveyor speed vector is $\mathbf{v} = [v_{\mathrm{c}}, 0, 0]$ and it is assumed known with $v_{\mathrm{c}} = 1$ m/s. The same transmitting and receiving UWB antenna is considered for both tags and readers: a 3D simulated radiation pattern of a dipole antenna attached to a reflector has been included in simulation. Frequency selectivity is not considered and we assume the radiation pattern equal to its value at the central frequency $f_{\mathrm{c}} = 4$ GHz. Reader antennas presents a maximum gain of $G_r(f_{\mathrm{c}}, \mathbf{\Theta}_r^{(\max)}) = 5.35$ dBi while tag antennas are such that the maximum value of $G_{\mathrm{t}}(f_{\mathrm{c}}, \mathbf{\Theta}_{\mathrm{t}}^{(\max)})/L_{\mathrm{tag}} = 3$. Reader antennas are set to have maximum gain toward the center of the monitored area, while the tag antennas have maximum gain towards the direction orthogonal to the object face to which the tag is attached. Wireless propagation and ranging errors are modeled based on geometric visibility. In particular, for a given reader, each tag is assumed undetected when it is in NLOS condition with respect to the reader (i.e., another object obstruct the reader-tag signal path) or when it is in LOS condition with the reader and the signal is received with $\mathsf{SNR}_{ij,r}^{(k)} \leq \mathsf{SNR}_{\mathrm{th}}$, where $\mathsf{SNR}_{\mathrm{th}}$ is a threshold corresponding to the received SNR when the tag is at a distance of 6 m, antennas are oriented in the direction of the maximum gain and $N_{\mathrm{p}} = 8192$.[18] If a tag is detected, we assume a TOA estimation error uniformly distributed in $[-1, 1]$ ns.[19] Results are obtained considering a maximum update rate $R_{\mathrm{u}} = 5, 10$, and 15 Hz. The tracking algorithm is based on PF with $N_{\mathrm{par}} = 100$, $\sigma_{\mathrm{p},k}^2 = 1$ for all k, and a value of $\sigma_{\mathrm{m},k}^2$ chosen such

[18] This distance has been measured considering these parameter within the European project SELECT (www.selectwireless.eu).

[19] This corresponds to an energy detector with $T_{\mathrm{ED}} = 2$ ns.

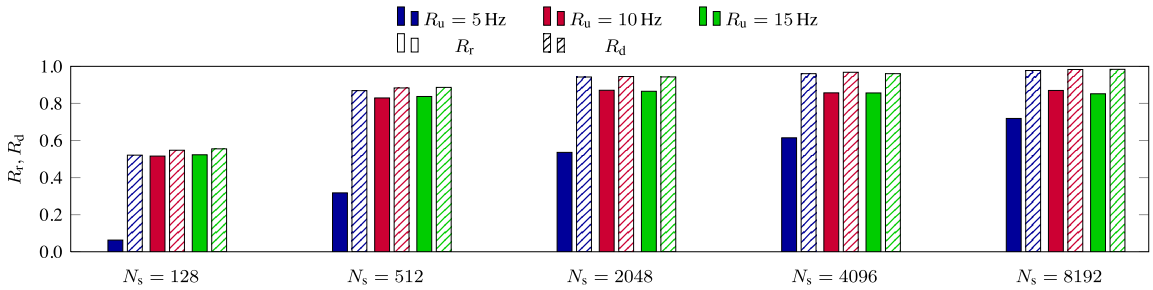

Figure 6.9: Relative OOA success rate and object detection rate for $N_{to} = 3$, $\Delta_L = 0.5\,\text{m}$, and different values of N_s and R_u.

	R_m			R_r		
N_{to}	$\Delta_L = 0.3\,\text{m}$	$\Delta_L = 0.5\,\text{m}$	$\Delta_L = 0.8\,\text{m}$	$\Delta_L = 0.3\,\text{m}$	$\Delta_L = 0.5\,\text{m}$	$\Delta_L = 0.8\,\text{m}$
1	0.53	0.43	0.32	0.42	0.55	0.68
2	0.29	0.16	0.08	0.57	0.80	0.91
3	0.15	0.06	0.01	0.65	0.87	0.98
4	0.08	0.02	0	0.66	0.91	0.99
5	0.05	0.01	0	0.69	0.91	1

Table 6.1: Relative OOA success rate and misdetection rate for $N_s = 2048$ and different values of N_{to} and Δ_L.

that the nth estimated particle at time k is within a circle centered at $\hat{\boldsymbol{\mu}}_n^{(k)}$ of radius $|\hat{\mathbf{v}}_k|\, T_L$.

Numerical Results

Figure 6.8 shows the absolute OOA success rate for $R_u = 10\,\text{Hz}$, various N_{to}, Δ_L, and N_s. It can be seen that, in each setting, R_a increases with N_s but with negligible improvement for $N_s > 2048$. Moreover, by increasing Δ_L the absolute OOA success rate becomes more sensitive to the number of tags per object. For example, varying N_{to} from 1 to 5 increases R_a from 0.03 to 0.08 when $\Delta_L = 0.3\,\text{m}$, whereas it increases R_a from 0.02 to 0.20 when $\Delta_L = 0.8\,\text{m}$. This is because decreasing the distance between two tags attached to two different objects strongly limits the detection rate by increasing the number of NLOS conditions between readers and tags.

Figure 6.9 shows the relative OOA success rate R_r and the object detection rate R_m for $\Delta_L = 0.5\,\text{m}$, $N_{to} = 3$, and various Δ_L and N_s. It can be seen that the detection rate is more sensitive to the number of collected pulses than the update rate. For example, varying the update rate from $R_u = 5\,\text{Hz}$ to $R_u = 15$ changes R_d from 0.52 to 0.56 with $N_s = 128$, while it changes from 0.52 to 0.86 by increasing

N_s from 128 to 512 when $R_u = 5\,\text{Hz}$. Differently, the relative OOA success rate is very sensitive to the update rate, especially when the number of pulses is low. For example, varying the update rate from $R_u = 5\,\text{Hz}$ to $R_u = 10$ changes R_r from 0.06 to 0.52. However, a floor is experienced for $R_u > 5\,\text{Hz}$. Note that this parameter and the floor is strictly related to the monitored area dimension and the speed of the conveyor. Similarly to Figure 6.8 the effects of the number of collected pulses becomes negligible for $N_s > 2048$ for both R_a and R_m. This is due to the fact that the number of collected pulses influences the R_d more than the localization accuracy.

The table in Figure 6.1 gives the the relative OOA success rate R_r and misdetection rate R_m for $N_s = 2048$ and different values of N_{to} and Δ_L. Note that, even when the number of detected object is above the 95%, increasing the number of tags per object is less effective than increasing the distance between two tags Δ_L for the OOA performance. Moreover, increasing the number of tags above 3 has negligible effects on R_r, while it improves significantly the detection rate, especially when the distance between tags Δ_L is short.

Chapter 7

Conclusion

The statistical modeling and algorithm design of wireless localization systems have been explored, with particular regard to semi-passive and passive systems (i.e., location and tracking of non-collaborative targets, passive radar systems that use signals of opportunity, and wireless systems for the identification and localization of semi-passive tag devices embedded in objects). The research activity has been also conducted within the framework of international projects in collaboration with other universities and companies.

A mathematical model for the range information is derived as a function of wireless environment, signal features, and energy detection techniques. Such a model is tractable and serves as a cornerstone for the design and analysis of wideband ranging systems enabling soft-decision and hard-decision localization. Using the proposed range information model, we have obtained explicit expressions for the range likelihood and range estimate, as well as the distribution of the range estimation error. These expressions form the basis for the design of the energy detector according to a variety of optimization criteria and physical constraints. A case study of a localization network operating in a wireless environment is presented and its performance, in terms of ranging and localization accuracy, is evaluated. The accuracy of the analysis is confirmed by sample-level simulations. The results show that soft-decision localization requiring only the knowledge of channel statistics can significantly outperform hard-decision localization. The proposed range information model provides a new perspective on range-based localization in wireless environments.

The intrinsic properties of sensor radar networks and the representativeness of their observations determine the localization accuracy, especially in harsh propagation environments. Blind methods for observation selection have been proposed

based on features extracted from the received waveforms. Our methodology inspects the network setting, propagation environment, waveform processing, observation selection, and localization algorithm in an absence of prior information. It shows the importance of selecting representative observations for high localization accuracy in NLOS conditions, especially by adopting the appropriate selection features. In fact, in addition to a reduction in the overall localization complexity, observation selection significantly improves the performance in the presence of obstacles. The localization performance of a network of UWB SRs operating in an indoor environment with multipath, clutter, and obstructions has been determined based on the proposed methods for observation selection and signal processing. Results show that, in the presence of obstructions due to walls, the proposed selection methods strongly improve the localization accuracy. For example, the localization error outage at 1m improves from 93% without observation selection to 23% with the proposed observation selection method.

The effects of radar networking and signal processing on the tracking accuracy of SRs operating in indoor environments have been characterized. The results show that submeter accuracy can be achieved with a proper allocation of resources for the different tasks. In particular, deploying more than three sensors per room increases the network cost without contributing significantly to localization accuracy. The monostatic SRs perform better than the multistatic ones when resources are severely limited, while the multistatic SRs perform better than the monostatic ones not when ample resources are available. Moreover, a smart selection of available observations can improve performance, especially when a large number of sensors is deployed. The results provide guidelines for the joint design of the radar network, waveform processing, and tracking algorithm for inferring the position of moving targets in indoor scenarios. A passive radar system based on LTE signals of opportunity has been proposed. A Bayesian framework for tracking mobile targets and estimating their velocity within a monitored environment has been developed. The performance is quantified for a case study accounting for the LTE extended pedestrian model with various network, propagation, and processing settings. Results show that the mitigation of static clutter and of direct signals plays a very important role on the tracking accuracy.

The detection of multiple semi-passive RFID tags adopting impulsive backscattered signals is also addressed The design of multi-tag detection and tag codes is developed in the presence of interference, wake-up synchronization offset, and clock

drift. The system performance in terms of detection and false alarm rate is determined for different code families in various scenarios. An UHF-UWB RFID system enabling OOA estimation for a stream of objects has been presented. The OOA estimation performance metrics has been defined to evaluate the effects of RFID configurations and signal processing techniques on the performance for a succession of objects moving on a conveyor belt. The results based on particle filtering show a success rate greater than 99% can be achieved with a proper setting of ranging technique, localization update rate, and number of tags per object. In particular, the minimum distance between tags attached to two different objects strongly affects the performance even when a high number of particles is used.

Bibliography

[1] C. Floerkemeier, M. Langheinrich, E. Fleisch, F. Mattern, and S. E. Sarma, *The Internet of Things*. Lecture notes in computer science, vol. 4952, Springer, 2008.

[2] M. I. Skolnik, *Radar Handbook*, 2nd ed. McGraw-Hill Professional, 1990.

[3] W. Hao, S. Wei-min, and G. Hong, "A novel Taylor series method for source and receiver localization using TDOA and FDOA measurements with uncertain receiver positions," in *Proc. IEEE CIE Int. Conf. on Radar (Radar)*, Chengdu, China, Oct. 2011, pp. 1037–1040.

[4] K. C. Ho, L. Xiaoning, and L. Kovavisaruch, "Source localization using TDOA and FDOA measurements in the presence of receiver location errors: Analysis and solution," *IEEE Trans. Signal Process.*, vol. 55, no. 2, pp. 684–696, Feb. 2007.

[5] M. Z. Win, A. Conti, S. Mazuelas, Y. Shen, W. M. Gifford, D. Dardari, and M. Chiani, "Network localization and navigation via cooperation," *IEEE Commun. Mag.*, vol. 49, no. 5, pp. 56–62, May 2011.

[6] M. Z. Win and R. A. Scholtz, "Ultra-wide bandwidth time-hopping spread-spectrum impulse radio for wireless multiple-access communications," *IEEE Trans. Commun.*, vol. 48, no. 4, pp. 679–691, Apr. 2000.

[7] D. Cassioli, M. Z. Win, and A. F. Molisch, "The ultra-wide bandwidth indoor channel: From statistical model to simulations," *IEEE J. Sel. Areas Commun.*, vol. 20, no. 6, pp. 1247–1257, Aug. 2002.

[8] S. Gezici and H. V. Poor, "Position estimation via ultra-wide-band signals," *Proc. IEEE*, vol. 97, no. 2, pp. 386–403, Feb. 2009.

[9] L. Stoica, A. Rabbachin, and I. Oppermann, "A low-complexity noncoherent IR-UWB transceiver architecture with TOA estimation," *IEEE Trans. Microw. Theory Tech.*, vol. 54, no. 4, pp. 1637–1646, Jun. 2006.

[10] S. Gezici, M. Chiang, H. V. Poor, and H. Kobayashi, "A genetic algorithm based finger selection scheme for UWB MMSE rake receivers," in *Proc. IEEE International Conference on Ultrawideband (ICU 2005)*, Zurich, Switzerland, Sep. 2005.

[11] N. Patwari, A.O. Hero III, M. Perkins, N. Correal, and R. O'Dea, "Relative location estimation in wireless sensor networks," *IEEE Trans. Signal Process.*, vol. 51, no. 8, pp. 2137 – 2148, Aug. 2003.

[12] S. Maranò, W. M. Gifford, H. Wymeersch, and M. Z. Win, "NLOS identification and mitigation for localization based on UWB experimental data," *IEEE J. Sel. Areas Commun.*, vol. 28, no. 7, pp. 1026–1035, Sep. 2010.

[13] A. Conti, M. Guerra, D. Dardari, N. Decarli, and M. Z. Win, "Network experimentation for cooperative localization," *IEEE J. Sel. Areas Commun.*, vol. 30, no. 2, pp. 467–475, Feb. 2012.

[14] B. Alavi and K. Pahlavan, "Modeling of the TOA-based distance measurement error using UWB indoor radio measurements," *IEEE Commun. Lett.*, vol. 10, no. 4, pp. 275–277, Apr. 2006.

[15] F. Gustafsson, F. Gunnarsson, N. Bergman, U. Forsell, J. Jansson, R. Karlsson, and P. J. Nordlund, "Particle filters for positioning, navigation and tracking," *IEEE Trans. Signal Process.*, vol. 50, no. 2, pp. 425–437, Feb. 2002.

[16] A. H. Welsh, *Aspects of Statistical Inference*. Wiley, 2011.

[17] J. Aspnes, D. Goldenberg, and Y. R. Yang, "On the computational complexity of sensor network localization," in *Proc. Int. Workshop on Algorithmic Aspects of Wireless Sensor Networks*, Turku, Finland, Jul. 2004, pp. 32–44.

[18] D. E. Knuth, *The Art of Computer Programming, Volume 3: (2nd Ed.) Sorting and Searching*. Redwood City, CA, USA: Addison Wesley Longman Publishing Co., Inc., 1998.

[19] N. Patwari, J. N. Ash, S. Kyperountas, A. O. Hero, R. L. Moses, and N. S. Correal, "Locating the nodes: Cooperative localization in wireless sensor networks," *IEEE Signal Process. Mag.*, vol. 22, no. 4, pp. 54–69, Jul. 2005.

[20] K. Pahlavan, X. Li, and J.-P. Mäkelä, "Indoor geolocation science and technology," *IEEE Commun. Mag.*, vol. 40, no. 2, pp. 112–118, Feb. 2002.

[21] J. Hightower and G. Borriello, "Location systems for ubiquitous computing," *Computer*, vol. 34, no. 8, pp. 57–66, Aug. 2001.

[22] Y. Shen and M. Z. Win, "Fundamental limits of wideband localization – Part I: A general framework," *IEEE Trans. Inf. Theory*, vol. 56, no. 10, pp. 4956–4980, Oct. 2010.

[23] Y. Shen, H. Wymeersch, and M. Z. Win, "Fundamental limits of wideband localization – Part II: Cooperative networks," *IEEE Trans. Inf. Theory*, vol. 56, no. 10, pp. 4981–5000, Oct. 2010.

[24] S. Gezici, Z. Tian, G. B. Giannakis, H. Kobayashi, A. F. Molisch, H. V. Poor, and Z. Sahinoglu, "Localization via ultra-wideband radios: A look at positioning aspects for future sensor networks," *IEEE Signal Process. Mag.*, vol. 22, no. 4, pp. 70–84, Jul. 2005.

[25] A. H. Sayed, A. Tarighat, and N. Khajehnouri, "Network-based wireless location: Challenges faced in developing techniques for accurate wireless location information," *IEEE Signal Process. Mag.*, vol. 22, no. 4, pp. 24–40, Jul. 2005.

[26] U. A. Khan, S. Kar, and J. M. F. Moura, "Distributed sensor localization in random environments using minimal number of anchor nodes," *IEEE Trans. Signal Process.*, vol. 57, no. 5, pp. 2000–2016, May 2009.

[27] Y. Shen, S. Mazuelas, and M. Z. Win, "Network navigation: Theory and interpretation," *IEEE J. Sel. Areas Commun.*, vol. 30, no. 9, pp. 1823–1834, Oct. 2012.

[28] U. A. Khan, S. Kar, and J. M. F. Moura, "DILAND: An algorithm for distributed sensor localization with noisy distance measurements," *IEEE Trans. Signal Process.*, vol. 58, no. 3, pp. 1940–1947, Mar. 2010.

[29] D. Dardari, A. Conti, U. J. Ferner, A. Giorgetti, and M. Z. Win, "Ranging with ultrawide bandwidth signals in multipath environments," *Proc. IEEE*, vol. 97, no. 2, pp. 404–426, Feb. 2009, special issue on *Ultra-Wide Bandwidth (UWB) Technology & Emerging Applications*.

[30] R. Niu and P. K. Varshney, "Target location estimation in sensor networks with quantized data," *IEEE Trans. Signal Process.*, vol. 54, no. 12, pp. 4519–4528, Dec. 2006.

[31] R. Niu, R. S. Blum, P. K. Varshney, and A. L. Drozd, "Target localization and tracking in noncoherent multiple-input multiple-output radar systems," *IEEE Trans. Aerosp. Electron. Syst.*, vol. 48, no. 2, pp. 1466–1489, Apr. 2012.

[32] M. Arik and O. B. Akan, "Collaborative mobile target imaging in UWB wireless radar sensor networks," *IEEE J. Sel. Areas Commun.*, vol. 28, no. 6, pp. 950–961, Aug. 2010.

[33] S. Bartoletti, A. Conti, A. Giorgetti, and M. Z. Win, "Sensor radar networks for indoor tracking," *IEEE Wireless Commun. Lett.*, vol. 3, no. 2, pp. 157–160, Apr. 2014.

[34] E. Paolini, A. Giorgetti, M. Chiani, R. Minutolo, and M. Montanari, "Localization capability of cooperative anti-intruder radar systems," *EURASIP J. Adv. Signal Process.*, vol. 2008, pp. 1–14, Apr. 2008.

[35] K. K. Mada, H.-C. Wu, and S. S. Iyengar, "Efficient and robust EM algorithm for multiple wideband source localization," *IEEE Trans. Veh. Technol.*, vol. 58, no. 6, pp. 3071–3075, Jul. 2009.

[36] L. Lu, H. Zhang, and H.-C. Wu, "Novel energy-based localization technique for multiple sources," *IEEE Syst. J.*, vol. 8, no. 1, pp. 142–150, Mar. 2014.

[37] D. Dardari, C.-C. Chong, and M. Z. Win, "Threshold-based time-of-arrival estimators in UWB dense multipath channels," *IEEE Trans. Commun.*, vol. 56, no. 8, pp. 1366–1378, Aug. 2008.

[38] H. Lu, S. Mazuelas, and M. Z. Win, "Ranging likelihood for wideband wireless localization," in *Proc. IEEE Int. Conf. Commun.*, Budapest, Hungary, Jun. 2013, pp. 4397–4401.

[39] H. Wymeersch, J. Lien, and M. Z. Win, "Cooperative localization in wireless networks," *Proc. IEEE*, vol. 97, no. 2, pp. 427–450, Feb. 2009, special issue on *Ultra-Wide Bandwidth (UWB) Technology & Emerging Applications*.

[40] I. Guvenc, C.-C. Chong, F. Watanabe, and H. Inamura, "NLOS identification and weighted least-squares localization for UWB systems using multipath channel statistics," *EURASIP J. Appl. Signal Process.*, vol. 2008, 2008.

[41] B. Denis and N. Daniele, "NLOS ranging error mitigation in a distributed positioning algorithm for indoor UWB ad-hoc networks," in *International Workshop on Wireless Ad-Hoc Networks*, Oulu, Finland, May/Jun. 2004, pp. 356–360.

[42] S. Venkatesh and R. M. Buehrer, "NLOS mitigation using linear programming in ultrawideband location-aware networks," *IEEE Trans. Veh. Technol.*, vol. 56, no. 5, pp. 3182–3198, Sep. 2007.

[43] A. Conti, D. Dardari, M. Guerra, L. Mucchi, and M. Z. Win, "Experimental characterization of diversity navigation," *IEEE Syst. J.*, vol. 8, no. 1, pp. 115–124, Mar. 2014.

[44] H. Urkowitz, "Energy detection for unknown deterministic signal," *Proc. IEEE*, vol. 55, no. 4, pp. 523–531, Apr. 1967.

[45] C. Xu and C. L. Law, "Delay-dependent threshold selection for UWB TOA estimation," *IEEE Commun. Lett.*, vol. 12, no. 5, pp. 380–382, May 2008.

[46] A. Giorgetti and M. Chiani, "Time-of-arrival estimation based on information theoretic criteria," *IEEE Trans. Signal Process.*, vol. 61, no. 8, pp. 1869–1879, Apr. 2013.

[47] X. Cheng, F. Vanhaverbeke, Y. L. Guan, and M. Moeneclaey, "Blind combining for weighted energy detection of UWB signals," *Electron. Lett.*, vol. 47, no. 1, pp. 55–57, Jan. 2011.

[48] A. Mariani, A. Giorgetti, and M. Chiani, "Effects of noise power estimation on energy detection for cognitive radio applications," *IEEE Trans. Commun.*, vol. 59, no. 12, pp. 3410–3420, Dec. 2011.

[49] J. W. Chong, D. K. Sung, and Y. Sung, "Cross-layer performance analysis for CSMA/CA protocols: Impact of imperfect sensing," *IEEE Trans. Veh. Technol.*, vol. 59, no. 3, pp. 1100–1108, Mar. 2010.

[50] I. Ramachandran and S. Roy, "On acquisition of wideband direct-sequence spread spectrum signals," *IEEE Trans. Wireless Commun.*, vol. 5, pp. 1537–1546, Jun. 2006.

[51] N. C. Beaulieu, "Closed-form approximate to PDF of time-average power of bandlimited Gaussian process," *IEE Electronics Letters*, vol. 32, no. 21, pp. 1948–1950, Oct. 1996.

[52] V. Kostylev, "Energy detection of a signal with random amplitude," in *Proc. IEEE Int. Conf. Commun.*, New York, USA, Apr. 2002, pp. 1606–1610.

[53] J. Salt and H. Nguyen, "Performance prediction for energy detection of unknown signals," *IEEE Trans. Veh. Technol.*, vol. 57, no. 6, pp. 3900–3904, Nov. 2008.

[54] F. Digham, M.-S. Alouini, and M. K. Simon, "On the energy detection of unknown signals over fading channels," *IEEE Trans. Commun.*, vol. 55, no. 1, pp. 21–24, Jan. 2007.

[55] A. Anttonen, A. Mammela, and A. Kotelba, "Error probability of energy detected multilevel pam signals in lognormal multipath fading channels," in *Proc. IEEE Int. Conf. Commun.*, Dresden, Germany, Jun. 2009, pp. 1–5.

[56] S. Atapattu, C. Tellambura, and H. Jiang, "Performance of an energy detector over channels with both multipath fading and shadowing," *IEEE Trans. Wireless Commun.*, vol. 9, no. 12, pp. 3662–3670, Dec. 2010.

[57] A. Rabbachin, T. Q. Quek, P. C. Pinto, I. Oppermann, and M. Z. Win, "Noncoherent UWB communication in the presence of multiple narrowband interferers," *IEEE Trans. Wireless Commun.*, vol. 9, no. 11, pp. 3365–3379, Nov. 2010.

[58] E. D. Banta, "Energy detection of unknown deterministic signals in the presence of jamming," *IEEE Trans. Aerosp. Electron. Syst.*, vol. 14, no. 2, pp. 384–386, Mar. 1978.

[59] D. B. Jourdan, D. Dardari, and M. Z. Win, "Position error bound for UWB localization in dense cluttered environments," *IEEE Trans. Aerosp. Electron. Syst.*, vol. 44, no. 2, pp. 613–628, Apr. 2008.

[60] T. Wang, "Cramér-Rao bound for localization with a priori knowledge on biased range measurements," *IEEE Trans. Aerosp. Electron. Syst.*, vol. 48, no. 1, pp. 468 –476, Jan. 2012.

[61] J. Shen, A. F. Molisch, and J. Salmi, "Accurate passive location estimation using TOA measurements," *IEEE Trans. Wireless Commun.*, vol. 11, no. 6, pp. 2182 –2192, Jun. 2012.

[62] N. Sidiropoulos, A. Swami, and B. Sadler, "Quasi-ML period estimation from incomplete timing data," *IEEE Trans. Signal Process.*, vol. 53, no. 2, pp. 733–739, Feb. 2005.

[63] M. Abramowitz and I. A. Stegun, *Handbook of Mathematical Functions*. Dover Publications, 1970.

[64] I. Guvenc and Z. Sahinoglu, "Threshold-based TOA estimation for impulse radio UWB systems," in *Proc. IEEE Int. Conf. on Ultra-Wideband*, Zurich, Switzerland, Sep. 2005, pp. 420–425.

[65] A. F. Molisch, D. Cassioli, C.-C. Chong, S. Emami, A. Fort, B. Kannan, J. Karedal, J. Kunisch, H. Schantz, K. Siwiak, and M. Z. Win, "A comprehensive standardized model for ultrawideband propagation channels," *IEEE Trans. Antennas Propag.*, vol. 54, no. 11, pp. 3151–3166, Nov. 2006, special issue on *Wireless Communications*.

[66] I. N. Sanov, "On the probability of large deviations of random variables," *Mat. Sbornik*, vol. 42, pp. 11–44, 1957.

[67] W. Feller, *An Introduction to Probability Theory and Its Applications*. Wiley, 1971, vol. 2.

[68] A. N. Shiryaev, *Probability*, 2nd ed. New York, NY: Springer-Verlag, 1995.

[69] T. Kailath, "Sampling models for linear time-variant filters," Massachusetts Institute of Technology, Research Laboratory of Electronics (RLE) Technical Report 352, May 1959.

[70] P. A. Bello, "Characterization of randomly time-variant linear channels," *IEEE Trans. Commun. Sys.*, vol. CS-11, no. 4, pp. 360–393, Dec. 1963.

[71] M. Z. Win and Z. A. Kostić, "Impact of spreading bandwidth on Rake reception in dense multipath channels," *IEEE J. Sel. Areas Commun.*, vol. 17, no. 10, pp. 1794–1806, Oct. 1999.

[72] M. Z. Win, G. Chrisikos, and N. R. Sollenberger, "Performance of Rake reception in dense multipath channels: Implications of spreading bandwidth and selection diversity order," *IEEE J. Sel. Areas Commun.*, vol. 18, no. 8, pp. 1516–1525, Aug. 2000.

[73] J. D. Parsons, *The Mobile Radio Propagation Channel*, 2nd ed. England: John Wiley & Sons Ltd., 2000.

[74] A. F. Molisch, *Wireless Communications*, 2nd ed. United Kingdom: IEEE Press, John Wiley & Sons Ltd., 2010.

[75] A. F. Molisch, L. J. Greenstein, and M. Shafi, "Propagation issues for cognitive radio," *Proc. IEEE*, vol. 97, no. 5, pp. 787–804, May 2009.

[76] H. Hashemi, "The indoor radio propagation channel," *Proc. IEEE*, vol. 81, no. 7, pp. 943–968, Jul. 1993.

[77] J. Lin, "Divergence measures based on the Shannon entropy," *IEEE Trans. Inf. Theory*, vol. 37, no. 1, pp. 145–151, Jan. 1991.

[78] I. Guvenc and Z. Sahinoglu, "TOA estimation with different IR-UWB transceiver types," in *Proc. IEEE Int. Conf. on Ultra-Wideband*, Zurich, Switzerland, Sep. 2005, pp. 426–431.

[79] J.-Y. Lee and R. A. Scholtz, "Ranging in a dense multipath environment using an UWB radio link," *IEEE J. Sel. Areas Commun.*, vol. 20, no. 9, pp. 1677–1683, Dec. 2002.

[80] R. A. Scholtz and J.-Y. Lee, "Problems in modeling UWB channels," *Electronic letters*, vol. 20, no. 9, pp. 1–10, Dec. 2002.

[81] S. Bartoletti, W. Dai, A. Conti, and M. Z. Win, "A mathematical model for wideband ranging," *IEEE J. Sel. Topics Signal Process.*, vol. 9, no. 2, pp. 216–228, Mar. 2015.

[82] Federal Communications Commission, "Revision of part 15 of the commission's rules regarding ultra-wideband transmission systems, first report and order (ET Docket 98-153)," Adopted Feb. 14, 2002, Released Apr. 22, 2002.

[83] L. Mucchi, E. D. Re, and T. Landi, "Multi-level environment identification method for impulsive radio systems," in *Proc. IEEE Int. Conf. on Ultra-Wideband*, Bologna, Italy, Sep. 2011, pp. 385–389.

[84] P. Closas, C. Fernández-Prades, and J. A. Fernandez-Rubio, "A Bayesian approach to multipath mitigation in GNSS receivers," *IEEE J. Sel. Topics Signal Process.*, vol. 3, no. 4, pp. 695–706, Aug. 2009.

[85] P. Closas and C. Fernández-Prades, "A statistical multipath detector for antenna array based GNSS receivers," *IEEE Trans. Wireless Commun.*, vol. 10, no. 3, pp. 916–929, Mar. 2011.

[86] P. Closas and M. F. Bugallo, "Improving accuracy by iterated multiple particle filtering," *IEEE Signal Process. Lett.*, vol. 19, no. 8, pp. 531–534, Aug. 2012.

[87] H.-C. Wu, Y. Wu, J. C. Principe, and X. Wang, "Robust switching blind equalizer for wireless cognitive receivers," *IEEE Trans. Wireless Commun.*, vol. 7, no. 5, pp. 1461–1465, May 2008.

[88] A. Athalye, V. Savic, M. Bolic, and P. M. Djuric, "Novel semi–passive RFID system for indoor localization," *IEEE Sensors J.*, vol. 13, no. 2, pp. 528–537, Feb. 2013.

[89] E. A. de Reyna and P. M. Djuric, "Indoor localization with range-based measurements and little prior information," *IEEE Sensors J.*, vol. 13, no. 5, pp. 1979–1987, May 2013.

[90] H. Godrich, A. Petropulu, and H. Poor, "Sensor selection in distributed multiple-radar architectures for localization: A knapsack problem formulation," *IEEE Trans. Signal Process.*, vol. 60, no. 1, pp. 247–260, Jan. 2012.

[91] L. Kaplan, "Global node selection for localization in a distributed sensor network," *IEEE Trans. Aerosp. Electron. Syst.*, vol. 42, no. 1, pp. 113–135, Jan. 2006.

[92] ——, "Local node selection for localization in a distributed sensor network," *IEEE Trans. Aerosp. Electron. Syst.*, vol. 42, no. 1, pp. 136–146, Jan. 2006.

[93] M. Z. Win and R. A. Scholtz, "Impulse radio: How it works," *IEEE Commun. Lett.*, vol. 2, no. 2, pp. 36–38, Feb. 1998.

[94] L. Yang and G. B. Giannakis, "Ultra-wideband communications: An idea whose time has come," *IEEE Signal Process. Mag.*, vol. 21, no. 6, pp. 26–54, Nov. 2004.

[95] Y. Shen and M. Z. Win, "On the accuracy of localization systems using wideband antenna arrays," *IEEE Trans. Commun.*, vol. 58, no. 1, pp. 270–280, Jan. 2010.

[96] S. Gezici, Z. Tian, G. B. Giannakis, H. Kobayashi, A. F. Molisch, H. V. Poor, and Z. Sahinoglu, "Localization via ultra-wideband radios: a look at positioning aspects for future sensor networks," *IEEE Signal Process. Mag.*, vol. 22, no. 4, pp. 70–84, Jul. 2005.

[97] R. J. Fontana and S. J. Gunderson, "Ultra-wideband precision asset location system," *Proc. IEEE Conf. on Ultra Wideband Syst. and Technol.*, vol. 21, no. 1, pp. 147–150, May 2002.

[98] A. Giorgetti and M. Chiani, "Time-of-arrival estimation based on information theoretic criteria," *IEEE Trans. Signal Process.*, vol. 61, no. 8, pp. 1869–1879, Apr. 2013.

[99] F. Ahmad and M. G. Amin, "Noncoherent approach to through-the-wall radar localization," *IEEE Trans. Aerosp. Electron. Syst.*, vol. 42, no. 4, pp. 1405–1419, Oct. 2006.

[100] K. Yu and I. Oppermann, "Performance of UWB position estimation based on time-of-arrival measurements," in *Proc. Int. Workshop on Ultra Wideband Syst.*, Oulu, Finland, May 2004, pp. 400–404.

[101] N. Maaref, P. Millot, C. Pichot, and O. Picon, "Through-the-wall radar using multiple UWB antennas," *Proc. IET Int. Conf. on Radar Systems*, pp. 1–4, Oct. 2007.

[102] J. Salmi and A. F. Molisch, "Propagation parameter estimation, modeling and measurements for ultrawideband MIMO radar," *IEEE Trans. Antennas Propag.*, vol. 59, no. 11, pp. 4257–4267, Nov. 2011.

[103] L. Ulander and T. Martin, "Bistatic ultra-wideband SAR for imaging of ground targets under foliage," in *Proc. IEEE Int. Radar Conf. (RadarCon)*, Arlington, VA, May 2005, pp. 419–423.

[104] S. Nag and M. Barnes, "A moving target detection filter for an ultra-wideband radar," in *Proc. IEEE Int. Radar Conf. (RadarCon)*, Huntsville, Ala, USA, May 2003, pp. 147–153.

[105] P. K. Dutta, A. K. Arora, and S. B. Bibyk, "Towards radar-enabled sensor networks," in *Proc. IEEE Inform. Processing in Sensor Networks*, Nashville, TN, Apr. 2006, pp. 467–474.

[106] M. Sato and K. Yoshida, "Bistatic UWB radar system," in *Proc. IEEE Int. Conf. on Ultra-Wideband*, Singapore, Sep. 2007, pp. 62–65.

[107]

[108] D. Dardari, R. D'Errico, C. Roblin, A. Sibille, and M. Z. Win, "Ultrawide bandwidth RFID: The next generation?" *Proc. IEEE*, vol. 99, no. 7, pp. 1570–1582, Jul. 2010, special issue on *RFID - A Unique Radio Innovation for the 21st Century.*

[109] D. G. Brennan, "Linear diversity combining techniques," *Proc. IRE*, vol. 47, no. 6, pp. 1075–1102, Jun. 1959.

[110] J. H. Winters, "Optimum combining in digital mobile radio with cochannel interference," *IEEE J. Sel. Areas Commun.*, vol. SAC-2, no. 4, pp. 528–539, Jul. 1984.

[111] M. Z. Win, N. C. Beaulieu, L. A. Shepp, B. F. Logan, and J. H. Winters, "On the SNR penalty of MPSK with hybrid selection/maximal ratio combining over IID Rayleigh fading channels," *IEEE Trans. Commun.*, vol. 51, no. 6, pp. 1012–1023, Jun. 2003.

[112] A. Conti, W. M. Gifford, M. Z. Win, and M. Chiani, "Optimized simple bounds for diversity systems," *IEEE Trans. Commun.*, vol. 57, no. 9, pp. 2674–2685, Sep. 2009.

[113] A. F. Molisch and M. Z. Win, "MIMO systems with antenna selection—An overview," *IEEE Microw. Mag.*, vol. 5, no. 1, pp. 46–56, Mar. 2004.

[114] V. S. Chernyak, *Fundamentals of Multisite Radar Systems: Multistatic Radars and Multistatic Radar Systems*. London, U.K.: CRC Press, 1998.

[115] A. Safaai-Jazi, S. Riad, A. Muqaibel, and A. Bayram, "Ultra-wideband propagation measurements and channel modeling; through-the-wall propagation and material characterization," *DARPA NETEX program*, 2002.

[116] N. Balakrishnan and C. D. Lai, *Continuous Bivariate Distributions*, 2nd ed. Springer, 2009.

[117] M. Hollander and D. A. Wolfe, *Nonparametric Statistical Method*. Wiley, 1973.

[118] E. Paolini, A. Giorgetti, M. Chiani, R. Minutolo, and M. Montanari, "Localization capability of cooperative anti-intruder radar systems," *EURASIP J. Adv. in Signal Process.*, vol. 2008, pp. 1–14, Apr. 2008.

[119] A. F. Molisch, D. Cassioli, C.-C. Chong, S. Emami, A. Fort, B. Kannan, J. Karedal, J. Kunisch, H. Schantz, K. Siwiak, and M. Z. Win, "A comprehensive standardized model for ultrawideband propagation channels," *IEEE Trans. Antennas Propag.*, vol. 54, no. 11, pp. 3151–3166, Nov. 2006.

[120] B. Boudamouz, P. Millot, and C. Pichot, "Through the wall MIMO radar detection with stepped frequency waveforms," in *Proc. European Radar Conference (EuRAD)*, Paris, France, Sep. 2010, pp. 400–402.

[121] F. Viani, P. Rocca, G. Oliveri, D. Trinchero, and A. Massa, "Localization, tracking, and imaging of targets in wireless sensor networks: An invited review," *Radio Science*, vol. 46, no. 5, pp. 1–12, Oct. 2011.

[122] S. Bartoletti, A. Giorgetti, and A. Conti, "UWB sensor radar networks for indoor passive navigation," in *Proc. Tyrrhenian Int. Workshop on Adv. in Radar and Remote Sens.*, Naples, Italy, Sep. 2012, pp. 140–145.

[123] I. Bradaric, G. T. Capraro, and M. C. Wicks, "Sensor placement for improved target resolution in distributed radar systems," in *Proc. IEEE Int. Radar Conference*, Rome, ITALY, May 2008, pp. 1–6.

[124] R. D'Errico, "An indoor backscattering channel characterization for UWB passive RFID applications," in *Proc. 4th European Conference on Antennas and Propagation*, Prague, Czech Republic, Mar. 2012, pp. 1169–1173.

[125] S. Bartoletti, A. Giorgetti, M. Z. Win, and A. Conti, "Blind selection of representative observations for sensor radar networks," *IEEE Trans. Veh. Technol.*, Apr. 2015.

[126] C. R. Berger, B. Demissie, J. Heckenbach, P. Willett, and Z. Shengli, "Signal processing for passive radar using OFDM waveforms," vol. 4, no. 1, pp. 226–238, Feb. 2010.

[127] C. R. Berger, S. Zhou, and P. Willett, "Signal extraction using compressed sensing for passive radar with OFDM signals," in *Proc. Int. Conf. Inf. Fusion (FUSION)*, Cologne, Germany, Jun. 2008, pp. 1514–1519.

[128] M. Glende, J. Heckenbach, H. Kuschel, S. Mueller, J. Schell, and C. Schumacher, "Experimental passive radar systems using digital illuminators (DAB/DVB-T)," in *Proc. Int. Radar Symp*, Cologne, Germany, Sep. 2007, pp. 411–417.

[129] H. Kuschel, J. Heckenbach, S. Mueller, and R. Appel, "On the potentials of passive, multistatic, low frequency radars to counter stealth and detect low flying targets," in *Proc. IEEE Radar Conf.*, Rome, Italy, May 2008, pp. 1443–1448.

[130] C. Coleman, H. Yardley, and R. Watson, "A practical bistatic passive radar system for use with DAB and DRM illuminators," in *Proc. IEEE Radar Conf.*, Rome, Italy, May 2008, pp. 1514–1519.

[131] A. Dammann, S. Sand, and R. Raulefs, "On the benefit of observing signals of opportunity in mobile radio positioning," in *Proc. of Int. ITG Conf. on Systems, Comm., and Coding (SCC)*, Munich, Germany, Jun. 2013, pp. 1–6.

[132] J. A. D. Peral-Rosado, J. Lopez-Salcedo, G. Seco-Granados, F. Zanier, and M. Crisci, "Achievable localization accuracy of the positioning reference signal of 3GPP LTE," in *Proc. Int. Conf. on Localization and GNSS (ICL-GNSS)*, Starnberg, Germany, Jun. 2012, pp. 1–6.

[133] A. Kangas and T. Wigren, "Angle of arrival localization in LTE using MIMO pre-coder index feedback," *IEEE Commun. Lett.*, vol. 17, no. 8, pp. 1584–1587, Aug. 2013.

[134] H. D. Griffiths and C. J. Baker, "Passive coherent location radar systems. part 1: performance prediction," *IEE Proc. Radar, Sonar Navigation*, vol. 152, no. 3, pp. 153–159, Jun. 2005.

[135] K. Finkenzeller, *RFID Handbook: Fundamentals and Applications in Contactless Smart Cards and Identification*, 2nd ed. Wiley, 2004.

[136] D. Dardari, E. Falletti, and M. Luise, *Satellite and Terrestrial Radio Positioning Techniques - A signal processing perspective.* Elsevier Ltd., London, 2011.

[137] N. Decarli, F. Guidi, and D. Dardari, "A novel joint RFID and radar sensor network for passive localization: Design and performance bounds," *IEEE J. Sel. Topics Signal Process.*, vol. 8, no. 1, pp. 80–95, Feb. 2014.

[138] R. D'Errico, M. Bottazzi, F. Natali, E. Savioli, S. Bartoletti, A. Conti, D. Dardari, N. Decarli, F. Guidi, F. Dehmas, L. Ouvry, U. Alvarado, N. Hadaschik, C. Frankek, Z. Mhanna, M. Sacko, Y. Wei, and A. Sibille, "An UWB-UHF semi-passive RFID system for localization and tracking applications," in *IEEE Int. Conf. on RFID-Technology and Applications (RFID-TA)*, Nice, France, Nov. 2012, pp. 1–6.

[139] A. Lazaro, A. Ramos, R. Villarino, and D. Girbau, "Active UWB reflector for RFID and wireless sensor networks," *IEEE Trans. Antennas Propag.*, vol. 61, no. 9, pp. 4767–4774, Sep. 2013.

[140] D. Dardari, F. Guidi, C. Roblin, and A. Sibille, "Ultra-wide bandwidth backscatter modulation: Processing schemes and performance," *EURASIP J. Wireless Commun. and Netw.*, pp. 1–15, Jul. 2011.

[141] C. Floerkemeier, "Bayesian transmission strategy for framed ALOHA based RFID protocols," in *IEEE Int. Conf. on RFID*, Grapevine, TX, Mar. 2007, pp. 228–235.

[142] L. Zhu and T. Yum, "Optimal framed Aloha based anti-collision algorithms for RFID systems," *IEEE Trans. Commun.*, vol. 58, no. 12, pp. 3583–3592, Dec. 2010.

[143] X. Jia, Q. Feng, and L. Yu, "Stability analysis of an efficient anti-collision protocol for RFID tag identification," *IEEE Trans. Commun.*, vol. 60, no. 8, pp. 2285–2294, Aug. 2012.

[144] F. Guidi, A. Sibille, C. Roblin, V. Casadei, and D. Dardari, "Analysis of UWB tag backscattering and its impact on the detection coverage," *IEEE Trans. Antennas Propag.*, vol. 62, no. 8, pp. 4292–4303, Aug. 2014.

[145] W. Lovelace and J. Townsend, "Threshold discrimination and blanking for large near-far power ratios in UWB networks," *IEEE Trans. Commun.*, vol. 53, no. 9, pp. 1447–1450, Sep. 2005.

[146] N. Decarli, F. Guidi, A. Conti, and D. Dardari, "Interference and clock drift effects in UWB RFID systems using backscatter modulation," in *Proc. IEEE Int. Conf. on Ultra-Wideband*, Syracuse, NY, Sep. 2012, pp. 1–5.

[147] V. Heiries, K. Belmkaddem, F. Dehmas, B. Denis, L. Ouvry, and R. D'Errico, "UWB backscattering system for passive RFID tag ranging and tracking," in *Proc. IEEE Int. Conf. on Ultra-Wideband*, Bologna, Italy, Sep. 2011, pp. 489–493.

[148] C. Xu and C. L. Law, "TOA estimator for UWB backscattering RFID system with clutter suppression capability," *EURASIP Journal on Wireless Communications and Networking*, pp. 1–14, Jun. 2010.

[149] D. Arnitz, U. Muehlmann, and K. Witrisal, "UWB ranging in passive UHF RFID: Proof of concept," *IEEE Electronics Lett.*, vol. 46, no. 20, pp. 1401–1402, Oct. 2010.

[150] E. Savioli, M. Bottazzi, F. Natali, N. Decarli, F. Guidi, N. Hadaschik, R. D'Errico, and L. Ouvry, "Semi-passive UHF-UWB RFID: Architecture and localization performance," in *Communications Workshops, IEEE International Conference on Communications*, Budapest, Hungary, Jun. 2013, pp. 1–5.

[151] F. Guidi, N. Decarli, D. Dardari, C. Roblin, and A. Sibille, "Performance of UWB backscatter modulation in multi-tag RFID scenario using experimental

data," in *Proc. IEEE Int. Conf. on Ultra-Wideband*, Bologna, Italy, Sep. 2011, pp. 1–5.

[152] C. Mutti and C. Floerkemeier, "CDMA-based RFID systems in dense scenarios: Concepts and challenges," in *IEEE Int. Conf. on RFID*, Las Vegas, NV, Apr. 2008, pp. 215–222.

[153] J. Kimionis, A. Bletsas, and J. N. Sahalos, "Increased range bistatic scatter radio," *IEEE Trans. Commun.*, vol. 62, no. 3, pp. 1091–1104, Mar. 2014.

[154] C. He and Z. Wang, "Closed-form BER analysis of non-coherent FSK in MISO double rayleigh fading/RFID channel," *IEEE Commun. Lett.*, vol. 15, no. 8, pp. 848–850, Aug. 2011.

[155] J. Kimionis, A. Bletsas, and J. N. Sahalos, "Bistatic backscatter radio for tag read-range extension," in *IEEE Int. Conf. on RFID - Technologies and Applications (RFID-TA)*, Nice, France, Nov. 2012, pp. 356–361.

[156] E. Vahedi, R. Ward, and I. Blake, "Performance analysis of RFID protocols: CDMA versus the standard EPC gen-2," *IEEE Trans. Automation Science and Engineering*, vol. 11, no. 4, pp. 1250–1261, Oct. 2014.

[157] F. Guidi, N. Decarli, S. Bartoletti, A. Conti, and D. Dardari, "Detection of multiple tags based on impulsive backscattered signals," *IEEE Trans. Commun.*, vol. 62, no. 11, pp. 3918–3930, Nov. 2014.

[158] S. Hu, H. Chen, C. Law, Z. Shen, L. Zhu, W. Zhang, and W. Dou, "Backscattering cross section of ultrawideband antennas," *IEEE Antennas Wireless Propag. Lett.*, vol. 6, pp. 70–73, Mar. 2007.

[159] F. Guidi, A. Sibille, and C. Roblin, "Interaction of UWB tag backscattering with close metallic reflectors," *IEEE Antennas Wireless Propag. Lett.*, vol. 13, pp. 245–248, 2014.

[160] B. Denis, J.-B. Pierrot, and C. Abou-Rjeily, "Joint distributed synchronization and positioning in UWB ad hoc networks using TOA," *IEEE Trans. Microw. Theory Tech.*, vol. 54, no. 4, pp. 1896–1911, Jun. 2006.

[161] F. Guidi, M. Sacko, A. Sibille, and C. Roblin, "Analysis of UWB RFID tag backscattering in the presence of scatterers," in *Proc. URSI General Assembly and Scientific Symp.*, Istanbul, Turkey, Aug. 2011, pp. 1–4.

[162] G. Masson, D. Morche, H. Jacquinot, P. Vincent, F. Dehmas, S. Paquelet, A. Bisiaux, O. Fourquin, J. Gaubert, and S. Bourdel, "A 1 nJ/b 3.2-to-4.7 GHz UWB 50 Mpulses/s double quadrature receiver for communication and localization," in *Proc. of the ESSCIRC*, Seville, Spain, Sep. 2010, pp. 502–505.

[163] M. Chiani, A. Conti, and R. Verdone, "Partial compensation signal-level-based up-link power control to extend terminal battery duration," *IEEE Trans. Veh. Technol.*, vol. 50, no. 4, pp. 1125–1131, Jul. 2001.

[164] D. Slepian and E. Sonnenblick, "Eigenvalues associated with prolate spheroidal wave functions of zero order," *Bell Sys. Tech. Journal*, vol. 44, 1965.

[165] M. Chiani, "Integral representation and bounds for Marcum Q-function," *IEEE Electronics Lett.*, vol. 35, no. 6, pp. 445–446, Mar. 1999.

[166] S. Bartoletti and A. Conti, "Passive network localization via UWB wireless sensor radars: the impact of TOA estimation," in *Proc. IEEE Int. Conf. on Ultra-Wideband*, Bologna, Italy, Sep. 2011, pp. 576–580.

[167] V. Heiries, K. Belmkaddem, F. Dehmas, B. Denis, L. Ouvry, and R. D'Errico, "UWB backscattering system for passive RFID tag ranging and tracking," in *Ultra-Wideband (ICUWB), 2011 IEEE International Conference on*, Bologna, IT, Sep. 2011, pp. 489 –493.

[168] R. D'Errico, "An indoor backscattering channel characterization for UWB passive RFID applications," in *Antennas and Propagation (EUCAP), 2012 6th European Conference on*, Prague, CZ, Mar. 2012, pp. 1169 –1173.

[169] S. Bartoletti, M. Guerra, and A. Conti, "UWB passive navigation in indoor environments," in *Proc. 4th Int. Symp. on Applied Sci. in Biomed. and Commun. Technol.*, Barcelona, Spain, Oct. 2011, pp. 1–5.

[170] V. Chawla and D.-S. Ha, "An overview of passive RFID," *IEEE Commun. Mag.*, vol. 45, no. 9, pp. 11–17, Sep. 2007.

[171] K. Michael, G. Roussos, G. Huang, A. Chattopadhyay, R. Gadh, B. S. Prabhu, and P. Chu, "Planetary-scale RFID services in an age of uberveillance," *Proc. IEEE*, vol. 98, no. 9, pp. 1663–1671, Sep. 2010.

[172] R. Miesen, R. Ebelt, F. Kirsch, T. Schafer, G. Li, H. Wang, and M. Vossiek, "Where is the tag?" *IEEE Microwave Mag.*, vol. 12, no. 7, pp. 49–63, Dec. 2011.

[173] A. Costanzo, D. Masotti, T. Ussmueller, and R. Weigel, "Tag, you're it: Ranging and finding via RFID technology," *IEEE Microw. Mag.*, vol. 14, no. 5, pp. 36–46, Aug. 2013.

[174] L. Geng, M. Bugallo, A. Athalye, and P. Djuric, "Indoor tracking with RFID systems," *IEEE J. Sel. Topics Signal Process.*, vol. 8, no. 1, pp. 96–105, Feb. 2014.

[175] Z.-M. Liu and R. Hillegass, "A 3 patch near field antenna for conveyor bottom read in RFID sortation application," in *Proc. IEEE Antennas and Propag. Soc. Int. Symp.*, Albuquerque, NM, Jul. 2006, pp. 1043–1046.

[176] Y. Zhang, M. G. Amin, and S. Kaushik, "Localization and tracking of passive RFID tags based on direction estimation," *Hindawi Int. J. of Antennas and Propag.*, vol. 2007, pp. 1–9, 2007.

[177] L. Shangguan, Z. Li, Z. Yang, M. Li, Y. Liu, and J. Han, "OTrack: Towards order tracking for tags in mobile RFID system," *IEEE Trans. on Parallel and Distributed Syst.*, Oct. 2013.

[178] R. Siragusa, P. Lemaitre-Auger, A. Pouzin, and S. Tedjini, "RFID tags localization along an axis using a tunable near-field focused circular-phase array antenna," in *Proc. URSI General Assembly and Scientific Symp.*, Istanbul, Turkey, Aug. 2011, pp. 1–4.

[179] A. Parr, R. Miesen, and M. Vossiek, "Inverse SAR approach for localization of moving RFID tags," in *Proc. IEEE Int. Conf. on RFID*, Orlando, FL, Apr. 2013, pp. 104–109.

[180] P. Nepa, F. Lombardini, and A. Buffi, "Location and tracking of items moving on a conveyor belt and equipped with UHF-RFID tags," in *IEEE Antennas and Propag. Society Int. Symp. (APSURSI)*, Chicago, IL, Jul. 2012, pp. 1–2.

[181] D. Arnitz, K. Witrisal, and U. Muehlmann, "Multifrequency continuous-wave radar approach to ranging in passive UHF RFID," *IEEE Trans. Microw. Theory Tech.*, vol. 57, no. 5, pp. 1398–1405, May 2009.

[182] P. Nikitin, R. Martinez, S. Ramamurthy, H. Leland, G. Spiess, and K. V. S. Rao, "Phase based spatial identification of UHF RFID tags," in *IEEE Int. Conf. on RFID*, Orlando, FL, Apr. 2010, pp. 102–109.

[183] R. Kronberger, T. Knie, R. Leonardi, U. Dettmar, M. Cremer, and S. Azzouzi, "UHF RFID localization system based on a phased array antenna," in *IEEE Int. Symp. on Antennas and Propag. (APSURSI)*, Spokane, WA, Jul. 2011, pp. 525–528.

[184] T. Hansen and M. Oristaglio, "Method for controlling the angular extent of interrogation zones in RFID," *IEEE Antennas and Wireless Propag. Lett.*, vol. 5, no. 1, pp. 134–137, Dec. 2006.

[185] S. Bartoletti, A. Conti, and A. Giorgetti, "Analysis of UWB radar sensor networks," in *Proc. IEEE Int. Conf. Commun.*, Cape Town, South Africa, May 2010, pp. 1–6.

[186] A. Savioli, M. Bottazzi, F. Natali, N. Decarli, F. Guidi, N. Hadaschik, R. DErrico, and L. Ouvry, "Semi-passive UHF-UWB RFID: Architecture and localization performance," in *Proc. IEEE Int. Conf. on Commun. Workshops (ICC)*, Budapest, Hungary, Jun. 2013, pp. 52–56.

Author's Publication List

Journal Papers

(J1) S. Bartoletti, A. Giorgetti, M. Z. Win, and A. Conti, "Blind selection of representative observations for sensor radar networks," *IEEE Trans. Veh. Technol.*, Apr. 2015.

(J2) S. Bartoletti, W. Dai, A. Conti, and M. Z. Win, "A mathematical model for wideband ranging," *IEEE J. Sel. Topics Signal Process.*, vol. 9, no. 2, pp. 216–228, Mar. 2015.

(J3) F. Guidi, N. Decarli, S. Bartoletti, A. Conti, and D. Dardari, "Detection of multiple tags based on impulsive backscattered signals," *IEEE Trans. Commun.*, vol. 62, no. 11, pp. 3918–3930, Nov. 2014.

(J4) S. Bartoletti, A. Conti, A. Giorgetti, and M. Z. Win, "Sensor radar networks for indoor tracking," *IEEE Wireless Commun. Lett.*, vol. 3, no. 2, pp. 157–160, Apr. 2014.

Conference Proceedings

(C1) S. Bartoletti, N. Decarli, A. Guerra, F. Guidi, D. Dardari, and A. Conti, "Order of Arrival Estimation via UHF-UWB RFID," in *Proc. IEEE Workshop on Advances in Network Localization and Navigation (ICC)* , Sydney, Australia, June 2014, pp. 133–137.

(C2) S. Bartoletti, A. Conti, and M. Z. Win, "Passive Radar via LTE Signals of Opportunity," in *Proc. IEEE Workshop on Advances in Network Localization and Navigation (ICC)* , Sydney, Australia, June 2014, pp. 181–185.

(C3) S. Bartoletti, A. Giorgetti, and A. Conti, "Sensor Radars with Subset Diversity," in *Proc. IEEE Workshop on Advances in Network Localization and Navigation (ICC)* , Budapest, Hungary, June 2013, pp. 32–36.

(C4) R. D'Errico, M. Bottazzi, F. Natali, E. Savioli, S. Bartoletti, A. Conti, D. Dardari, N. Decarli, F. Guidi, F. Dehmas, L. Ouvry, U. Alvarado, N. Hadaschik, C. Frankek, Z. Mhanna, M. Sacko, Y. Wei, and A. Sibille, "An UWB-UHF semi-passive RFID system for localization and tracking applications," in *IEEE Int. Conf. on RFID-Technology and Applications (RFID-TA)*, Nice, France, Nov. 2012, pp. 1–6.

(C5) S. Bartoletti, A. Giorgetti, and A. Conti, "UWB sensor radar networks for indoor passive navigation," in *Proc. Tyrrhenian Int. Workshop on Adv. in Radar and Remote Sens.*, Naples, Italy, Sep. 2012, pp. 140–145.

(C6) S. Bartoletti, M. Guerra, and A. Conti, "UWB passive navigation in indoor environment," in *Proc. 4th Int. Symp. on Appl. Sci. in Biomed. and Commun. Tech.*, Barcelona, Spain, Oct. 2011, pp. 1–5.

(C7) S. Bartoletti and A. Conti, "Passive network localization via UWB wireless sensor radars: the impact of TOA estimation," in *Proc. IEEE Int. Conf. on Ultra-Wideband*, Bologna, Italy, Sep. 2011, pp. 576–580.

(C8) S. Bartoletti, A. Conti, and A. Giorgetti, "Analysis of UWB radar sensor networks," in *Proc. IEEE Int. Conf. Commun.*, Cape Town, South Africa, May 2010, pp. 1–6.

Coauthored Project Deliverables

(D1) GRETA "Report on the First Year of Activity," D2, 2014.

(D2) SELECT "Demo System 1," D7.1 2014.

(D3) GRETA "Reference Scenarios and Applications Requirements Definition," D1, 2013.

(D4) WEBS "Report PL59, PL60," 2013.

(D5) WEBS "Report PL57, PL58," 2012.

(D6) SELECT "Intermediate report on Dissemination & Exploitation plan and activities," D6.3 2012.

(D7) SELECT "Multi-functional network design: final system specification," D2.3.2, 2012.

(D8) SELECT "Signal processing techniques: final report," D2.2.2, 2012.

(D9) SELECT "Backscatter propagation modelling: final report," D2.1.2, 2012.

(D10) SELECT "Signal processing techniques: interim report," D2.2.1, 2011.